

UNIVERSIDAD DE CANTABRIA

PROGRAMA DE DOCTORADO DE INGENIERÍA DE COSTAS,
HIDROBIOLOGÍA Y GESTIÓN DE SISTEMAS ACUÁTICOS (IH2O)



TESIS DOCTORAL

**Wave runup en playas: el papel del estado
morfodinámico de la playa**

PHD THESIS

**Wave runup on beaches: the role of the beach
morphodynamic state**

Realizada por: PAULA GOMES DA SILVA

Dirigida por: Prof./Dr. Mauricio González

Prof./Dr. Raúl Medina

Escuela de Doctorado de la Universidad de Cantabria

Santander 2018

Aos meus queridos pais

"Um homem precisa viajar para lugares que não conhece para quebrar essa arrogância que nos faz ver o mundo como o imaginamos, e não simplesmente como é ou pode ser. Que nos faz professores e doutores do que não vimos, quando deveríamos ser alunos, e simplesmente ir ver."

("A man needs to travel to places he doesn't know for breaking this arrogance that causes us to see the world as we imagine it, and not simply as it is or may be. That makes us teachers and doctors of what we have never seen, when we should just be learners, and simply go and see it.")

Amyr Klink (Mar sem fim/Endless sea)

Acknowledgements

Llegando al fin de mi jornada como doctoranda tengo muchas personas a las que agradecer por haber, de alguna manera, apoyado el desarrollo de esta tesis.

Primeramente, doy las gracias a mis directores Mauricio y Raúl, por haberme abierto las puertas de IHCantabria, por la confianza que han depositado en mí y por compartir sus experiencias y conocimientos durante este proceso que me ha engrandecido profesional y personalmente.

Agradezco a los profesores e investigadores de IHCantabria. Por suerte, he tenido la oportunidad de contar con el apoyo de los mejores durante el desarrollo de mi trabajo. Agradezco especialmente a Cesar Vidal, por los consejos a la hora de planificar las campañas de campo y analizar los datos. Agradezco también a Gabriel Diaz, por la disponibilidad, e incluso ilusión, en ayudarme las miles de veces que necesité auxilio con las simulaciones y análisis de los datos. Agradezco a Roland Garnier por el apoyo con la logística y ejecución de las campañas de campo, por la ayuda diaria en la interpretación de nuestros datos y por las ganas que tiene de hacer siempre un trabajo de excelencia.

Tengo que agradecer a todos los que han dado soporte a las campañas de campo. Al personal del laboratorio de ensayos físicos de IHCantabria, en particular Álvaro Sainz, David Blanco y José Salas, por la mano que me han echado con los equipos de medición. A mis compañeros de grupo que han hecho todo el esfuerzo para que las campañas fueran un éxito. Al Laboratorio de Ingeniería Geográfica de la Universidad de Cantabria, en especial al profesor Javier Sánchez, por prestar los equipos topográficos para las mediciones y por todo el auxilio que hemos necesitado durante las campañas.

Agradezco al Profesor Antonio Klein, por la motivación para emprender esta jornada y por disponibilizar los datos medidos en la Ensenada de Itapocorói durante la realización del Proyecto Piçarras (Proc. No. 575008/2008-3).

Agradezco también a los compañeros de IH con los que compartí todo el proceso, las alegrías, los cafés, las comidas, las barbacoas y los agobios: Carlos (y Nati), Nacho, Camino, Laura, Camilo, June, Alfonso, Paula e Íñigo. Muchas Gracias! A Felipe doy las gracias por preocuparse y por compartir también las cañas y los hobbies.

A los buenos amigos que hice en Santander, en especial Jana, Gema y Ana por las escapadas necesarias del ambiente de trabajo y por estar siempre pendientes.

E aos amigos da vida, os de sempre, que estiveram e vão estar em todos os meus agradecimentos, especialmente Morja e Bri que, de longe (e nem tão longe), sempre tiraram um tempinho pra me entender e aconselhar.

A David, un "muito obrigado" especial por las correcciones en el texto, por el apoyo incondicional y por la paciencia infinita.

Finalmente, agradeço muito à minha família por ser meu suporte, por apoiar-me e incentivar-me em todas as jornadas mais duras e distantes, e por estarem presentes através do oceano.

El presente estudio ha sido realizado con el apoyo de:

- CNPq, Conselho Nacional de Desenvolvimento Científico e Tecnológico - Brasil
- Instituto de Hidráulica Ambiental de la Universidad de Cantabria
- Proyecto MUSCLE-Beach (Plan nacional - BIA2014-59643-R)
- Proyecto SMC2020 (Sodercan - ID16-IN-045)

Contents

Acknowledgements	VII
Contents	x
List of Figures	xv
List of Tables	xxi
Abbreviations	xxiii
Symbols	xxv
0. Resumen en Español	1
0.1. Introducción	1
0.1.1. Estado del Arte	3
0.1.2. Objetivos de la tesis	6
0.2. Experimentos de campo	6
0.3. Análisis y estimación del swash infragravitatorio	9
0.3.1. Metodología	9
0.3.2. Resultados	10
0.4. Análisis y estimación del swash incidente	13
0.4.1. Metodología	13
0.4.2. Resultados	15
0.5. Aplicación de las fórmulas de swash en el cálculo del runup	18
0.5.1. Methods	18
0.5.2. Resultados	19
0.6. Conclusiones	20
0.6.1. Principales conclusiones en el análisis de las mediciones de oleaje, morfología y runup	20
0.6.2. Principales conclusiones en el análisis y estimación del swash infragravitatorio	20
0.6.3. Principales conclusiones en el análisis y estimación del swash incidente	21
0.6.4. Principales conclusiones en la aplicación de las fórmulas de swash en el cálculo del runup	22

1. Introduction	23
1.1. Motivation: the importance of the wave runup on coastal studies . . .	23
1.2. State of the Art	26
1.2.1. Empirical runup parameterizations	27
1.2.2. Wave runup and wave reflection on the coast	33
1.3. Thesis Objectives	37
1.4. Outline	38
2. Field experiments	41
2.1. Introduction	41
2.2. Field Site - Somo Beach	42
2.3. Experiments set-up	43
2.3.1. MUSCLE-Beach experiment (2016)	43
2.3.2. MUSCLE-Beach experiment (2017)	46
2.4. Data process	48
2.5. Results	50
2.5.1. MUSCLE-Beach experiment 2016	50
2.5.2. MUSCLE-Beach experiment 2017	57
2.6. Summary and Conclusions	60
3. Infragravity swash analysis and parameterization	65
3.1. Introduction	65
3.2. Methods	66
3.2.1. Previous studies dataset	66
3.2.2. Data analysis methodology	68
3.3. Results	69
3.3.1. Infragravity swash estimation using the R2001 and S2006 formulas	69
3.3.2. Infragravity swash parameterization	71
3.3.3. The role of the morphodynamic beach state	74
3.3.4. Evaluation of the infragravity swash parameterization	76
3.4. Discussion	79
3.5. Summary and Conclusions	81
4. Incident swash analysis and parameterization	85
4.1. Introduction	85
4.2. Methods	87
4.2.1. Dataset	87
4.2.2. S_{inc} estimation using G1984 and S2006 formulas	87
4.2.3. Wave reflection and the incident swash at Somo beach	88
4.2.4. S_{inc} parameterization for different morphodynamic condi- tions based on G1984 model	92
4.2.5. Evaluations of S_{inc} parameterization	93
4.3. Results	93
4.3.1. S_{inc} estimation using G1984 and S2006 formulas	93

4.3.2.	Wave reflection and the incident swash at Somo beach . . .	96
4.3.3.	S_{inc} parameterization for different morphodynamic conditions based on G1984 model	101
4.4.	Discussion	104
4.5.	Summary and Conclusions	109
5.	Application of the swash formulas to wave runup estimation	111
5.1.	Introduction	111
5.2.	Methods	111
5.2.1.	Evaluations of wave runup estimation (R_2)	111
5.2.2.	Application to Itapocorói Bay	112
5.3.	Results	117
5.3.1.	Evaluation of wave runup estimation (R_2)	117
5.3.2.	Application to Itapocorói Bay	119
5.4.	Discussion	121
5.5.	Summary and Conclusions	122
6.	Conclusions and future research	125
6.1.	Conclusions	125
6.1.1.	Main conclusions on the analysis of measured wave, morphology and runup	125
6.1.2.	Main conclusions on the analysis and parameterization of the infragravity swash	126
6.1.3.	Main conclusions on the analysis and parameterization of the incident swash	127
6.1.4.	Main conclusion on the application of the swash formulas to runup estimation	128
6.2.	Scientific contributions	129
6.3.	Future research	130
A.	Appendix 1 - Tables	133
	Bibliography	137

List of Figures

1.	Componentes del runup (setup $\langle \eta \rangle$ y swash S) y parámetros importantes (altura de onda H , pendiente de la playa $\tan\beta$ y nivel del agua SWL).	2
2.	Ubicación del experimento y de las mediciones. En el detalle, la vista desde la estación de video cámaras.	8
3.	Regresión lineal entre el S_{igH} medido y los valores calculados con el modelo empírico utilizando $K = f(\Omega^*)$	12
4.	Dispersión entre datos medidos y calculados para cada estado morfodinámico (arriba) y ajuste final de los datos (abajo) utilizando la ec. 12. La línea diagonal representa la bisectriz sobre la cual los valores están perfectamente correlacionados.	17
1.1.	Runup components setup ($\langle \eta \rangle$), swash (S) and important parameters wave height (H), beach slope ($\tan\beta$) and still water level (SWL)	24
1.2.	Example of the effects of wave runup, tide and surge during extreme events. A) Niterói - Brazil; B) Haumoana - New Zealand and C) Santander - Spain. (Photos: Grasiela de Oliveira; Alan Blacklock and Eva Minguez)	25
1.3.	Spectral signature of swash according to the morphodynamic beach state. The dashed line represents the boundary between infragravity and incident frequencies (figure adapted from Hughes et al., 2012).	29
1.4.	Linear regression between S_{ig} and S2006 parameter $(H_0L_0)^{0.5}$. Symbols represent each experiment analysed by S2006. Red circles indicate an example of S_{ig} calculated under similar sea state in a dissipative (Agate) and a reflective (Duck) beach.	32
1.5.	Regression fit between the R_2 and H (left) and between R_2 and the parameter including the beach slope (S) and L (right). (Adapted from Ruggiero et al, 2001)	33
1.6.	The wave runup as an approximation of the standing wave height at the shoreline.	34
1.7.	Guza et al. (1984) dataset along the three conditions observed. (Adapted from Guza et al, 1984)	36
2.1.	Location of the field experiment and measurements position. In detail, the view from the video station.	42

2.2.	Pressure Sensors and ADV installed at low tide (up) and been submerged during the flooding tide (down).	44
2.3.	Example of the process carried out to identify the pixels correspondent to the profiles on images.	45
2.4.	Runup measurement with GPS in the three profiles (up) and measured values over the tide series (down).	46
2.5.	Equipments installed at P2 at different tidal moments.	47
2.6.	Topobatismetry measured on October 2017.	47
2.7.	Generation of timestacks from the images: a) image obtained from the video camera – the white line represents the transect over which the pixels were extracted; b) runup timestack generated with the time sequence of cross-shore pixels and c) runup time series digitalized from timestack image; d) fit to a cumulative distribution function (CDF) to obtain the R_2	49
2.8.	Topography of Somo profiles (a) and examples of wave spectra obtained by the pressure sensors (PS) at P1, P2, P3 and at ADCP position (b). See equipment and profile position in Figure 2.1. . . .	52
2.9.	Wave parameters, $\tan\beta$ and swash values obtained at the three profiles during the high tide.	53
2.10.	Total swash spectra obtained at Somo beach profiles P1, P2 and P3. The vertical dashed line represents the limit between infragravity and incident bands ($f = 0.05$ Hz). Diagonal black line shows the f^{-3} dependence of swash energy.	54
2.11.	Wave parameters time series measured by the Virgen del Mar Waverider buoy. The green shaded area represents the day of the experiment, while the gray shaded area represents the previous 30-days period used to calculate the beach state according to previous wave condition. Red lines indicate the energetic events that preceded the field experiment.	55
2.12.	Methodology applied to calculate the beach state taking into account the beach memory.	56
2.13.	Wave spectra measured at the ADCP position on 19th and 21st September.	58
2.14.	Wave parameters, foreshore slope and swash values obtained during the 2017 experiment.	59
2.15.	Total swash spectra measured at profile P2 on the 19th and 21st September. The vertical dashed line represents the limit between infragravity and incident bands ($f = 0.05$ Hz). Diagonal black line shows the f^{-3} dependence of swash energy.	60
2.16.	Topography of the profile P2 measured at 19/09/2017 and wave spectra obtained from each of the 9 sensors.	62
2.17.	Topography of the profile P2 measured at 21/09/2017 and wave spectra obtained from each of the 9 sensors.	63
3.1.	Location of the experiments presented by Stockdon et al (2006) and Senechal et al (2011).	67

3.2.	Linear regression between S_{ig} observed and calculated with S2006 (up) and R2001 (down) parameterizations.	70
3.3.	Linear regression between S_{ig} y $(H_0L_0/\tan\beta)^{0.5}$ (passing through the origin). Colors represent three groups of beaches: coarse sediment beaches (black), beaches with intermediate sediment size (blue) and fine sediment beaches (red).	72
3.4.	Regression fit between S_{igH} and $(H_0L_0/\tan\beta)^{0.5}$	73
3.5.	Points of the GOW database used to calculate Ω^* for each experiment.	75
3.6.	Linear regression between K and Ω^* from each experiment. Symbols represent the dataset from each experiment and the red line is the best fit obtained.	75
3.7.	Regression fit between measured horizontal infragravity swash S_{igH} and the values calculated S_{igHc} with the parameterization using $K = f(\Omega^*)$	76
3.8.	Correlation coefficient obtained from the linear regression analysis between measured and calculated infragravity swash for beaches under intermediate and dissipative conditions.	78
3.9.	Linear regression fit between measured S_{ig} and the Hunt scaling.	79
3.10.	Linear regression fit between measured and calculated S_{igH} (using eq. 3.5) for data obtained during different tidal moments (high, mid and low tide).	82
4.1.	Methodology applied to verify the relation between S_{inc}/H_0 and K_r^2	89
4.2.	Location of the collocated pressure sensor and velocimeter used to calculate K_r^2	90
4.3.	Energy spectra of cross-shore velocity U and longshore velocity V at the mesurement points.	91
4.4.	Distribution of the dataset used in this work according to the conditions proposed by Guza et al (1984). ξ_0 is the Iribarren number and ξ_c is the minimum value for complete reflection.	93
4.5.	Linear regression between S_{inc} observed and calculated with S2006 (up) and G1984 (down) parameterizations. The dashed line represents the ideal fit over which the values would be perfect correlated. The red line is the fit between measured and calculated values.	94
4.6.	a) Relation between S_{inc}/H_0 and ξ_0 for dissipative beaches. Red and blue lines represent the linear and the quadratic relation between both variables respectively. Black Symbols represent the same beaches as presented in previous figures. b) Error associated with each fit ($Error = (Predicted - Observed)/Observed $). Note that the morphodynamic beach state was determined using Ω^*	96
4.7.	Example of the shoreward and seaward (reflected) wave series (upper panels), wave energy density (middle panels) and $K_r^2(f)$ (lower panels) at profiles P2 and P3, during the first experiment (05/2016).	97

4.8.	Example of the shoreward and seaward (reflected) wave series (upper panels), wave energy density (middle panels) and $K_r^2(f)$ (lower panels) at profiles P2, for the two days of the second experiment (09/2017).	98
4.9.	Relation between the reflection coefficient K_r^2 and the foreshore slope $\tan\beta$ (a), the mean frequency f_m (b) and the Miche's number M (c).	99
4.10.	Relation between S_{inc}/H_0 and the measured reflection coefficient (a) and the Miche's number M (b).	100
4.11.	Relation between S_{inc}/H_0 and the parameter M using the whole database available in this work.	101
4.12.	Scatterplot between measured S_{inc} and S_{inc} calculated using the coefficients obtained with the fit for the whole dataset ($a = 0.42$, $b = 0.99$ and $c = -0.65$) and resultant $\rho^2 = 0.32$. Light colored dots represent the distribution of S_{inc} calculated with S2006 model. The dashed line represents the ideal fit over which the values would be perfectly correlated.	102
4.13.	Scatterplot between measured and calculated S_{inc} for each beach type (up) and the final regression fit (down) using the three formulas. The dashed line represents the fit over which the values would be perfect correlated.	103
4.14.	Distribution of the dataset used in this work according to the conditions proposed by Guza et al (1984). Symbols represent the same beaches as presented in previous figures. Black, blue and red symbols represents reflective, intermediate and dissipative conditions (according to Ω^*), respectively.	106
4.15.	Linear regression fit between measured and calculated S_{inc}/H_0 (using eq. 4.9) for the data obtained during different tidal moments (high, mid and low tide).	108
5.1.	Location and measurement distribution along Itajuba, Piçarras and Alegre beaches.	113
5.2.	Example of the topography (blue line) and runup (red dots) measured in each beach profile. Black triangles indicate the limits between which the foreshore slope was calculated.	115
5.3.	$D50$, mean $\tan\beta$ and Ω^* distribution along the beach. On the box-plot, the central mark is the median, the edges of the box are the 25th and 75th percentiles, the whiskers extend to the most extreme datapoints.	116
5.4.	GOW point used to calculate the beach state according to the beach memory (Ω^*).	116

5.5.	Scatterplot between measured and calculated R_2 . Coloured symbols indicate the beach morphodynamic state according to Ω^* . Black thin line represents the ideal fit, black thick line represents the fit obtained when using the formulas proposed here (eq. 5.2) and gray dashed line is the fit obtained using the formulas proposed by Stockdon et al. (2006) (eq. 1.11).	117
5.6.	Scatterplot between measured and calculated values of the wave runup components: a)swash amplitude ($S/2$) calculated using both infragravity and incident swash formulas proposed in this work and b) setup level ($\langle \eta \rangle$) calculated according to S2006. Coloured symbols indicate the beach morphodynamic state according to Ω^*	118
5.7.	Setup $\langle \eta \rangle$, infragravity swash S_{ig} , incident swash S_{inc} and wave runup R_2 calculated with the formulas proposed in this work for Itapocorói bay.	120
5.8.	Estimated vs observed R_2 from reflective conditions on Itapocorói bay. Blue circles indicate the main overestimation resultant from S2006 model and reduced with the formula proposed here.	121
5.9.	Difference between the errors from S2006 and from the model proposed here as stated in eq. 5.3.	123
A.1.	Field experiment sites.	133

List of Tables

3.1.	Performance evaluation of the infragravity swash parameterization for each experiment, using S2006 (eq. 3.1) and R2001 (eq. 3.2) parameterizations	69
3.2.	Results of the linear regression ($y = Kx$) between the measured S_{ig} and different parameters.	71
3.3.	Performance evaluation of infragravity swash parameterization for each experiment using Eq. 3.4 (K constant) and Eq. 3.5 (K as a function of Ω^*).	77
3.4.	Performance evaluation of infragravity swash parameterization for intermediate and dissipative beaches using Eq. 3.4 (K constant) and Eq. 3.5 (K as a function of Ω^*).	77
4.1.	Performance evaluation of G1984 and S2006 for all dataset and for different morphodynamic conditions	95
4.2.	Correlation between the reflection coefficient and different wave and beach parameters ($y = Kx$).	99
4.3.	Coefficients of the regression between S_{inc}/H_0 and the parameters proposed in eq. 4.7 ($S_{inc}/H_0 = a * \tan\beta^b(H_0/L_0)^c$) for different beach types	104
5.1.	Values attributed to coefficients a , b and c for dissipative, intermediate and reflective conditions.	112
5.2.	Performance assessment of the R_2 calculated with the S_{inc} and S_{ig} parameterization from S2006 and from those proposed in this work, using the dataset from Somo beach and those recompiled from previous works.	119
A.1.	Summary of the environmental parameter from Somo (Gomes da Silva et al, 2017); Truc Vert (Senechal et al, 2011), Itapocorói (Vieira da Silva et al, 2017) beaches. Sub-index 0 indicates parameters obtained from measurement points and deshoaled to a depth of 80 m. N is the number of data in each dataset.	134
A.2.	Summary of the environmental parameters from Stockdon et al (2006) used in this work. Sub-index 0 indicates parameters obtained from measurements points deshoaled to a depth of 80 m. N is the number of data in each dataset.	135
A.3.	Summary of the runup, setup and swash statistics for all field experiments analysed in this thesis.	136

Abbreviations

ADCP = Acoustic Doppler Current Profiler

ADV = Acoustic Doppler Velocimeter

AST = Acoustic Surface Tracking

CDF = Cumulative Distribution Function

GOW = Global Ocean Waves database

G1984 = refers to the work Guza et al (1984)

PS = Pressure sensor

PSD = Power Spectral Density in wave and swash spectra

Psync = Synchronized pressure sensor

RMSE = Root Mean Square Error

R2001 = refers to the work Ruggiero et al (2001)

S2006 = refers to the work Stockdon et al. (2006)

Symbols

a = first coefficient in the basic form of Guza's equation

A_s = swash amplitude

A_0 = deep water wave amplitude

b = second coefficient in the basic form of Guza's equation

c = third coefficient in the basic form of Guza's equation

D_{50} = median sediment size

D = number of days used to calculate the beach state in Ω^* equation

$E(f)$ = wave energy spectra

E^+ = shoreward wave energy

E^- = seaward wave energy

f = wave frequency

f_m = mean wave frequency

f_p = peak wave frequency

g = acceleration of gravity

h = water depth

H = wave height

H_0 = deep water significant wave height

H_{0rms} = deep water root mean square wave height

H_i = incident (shoreward) wave height

H_r = reflected (seaward) wave height

H_s = significant wave height

H_{SW} = standing wave height

K = slope of the linear regression fit ($y=Kx$)

- $K_r^2(f)$ = squared reflection coefficient
 K_r^2 = squared reflection coefficient integrated over the incident frequency band
 L_0 = deep water wave length
 L_{zum} = vertical scale Rayleigh distribution
 M = Miche's number
 R = wave runup
 R_2 = wave runup exceeded by 2% of the waves
 R_{2c} = calculated wave runup exceeded by 2% of the waves
 R_{2cm} = measured wave runup exceeded by 2% of the waves
 R_{ig} = infragravity runup
 R_{max} = maximum runup
 S = swash
 S_{ig} = infragravity swash
 S_{igc} = calculated infragravity swash
 S_{igH} = horizontal infragravity swash
 S_{igHc} = calculated horizontal infragravity swash
 S_{inc} = incident swash
 T = wave period
 T_p = wave peak period
 U = cross-shore velocity
 V = longshore velocity
 Z = vertical topographic value
 β = foreshore slope
 η = free surface elevation
 η^+ = shoreward free surface elevation
 η^- = seaward free surface elevation
 $\langle \eta \rangle$ = wave setup
 ϵ_s = non-dimensional swash
 ϵ_0 = non-dimensional wave height
 ϕ = decay rate used to calculate the beach state in Ω^* equation
 ξ_0 = Surf similarity parameter (Iribarren number)

ξ_c = minimum ξ_0 value for total reflection

Ω = non-dimensional fall velocity parameter used to determine the beach state

Ω^* = beach state taking into account the previous sea states (beach memory)

ω_s = dimensional fall velocity parameter

ρ^2 = correlation coefficient

σ = radian frequency

θ = wave direction

Chapter 0

Resumen en Español

0.1. Introducción

A lo largo de las últimas décadas, las costas de todo el mundo han sido objeto de interés para la comunidad científica y los ingenieros. Los impactos de las dinámicas marinas sobre la población que vive en la costa y sobre las estructuras y recursos costeros son temas que causan preocupación y han recibido atención especial. Los análisis de riesgo de erosión e inundación son, hoy día, elementos básicos de cualquier estrategia de gestión de la costa. Entre los elementos fundamentales para los estudios de riesgo, el runup de las olas es uno de los más críticos.

El runup es definido como la oscilación vertical de la línea de costa en la playa. Cuando las olas se acercan a la costa, parte de la energía se pierde por la rotura en la zona de rompientes. El resto de la energía alcanza la playa y genera las oscilaciones del runup. En términos prácticos, el runup está compuesto por una sobreelevación (quasi) estacionaria del nivel del agua (setup - $\langle \eta \rangle$), y por fluctuaciones alrededor de esta sobreelevación (swash - S) (Guza and Thornton, 1982; Miche, 1951) (Figure 1). Los procesos que desencadenan las oscilaciones de altas y bajas frecuencias en la zona de ascenso y descenso son bastante diferentes y, por esta razón, el swash incidente (S_{inc} : 0.05 to 0.5 Hz) y el swash infragravitatorio (S_{ig} : 0.003 to 0.05 Hz) normalmente son analizados separadamente.

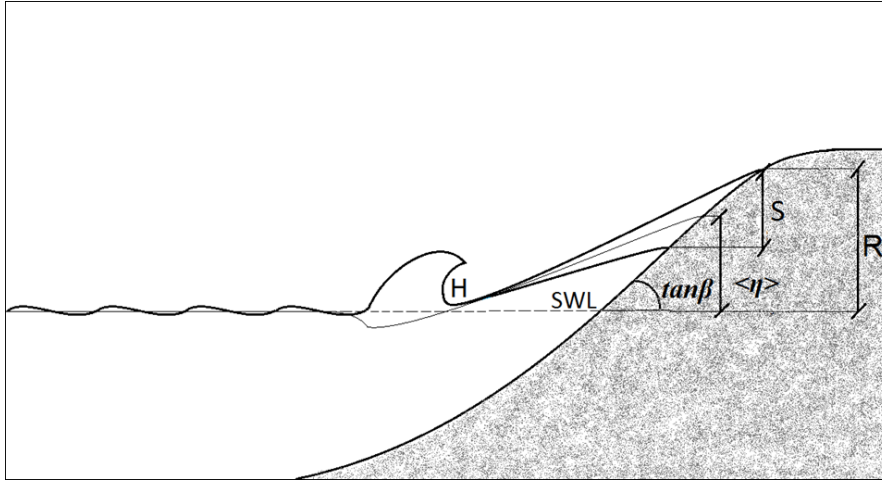


Figure 1: Componentes del runup (setup $\langle \eta \rangle$ y swash S) y parámetros importantes (altura de onda H , pendiente de la playa $\tan\beta$ y nivel del agua SWL).

La importancia de conocer y cuantificar el runup en playas, radica en el hecho de que dichas oscilaciones son responsables de una cantidad considerable de los cambios de sedimento entre las partes subaérea y emergida del perfil de la playa (Masselink and Puleo, 2006). El runup también juega un papel importante en la inundación y la erosión costera, principalmente en condiciones extremas de temporal, en las que puede llegar a alcanzar valores catastróficos si se suma a las elevaciones de mareas astronómicas y meteorológicas (Gomes da Silva et al., 2016; Medina and Méndez, 2006; Sallenger, 2000). Por ello, el runup es comúnmente utilizado como criterio importante en diseños de estructuras costeras y alimentación artificial de playas, así como en análisis de riesgo de erosión e inundación de la costa.

Debido a la complejidad de los procesos de transformación del oleaje cerca a la costa, el cálculo del runup suele hacerse por medio de formulaciones empíricas que lo relacionan directamente con la pendiente de la playa y las características del oleaje offshore (e.g. Ruessink et al., 1998; Senechal et al., 2011; Vousdoukas et al., 2009). Sin embargo, todavía existe un debate considerable acerca de como el runup se relaciona a dichos parámetros, así como acerca del rango de aplicación de los modelos empíricos debido a procesos que pueden ocurrir entre el punto de medición del oleaje y la playa.

Muchos de los procesos más complejos que dan lugar a las variaciones del runup están relacionados con las condiciones morfodinámicas de la playa. Tal complejidad hace que sea difícil establecer una fórmula empírica de runup que sea válida para todos tipos de playas. Esta problemática fue discutida por Gomes da Silva et al. (2016), que han identificado debilidades en las formulaciones recientes para distinguir el runup en distintos tipos de playas. Estos hechos han traído a la luz una serie de preguntas de investigación:

¿Cuál es la capacidad de predicción de la fórmulas empíricas para el cálculo del runup en los diferentes tipos de playa?

¿Qué informaciones específicas del sitio de estudio deben ser incluidas en las fórmulas de runup?

¿Cómo se puede mejorar las predicciones del runup de bajas y altas frecuencias al tener en cuenta información de la morfodinámica de la playa?

¿Es posible establecer una única fórmula que cumpla con el cálculo del runup en condiciones morfodinámicas distintas?

En base a la importancia del cálculo del runup en estudios costeros y gestión de la costa, se ha desarrollado esta tesis con el objetivo de contestar las cuestiones presentadas arriba. La idea es profundizar en los conocimientos de los procesos del runup y proponer fórmulas empíricas que mejoren las predicciones de dicha variable en playas de los más diversos estados morfodinámicos.

0.1.1. Estado del Arte

Uno de los primeros trabajos presentados en el sentido de proponer un modelo empírico para el cálculo de runup fue presentado por Hunt (1959). Basándose en experimentos de laboratorio con ondas monocromáticas actuando sobre estructuras, el autor probó una serie de parámetros de ondas y de la geometría de la estructura, y observó que el runup normalizado (R/H) está relacionado con el

parámetro de Iribarren - $\xi = \tan\beta/\sqrt{H/L}$ (Battjes, 1975; Iribarren, 1949) como presentado en la ec. 1:

$$\frac{R}{H} = K\xi \quad (1)$$

donde R es el runup, K es una constante, $\tan\beta$ es la pendiente de la playa y H y L son la altura y longitud de onda respectivamente.

Desde entonces, se ha dedicado mucho esfuerzo a demostrar que ξ podría ser utilizado también para describir el runup del oleaje irregular en playas naturales (Holman and Sallenger, 1985; Senechal et al., 2011; Vousdoukas et al., 2009). La correlación con ξ_0 (número de Iribarren calculado con los parámetros de oleaje en profundidades indefinidas) indica el efecto de los procesos que ocurren en la zona de rompientes sobre los valores del runup, ya que este mismo parámetro es utilizado para describir el tipo de rotura del oleaje, la cantidad de reflexión, el estado morfodinámico de la playa, entre otros procesos de oleaje (Battjes, 1975).

Siguiendo lo presentado en los trabajos anteriores, Stockdon et al. (2006) (a partir de ahora S2006) combinaron datos medidos en 10 experimentos de campo, y obtuvieron la formulación empírica de runup más extensiva presentada hasta el momento (ec. 2 to ec. 5). Dichos autores propusieron un modelo empírico del runup, en el cual el setup ($\langle \eta \rangle$), el swash infragravitatorio (S_{ig}) y el incidente (S_{inc}) son calculados separadamente. Los tres valores fueron relacionados con el parámetro $\tan\beta(H_0L_0)^{0.5}$:

$$R_2 = 1.1 \left(\langle \eta \rangle + \frac{\sqrt{S_{inc}^2 + S_{ig}^2}}{2} \right) \quad (2)$$

$$\langle \eta \rangle = 0.35(H_0L_0)^{0.5}\tan\beta \quad (3)$$

$$S_{inc} = 0.75(H_0L_0)^{0.5}\tan\beta \quad (4)$$

$$S_{ig} = 0.06(H_0L_0)^{0.5} \quad (5)$$

De acuerdo a S2006, la componente vertical del swash infragravitatorio está relacionada al parámetro $(H_0L_0)^{0.5}$ y es independiente de la pendiente de la playa. Sin embargo, la aplicación de la ec. 5 resultaría en valores de swash infragravitatorio semejantes en playas compuestas por gravas y playas con sedimento muy fino. Tal equivalencia entre diferentes tipos de playa no refleja la realidad del proceso del swash. Para un determinado estado de mar, playas de sedimento fino tienden a presentar condiciones más disipativas; la disipación por rotura es más significativa y se espera una gran cantidad de energía infragravitatoria en la línea de costa (Wright and Short, 1984).

Ruggiero et al. (2001) (a partir de ahora R2001), por otra parte, propone que el runup de bajas frecuencias puede ser descrito en diferentes tipos de playas a través de una relación en la que se incluye la pendiente de la zona de ascenso y descenso:

$$R_2 = 0.27(\tan\beta H_0L_0)^{0.5} \quad (6)$$

Cuando el peralte del oleaje es pequeño, las olas alcanzan la playa sin que ocurra la disipación de la energía por rotura. Siendo este el caso, las olas son totalmente o parcialmente reflejadas en la línea de costa, y el runup va a depender de la cantidad de energía reflejada. En casos de fuerte reflexión, se puede observar la amplificación de los valores de swash debido a la presencia de una onda estacionaria perpendicular a la playa (Méhauté et al., 1968). En estos casos, el runup puede ser relacionado a la altura de la onda estacionaria (H_{oe}) en la costa: $R = H_{oe} = H(\pi/2\tan\beta)^{0.5}$.

Guza et al. (1984) observaron que el swash de ondas monocromáticas responde a tres regímenes: i) reflexión completa; ii) saturación y iii) una condición transitoria entre las otras dos. Los resultados indicaron que el swash relativo S/H en cada uno de los regímenes puede ser descrito por la siguientes relaciones:

$$\frac{S}{H} = \begin{cases} 3\xi_0^2/\pi & \text{if } \xi_0 < \xi_c \text{ (regimen de saturación)} \\ (2\pi\beta)^{-1/4}\xi_0 & \text{if } \xi_c/3 < \xi_0 < \xi_c \text{ (regimen de transición)} \\ (\pi/2\tan\beta)^{1/2} & \text{if } \xi_c < \xi_0 \text{ (regimen reflejante)} \end{cases} \quad (7)$$

donde $\xi_c = \left| \frac{\pi^3}{2\tan\beta} \right|^{1/4}$. La necesidad de diferentes expresiones, evidencia el problema de generar una única fórmula para calcular el swash en playas con diferentes condiciones morfodinámicas.

0.1.2. Objetivos de la tesis

El objetivo general de esta tesis es ampliar los conocimientos acerca de los procesos en la zona de ascenso y descenso y mejorar los modelos empíricos de swash teniendo en cuenta las condiciones morfodinámicas de la playas. Para alcanzar dicho objetivo, se establecieron las siguientes tareas:

1. Analizar los procesos del oleaje y del swash en la playa de Somo, con base en mediciones de campo.
2. Analizar el papel de la forma del perfil y de las condiciones morfodinámicas de las playa en los valores del swash infragravitatorio.
3. Evaluar el efecto del estado morfodinámico de la playa y de la cantidad de energía reflejada en el swash incidente.
4. Verificar la mejora en el cálculo del runup al utilizar las formulaciones propuestas en este trabajo.

0.2. Experimentos de campo

Para alcanzar los objetivos propuestos en esta tesis, se han realizado dos campañas de campo en la playa de Somo, costa norte de España. Los experimentos son

parte del proyecto MUSCLE-Beach y se han llevado a cabo en mayo de 2016 y en septiembre de 2017. A continuación se presenta una breve descripción de las campañas de campo.

Experimento MUSCLE-Beach 2016

La primera campaña se ha realizado el 04 de mayo de 2016 con el objetivo de verificar los procesos relacionados al swash en perfiles con diferentes estados morfodinámicos. De esta forma, se han medido datos de oleaje, corrientes, runup, topografía, batimetría y granulometría en tres perfiles de playa (llamados P1, P2 y P3). También se midieron datos de oleaje en un punto a 25 m de profundidad, en medio a la ensenada del Sardinero. La Figura 2 presenta la ubicación de las mediciones en el area de estudio.

Los datos de sedimento y oleaje fueron utilizados para clasificar los perfiles según su estado morfodinámico. Se observó que la condición morfodinámica de los perfiles está condicionada por los estados de mar en los días que antecedieron a la campaña; y la mejor clasificación, de acuerdo al estado verificado in situ, se obtuvo utilizando el parámetro adimensional de velocidad de caída del grano, teniendo en cuenta las condiciones previas del estado de mar (Ω^*) (Wright et al., 1985) como presentado en la ec. 8. Los resultados indicaron condición reflejante en el perfil P1, mientras los perfiles P2 y P3 fueron clasificados como intermedios del tipo "terrazza de bajamar".

$$\Omega^* = \left[\sum_{n=1}^D D^{-i/\phi} \right]^{-1} \sum_{n=1}^D \Omega 10^{-i/\phi} \quad (8)$$

donde $i = 1$ en el día del experimento e $i = D$ en D días anterior a las mediciones. ϕ es la tasa de decaimiento en días de tal manera que el factor peso alcanza 10% después de ϕ días.

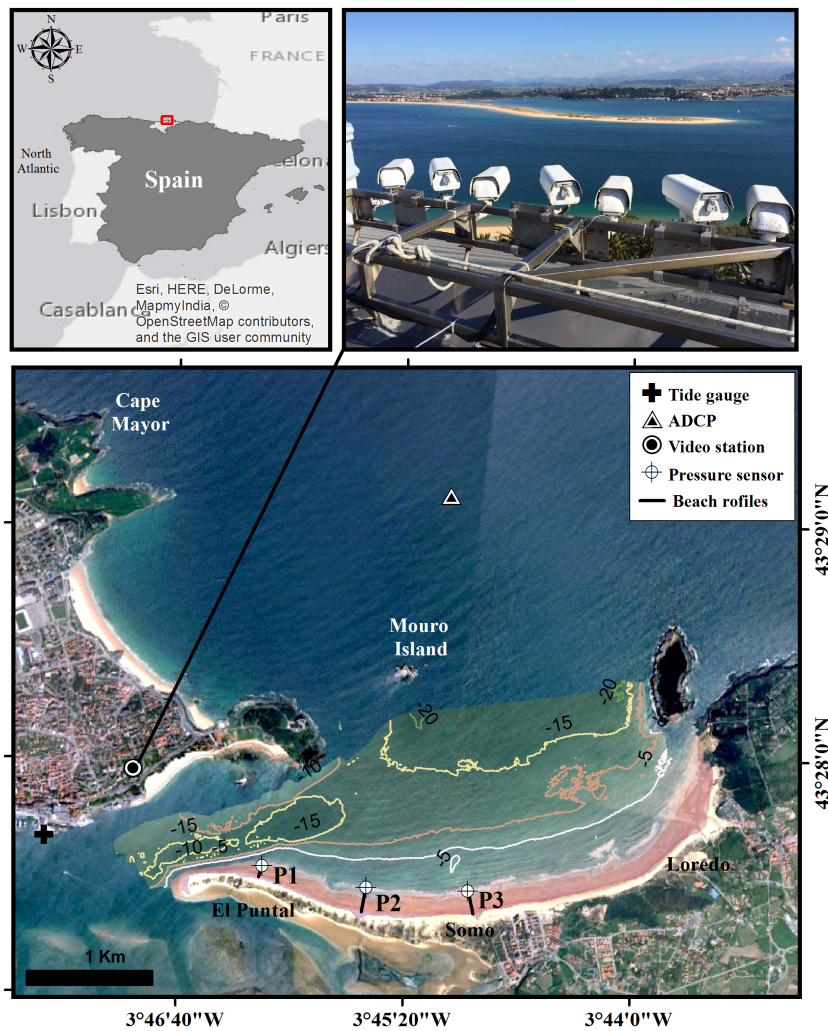


Figure 2: Ubicación del experimento y de las mediciones. En el detalle, la vista desde la estación de video cámaras.

Experimento MUSCLE-Beach 2017

El segundo experimento se realizó en los días 19 y 21 de Septiembre de 2017. Esta vez, el objetivo fue analizar la transformación del oleaje a lo largo de la zona de rompientes. 7 sensores de presión y 2 ADV fueron instalados a lo largo del perfil P2 en los dos días de campaña. La topografía, granulometría y el runup fueron medidos como en la primera campaña de campo, y un equipo ADCP fue instalado en la misma posición (a 25 m de profundidad).

En este experimento se observaron condiciones más reflejantes, aunque la clasificación de acuerdo al parámetro Ω^* indicó condiciones de terraza de bajamar, misma

condición verificada en P2 durante el primer experimento. Al observar la evolución del oleaje a lo largo del perfil de la playa en el 21 de septiembre, se verificó la posible presencia de una onda estacionaria perpendicular a la costa.

0.3. Análisis y estimación del swash infragravitatorio

Como ya se ha mencionado anteriormente, según Stockdon et al. (2006) (S2006), la componente vertical del swash infragravitatorio (S_{ig}) puede ser explicada por el parámetro $(H_0L_0)^{0.5}$, sin tener en cuenta la morfología de la playa. Sin embargo, el uso de dicho parámetro no permite diferenciar el swash infragravitatorio en playas con condiciones morfodinámicas distintas. Ruggiero et al. (2001) (R2001), por otro lado, demostró que el runup de bajas frecuencias puede ser representado a través de la relación $R_{ig} \propto (\tan\beta H_0L_0)^{0.5}$. En este apartado, se presentan los análisis realizados con respecto al swash infragravitatorio, teniendo como base los trabajos de S2006 y R2001.

0.3.1. Metodología

Los datos medidos en la playa de Somo, y los obtenidos a través de la recopilación de estudios anteriores (8 experimentos), fueron utilizados en los análisis del swash de bajas frecuencias. El análisis se realizó de acuerdo a los siguientes pasos:

- i) Los datos medidos en la playa de Somo fueron analizados con el objetivo de comprender los procesos del oleaje que influyen en los valores del swash infragravitatorio;
- ii) Se verificó la capacidad de predicción de las formulaciones propuestas por S2006 y R2001, comparando datos medidos y calculados;
- iii) Un conjunto de parámetros fue seleccionado y su relación con el swash infragravitatorio fue verificada;

- iv) En base a los análisis anteriores, se desarrolló una nueva formulación empírica para el cálculo del swash infragravitatorio;
- v) Los resultados de la nueva fórmula fueron comparados con los ajustes obtenidos utilizando las formulaciones propuestas en estudios anteriores.

0.3.2. Resultados

Cálculo del swash infragravitatorio utilizando R2001 y S2006

La capacidad de predicción de las fórmulas propuestas por R2001 y S2006 fue evaluada a través de parámetros estadísticos obtenidos de la correlación entre datos medidos y simulados. El modelo R2001 mostró mejor correlación, con un coeficiente de correlación ρ^2 de 0.73 frente a 0.68 resultante del modelo de S2006. En contraste, el cálculo de S_{ig} utilizando S2006 resultó en un RMSE ligeramente menor. Eso indica que R2001 describe mejor la tendencia de los datos, pero con mayor dispersión. En general, altos valores de ρ^2 y bajos RMSE indicaron un buen ajuste de ambos modelos a los datos medidos.

Modelo empírico de swash infragravitatorio

Se analizó una serie de parámetros relacionados a la morfología y a la dinámica de la playa, con vistas a verificar su relación con el swash infragravitatorio. La mejor relación se obtuvo con el parámetro propuesto por R2001 ($\rho^2 = 0.71$), seguido por el parámetro propuesto por S2006 ($\rho^2 = 0.67$). Se verificó un patrón interesante al relacionar S_{ig} con el parámetro $(H_0L_0/\tan\beta)^{0.5}$. Los resultados de dicha relación indicaron tres grupos de playas que presentan comportamiento diferente con respecto al swash infragravitatorio. Las playas de cada grupo presentaron las mismas características morfodinámicas con tamaños semejantes de sedimento.

El parámetro $(H_0L_0/\tan\beta)^{0.5}$ corresponde a la componente horizontal del swash infragravitatorio si se utiliza el modelo de R2001 (*i.e.* $S_{igH} = S_{ig}/\tan\beta$). Así, se

analizó la relación entre el parámetro citado y el swash horizontal de la siguiente forma:

$$S_{igH} = K \left(\frac{H_0 L_o}{\tan \beta} \right)^{0.5} \quad (9)$$

donde K es la pendiente de la regresión. La regresión lineal verificada con la ec. 9 resultó en un coeficiente de correlación ρ^2 igual a 0.79, lo que supone una mejora de 12% y 8% comparado a S2006 y R2001 respectivamente. El mejor ajuste se obtuvo con $K = 0.26$. El ajuste en función del parámetro $\tan \beta^{-0.5}$ puede estar relacionado al comportamiento de ondas estacionarias en la costa. Cuando el peralte de la onda es pequeño, como es el caso del peralte de ondas largas, la onda es reflejada en la costa y el swash puede ser relacionado con la altura de la onda estacionaria. Dicha altura, a su vez, es función de $\tan \beta^{-0.5}$.

La mejora en las predicciones al utilizarse la componente horizontal del swash en lugar de la componente vertical, puede estar relacionada con la representación del swash en playas de pendiente muy suave. En condiciones muy disipativas, debido a perfiles muy tendidos, la excursión vertical del swash es mínima, mientras que la variación horizontal (inundación) es bastante importante. Parece intuitivo entonces, utilizar el swash horizontal en lugar de su componente vertical.

El papel del estado morfodinámico

Los ajustes observados con la ec.9 todavía mostraron alguna discrepancia entre playas con diferentes estados morfodinámicos. Los valores del swash infragravitatorio para playas disipativas quedaron ligeramente arriba de la línea de ajuste, indicando sobrestimación en los valores calculados. En este punto, se planteó la hipótesis de que la pendiente K de la ecuación no sería constante, sino una función del estado morfodinámico del perfil. Los valores de K fueron entonces relacionados con el Ω^* de cada experimento. Los resultados indicaron una correlación significativa entre K y Ω^* ($\rho^2 = 0.48$). Con esto se obtuvo el modelo empírico del

swash infragravitatorio, teniendo en cuenta la pendiente de la playa y el estado morfodinámico:

$$S_{igH} = (0.19 + 0.008\Omega^*) \left(\frac{H_0 L_o}{\tan\beta} \right)^{0.5} \quad (10)$$

Evaluación de la nueva fórmula

La correlación entre los valores medidos de swash infragravitatorio y aquellos calculados utilizando las fórmulas presentadas en las ec. 9 y ec. 10 fue verificada. Un análisis general de todos los datos demostró un buen ajuste entre datos medidos y simulados (Figura 3).

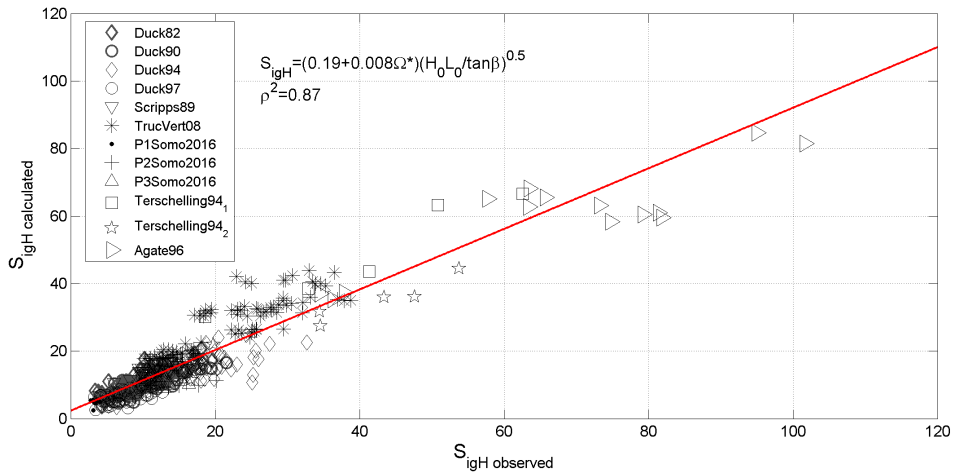


Figure 3: Regresión lineal entre el S_{igH} medido y los valores calculados con el modelo empírico utilizando $K = f(\Omega^*)$.

El cálculo del swash infragravitatorio utilizando la ec. 10 ($K = f(\Omega^*)$) resultó en una mejora en la predicción, comparado con el calculado utilizando la ec. 9 ($K = cte$), con ρ^2 igual a 0.87.

De cara a verificar el desempeño de las ecuaciones propuestas en este trabajo cuando son aplicadas a playas con diferentes condiciones morfodinámicas, se analizó la correlación entre datos medidos y simulados para cada tipo de playa. Los resultados fueron comparados con aquellos obtenidos utilizando R2001 y S2006.

Una vez que solo P1 fue clasificado como reflejante, los análisis se limitaron a playas intermedias y disipativas.

Los resultados obtenidos con las ecuaciones 8 y 9 mostraron mejor correlación (mayor ρ^2) con los datos medidos, si los comparamos con los valores obtenidos con R2001 y S2006. La diferencia más significativa fue observada en las predicciones para playas disipativas, para las cuales los valores de ρ^2 aumentaron de 0.77 y 0.55 utilizando R2001 y S2006, a 0.91 y 0.92 utilizando las ec. 9 y 10. Las diferencias en los valores de ρ^2 observadas entre la utilización de R2001 y la ec. 9 (versión horizontal de R2001) para los dos tipos de playas, indica la importancia de utilizar la componente horizontal del swash en lugar de la componente vertical.

0.4. Análisis y estimación del swash incidente

Una vez que se ha determinado la fórmula para el cálculo del swash de bajas frecuencias S_{ig} ($f < 0.05Hz$), el siguiente paso es el análisis del swash incidente S_{inc} ($f > 0.05Hz$). Dicho análisis se realizó en base a dos aproximaciones distintas. En un primer momento, se utilizaron los datos medidos en la playa de Somo para evaluar la importancia del coeficiente de reflexión en los valores de swash de altas frecuencias. Luego, se tomó la formulación presentada por Guza et al. (1984) (a partir de ahora G1984) como base para establecer la nueva fórmula de cálculo del swash incidente.

0.4.1. Metodología

Cálculo del swash incidente utilizando S2006 y G1984

Antes de presentar el desarrollo de la nueva fórmula de cálculo del swash incidente, se analizó la capacidad de predicción del mismo por parte de los modelos empíricos presentados anteriormente por G1984 and S2006. Con este fin, se aplicaron las

fórmulas a los datos de este trabajo y se compararon los resultados con los datos medidos.

Reflexión del oleaje y el swsh incidente en la playa de Somo

El análisis de la relación entre el coeficiente de reflexión y los valores de S_{inc} se realizó en base a las siguientes etapas:

- i) El coeficiente de reflexión fue calculado en base a las series de superficie libre y se verificó su relación con diferentes parámetros ambientales.
- ii) Se analizó la relación entre el coeficiente de reflexión (medido y teórico) y el swash incidente relativo (S_{inc}/H_0).

Modelo empírico de swash incidente basado en la fórmula de G1984

Si analizamos la formulación propuesta por G1984 para el cálculo del swash de ondas monocromáticas, se verifica una única forma básica que puede ser aplicada a los regímenes de saturación, transición y reflexión a la vez:

$$\frac{S}{H} = a * \tan \beta^b \left(\frac{H}{L} \right)^c \quad (11)$$

donde a , b y c son coeficientes que cambian de acuerdo al régimen. El parámetro de Hunt, utilizado por S2006, también sigue la misma forma (con $b = 1$ y $c = -0.5$). Por tanto, en esta parte del trabajo, se ha establecido el modelo empírico de cálculo del swash con base en la relación presentada en la ec. 11. Los coeficientes de dicha formulación han sido ajustados de acuerdo al estado morfodinámico (disipativo, intermedio y reflejante) de la playa. La fórmula fue entonces evaluada y los resultados fueron comparados a los obtenidos con los modelos propuestos en trabajos anteriores.

0.4.2. Resultados

Cálculo del swash incidente utilizando S2006 y G1984

Se evaluó la predicción del swash incidente utilizando los modelos empíricos propuestos por S2006 y G1984. S2006 representó bien la tendencia de los datos medidos de swash incidente, con una correlación de $\rho^2 = 0.31$. Dicho modelo también demostró buena capacidad de predicción del swash en todas las condiciones morfodinámicas y, particularmente, en playas intermedias.

El modelo propuesto por G1984, a su vez, no mostró en buena correlación con los datos medidos, algo esperado teniendo en cuenta que dicho modelo ha sido establecido basándose en datos de oleaje monocromático. No obstante, los valores calculados para playas disipativas indicaron mejores resultados que los observados con el modelo de S2006. En condiciones disipativas, la rotura del oleaje es importante, resultando en la saturación del swash de bajas frecuencias. Por esta razón, aunque el modelo propuesto por G1984 haya sido establecido en base a datos de oleaje monocromático, la fórmula propuesta por los autores para describir el régimen de saturación (régimen en el que están incluidos los datos de playas disipativas) predice mejor los valores de swash incidente en este tipo de playas.

Reflexión del oleaje y el swash incidente en la playa de Somo

El análisis del coeficiente de reflexión medido en la playa de Somo indicó mayor cantidad de energía reflejada durante el segundo día de la segunda campaña de campo (MUSCLE-Beach 2017), mismo día en el que se verificó una posible estructura estacionaria perpendicular a la playa. El K_r^2 observado el 21 de septiembre fue de 0.25, mientras en los demás días los valores no pasaron de 0.1.

Se verificó una relación entre los valores del coeficiente de reflexión y el swash incidente relativo S_{inc}/H_0 . Lo mismo se verificó al utilizar el coeficiente de reflexión teórico M . La aplicación de dicha relación a los datos de las demás playas, sin embargo, no resultó en mejoras en las predicciones del swash incidente, si se compara

con los resultados obtenidos con el modelo de S2006. Una limitación evidente en esta aproximación es la necesidad de utilizarse coeficientes de reflexión teóricos, un tema bastante limitado en la literatura actual.

Modelo empírico de swash incidente con base en la fórmula de G1984

El análisis basado en la segunda aproximación propuesta se hizo utilizando la fórmula básica verificada en las expresiones presentadas por G1984. Los coeficientes de la ecuación fueron ajustados para cada estado morfodinámico de playas: reflejantes ($\Omega^* \leq 1.5$), intermedias ($1.5 < \Omega^* \leq 5.5$) y disipativas ($\Omega^* > 5.5$). La fórmula y los coeficientes resultantes están presentados en la ec. 12.

$$\frac{S_{inc}}{H_0} = a \cdot \tan \beta^b \left(\frac{H_0}{L_0} \right)^c \begin{cases} a = 2.83; b = 2.12; c = -0.82 \text{ (disipativas: } \Omega^* > 5.5) \\ a = 0.15; b = 0.56; c = -0.64 \text{ (intermedias: } 1.5 < \Omega^* \leq 5.5) \\ a = 0.50; b = -0.37; c = -0.15 \text{ (reflejantes: } \Omega^* \leq 1.5) \end{cases} \quad (12)$$

La Figura 4 presenta el ajuste entre datos medidos y los valores calculados con la formulación propuesta aquí para cada estado morfodinámico y para todos los datos (uniendo los resultados de las tres ecuaciones - ajuste final). La correlación entre el S_{inc} y los parámetros propuestos fue alta para todos los estados morfodinámicos ($\rho^2 > 0.42$), especialmente para los datos de playas intermedias y disipativas ($\rho^2 = 0.71$ and $\rho^2 = 0.70$). El ajuste final entre datos medidos y calculados resultó en ρ^2 igual a 0.56, lo que demuestra una mejora de 25% en comparación a la estimación obtenida del modelo de S2006 ($\rho^2 = 0.31$).

Los coeficientes b y c , resultantes del ajuste para playas disipativas y reflejantes, son bastante semejantes a los valores propuestos por G1984 para caracterizar el swash en los regímenes de saturación ($b = 2$ and $c = -1$) y reflectivo ($b = -0.5$ and $c = 0$), aunque de los datos utilizados, ninguno ha sido clasificado en regimen

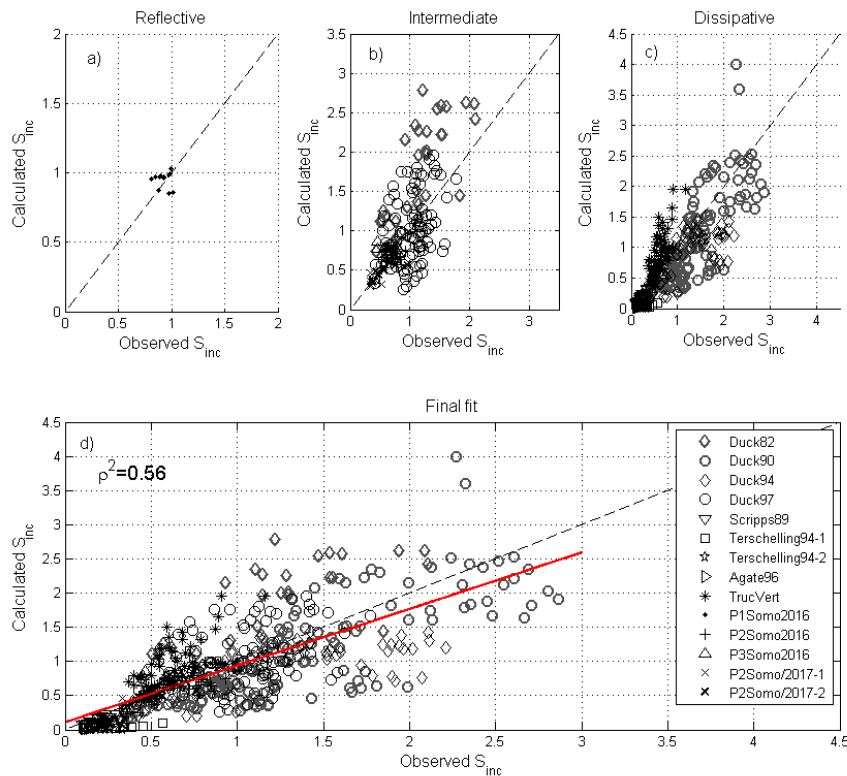


Figure 4: Dispersión entre datos medidos y calculados para cada estado morfodinámico (arriba) y ajuste final de los datos (abajo) utilizando la ec. 12. La línea diagonal representa la bisectriz sobre la cual los valores están perfectamente correlacionados.

reflejante (de acuerdo a la clasificación de G1984). Estos resultados indican que las fórmulas para cálculo del swash de olas monocromáticas en régimen reflejante y de saturación pueden ser extendidas y aplicadas al swash de oleaje irregular en playas reflejantes y disipativas. Sin embargo, los límites propuestos por G1984 para clasificar los tres regímenes no se aplican para diferenciar los datos procedentes de los tres estados morfodinámicos analizados aquí.

La solución propuesta en este trabajo, con base en la formulación de Guza et al. (1984), mostró ser una solución plausible para representar el swash en diferentes tipos de playa. El exponente del término de la pendiente del perfil y del peralte de las olas en las fórmulas propuestas varían de acuerdo al estado de la playa. Así, se concluye que una única fórmula basada en ξ_0 no sería capaz de captar las diferencias en el swash incidente en condiciones morfodinámicas distintas.

0.5. Aplicación de las fórmulas de swash en el cálculo del runup

Una vez que se han establecidos los modelos empíricos de swash infragravitatorio e incidente, el último paso fue verificar el impacto que tiene el uso de las nuevas fórmulas en el cálculo del runup. Este ítem es dedicado a i) demostrar el efecto de las nuevas fórmulas en los valores calculados de runup y ii) verificar el desempeño de dichas fórmulas para el cálculo del runup cuando se aplica a otras playas.

0.5.1. Methods

Evaluación del cálculo del runup R_2

Para analizar el efecto de aplicarse la formulación de S_{inc} y S_{ig} en el cálculo del runup se utilizó la estructura de la fórmula de S2006 (ec. 2). La fórmula final del runup incluyendo los nuevos parámetros es:

$$R_2 = 1.1 \left(0.35 \tan\beta (H_0 L_0)^{0.5} + \frac{\sqrt{\left[(0.19 + 0.008\Omega^*) \left(\frac{H_0 L_0}{\tan\beta} \right)^{0.5} \tan\beta \right]^2 + \left[a * \tan\beta^b H_0 \left(\frac{H_0}{L_0} \right)^c \right]^2}}{2} \right) \quad (13)$$

Aplicación a las playas de la ensenada de Itapocorói, Brasil

Para verificar la validez de las predicciones del runup en otras playas, se utilizaron los datos del experimento de campo realizado en las playas de Itajuba, Piçarras y Alegre (Vieira da Silva et al., 2017), localizadas en la ensenada de Itapocorói, costa sur de Brasil. Los datos de dicho experimento han sido medidos cada dos días a lo largo de una campaña que ha durado 1 mes. Específicamente se utilizaron los datos de batimetría, oleaje medidos por ADCPs, runup máximo medido con

GPS y tamaño de sedimento en 8 perfiles (P01, P03, P05, P07, P25, P40, P47 y P50) a lo largo de las playas.

0.5.2. Resultados

Evaluación del cálculo del runup R_2

Los valores del runup calculados con las fórmulas presentadas en este trabajo mostraron buen ajuste a los datos medidos en campo. La comparación de la correlación entre datos medidos y calculados demostró mejoras en el cálculo del runup respecto a los valores obtenidos con las fórmulas de S2006, y se comprueba una mejora en los valores más altos valores que eran subestimados por la formulación anterior.

A pesar de los resultados positivos obtenidos con la nueva formulación, la dispersión entre datos medidos y simulados todavía es significativa, especialmente para playas disipativas. No obstante, parte del error en dichas playas puede estar asociado al cálculo del setup, variable no abordada en el presente estudio.

Aplicación a las playas de la ensenada de Itapocorói, Brasil

De los datos medidos en las playas de la ensenada de Itapocorói, se observaron condiciones intermedias y reflejantes. El cálculo del runup en ambos estados morfodinámicos demostró mejora con respecto a las predicciones utilizando fórmulas anteriores. Se observó una reducción en el error en las predicciones de hasta 1.2 m al comparar los resultados utilizando las fórmulas de este trabajo con los valores obtenidos con las fórmulas propuestas por S2006. La parametrización propuesta resultó en una reducción de la dispersión entre datos medidos y simulados, corrigiendo sobrestimaciones particularmente importantes en los datos de condiciones reflejantes.

0.6. Conclusiones

0.6.1. Principales conclusiones en el análisis de las mediciones de oleaje, morfología y runup

Se han realizado dos campañas de campo en la playa de Somo, en el norte de España. El primer experimento (MUSCLE-Beach 2016) estuvo enfocado a determinar las características del swash y de la playa en perfiles con condiciones morfodinámicas distintas. Los resultados de este primer experimento indicaron características diferentes del swash en cada uno de los perfiles medidos. Se destacó el efecto del estado de mar en los días previos a la fecha del experimento en el estado morfodinámico actual de la playa.

El segundo experimento (MUSCLE-Beach 2017) se realizó con el objetivo de comprender la evolución del oleaje en la zona de rompientes, hasta llegar a la zona de ascenso y descenso. Se verificó una estructura nodal con frecuencia incidente, típica de ondas parcialmente estacionarias, lo que resaltó la importancia del proceso de reflexión en la estimación del swash en la playa.

0.6.2. Principales conclusiones en el análisis y estimación del swash infragravitatorio

En este capítulo se analizó el papel del estado morfodinámico de la playa en las oscilaciones de bajas frecuencias. La ausencia de parámetros indicativos de la morfología de la playa fue señalada como la principal limitación en las formulas propuestas anteriormente.

Se propuso un nuevo parámetro en el que se incluyó la pendiente de la playa $[(H_0 L_0 / \tan \beta)^{0.5}]$. La mejora en las predicciones del swash infragravitatorio al incluir dicho parámetro indica que hay una relación entre S_{ig} y la pendiente de la playa. No obstante, se trata de una relación lineal y por ese motivo no se verificó una correlación con $\tan \beta$ en los estudios anteriores. La correlación con $\tan \beta^{-0.5}$

puede estar relacionada al comportamiento reflejante de las ondas largas, que resultan en una estructura estacionaria normal a la playa. La componente horizontal del swash mostró estar relacionada con el parámetro propuesto, y la pendiente del ajuste es una función del parámetro adimensional de caída del sedimento, que representa el estado morfodinámico de la playa.

Finalmente, se han propuesto dos fórmulas para el cálculo del swash infragravitatorio en playas. La decisión de utilizar una u otra, deberá basarse en los datos disponibles.

0.6.3. Principales conclusiones en el análisis y estimación del swash incidente

En este capítulo se analizó el papel de la cantidad de energía reflejada en la playa en los valores del swash de altas frecuencias. Los análisis se llevaron a cabo en dos aproximaciones distintas. Primero se verificó la relación entre el coeficiente de reflexión y el swash incidente relativo (S_{inc}/H). Luego, utilizando como base el modelo propuesto por G1984, se ha propuesto una nueva fórmula para el cálculo del swash incidente.

Los análisis iniciales sobre los datos medidos en la playa de Somo confirmaron la presencia de la onda estacionaria durante el experimento. Se verificó una relación entre el S_{inc}/H_0 y el coeficiente de reflexión. No obstante, establecer una parameterización con el coeficiente de reflexión requiere el uso de coeficientes teóricos, un tema poco desarrollado en la literatura actual.

Con base en el trabajo de G1984, se propuso una fórmula general para describir el swash incidente en playas. La principal diferencia entre dicha fórmula y las presentadas anteriormente es el exponente del término de la pendiente y del peralte de la ola. Partimos de la hipótesis de que los coeficientes (exponentes) cambian de acuerdo al estado morfodinámico de la playa. En base a esto, se establecieron tres fórmulas para el cálculo del swash incidente en playas reflejantes, intermedias y disipativas.

0.6.4. Principales conclusiones en la aplicación de las fórmulas de swash en el cálculo del runup

Al utilizarse las fórmulas del swash incidente e infragravitatorio en las predicciones del runup se obtuvo una buena relación entre datos medidos y calculados en todas las condiciones morfodinámicas. Las contribuciones más relevantes se verificaron para las playas intermedias y disipativas. Mejoras en el cálculo del runup en playas disipativas son de especial interés, dado que gran parte de los eventos extremos de temporal son caracterizados como disipativos.

Los resultados del cálculo del runup para las playas de Brasil comprobaron la validez de las ecuaciones propuestas aquí para playas intermedias y reflejantes.

Chapter 1

Introduction

1.1. Motivation: the importance of the wave runup on coastal studies

Over the past few decades, the coasts around the world have become a subject of special interest to the scientific and engineering community. The impacts of the marine dynamics on the coastal population, coastal structures and coastal resources are issues of concern and have received particular attention. Flooding and erosion risk analysis are, now, basic elements of any coastal management strategy. All those themes have been topic of recent coastal studies. Among the fundamental elements used in the studies cited here, the wave runup is one of the most critical.

The wave runup (R), or simply runup, is defined as the vertical oscillation of the coast line over the foreshore. As waves approach the coast, part of the energy dissipates by breaking in the surf zone. The remaining energy reaches the beach and result in runup oscillations. In practical terms, the wave runup is composed of a (quasi) steady superelevation of the mean water level (setup - $\langle \eta \rangle$), and by time-varying fluctuations around this superelevation (swash- S) (Guza and Thornton, 1982; Miche, 1951) (Figure 1.1). Different processes trigger high and low frequency swash oscillations and, because of that, the swash is commonly in

terms of incident (S_{inc} : 0.05 to 0.5 Hz) and infragravity (S_{ig} : 0.003 to 0.05 Hz) frequencies, separately.

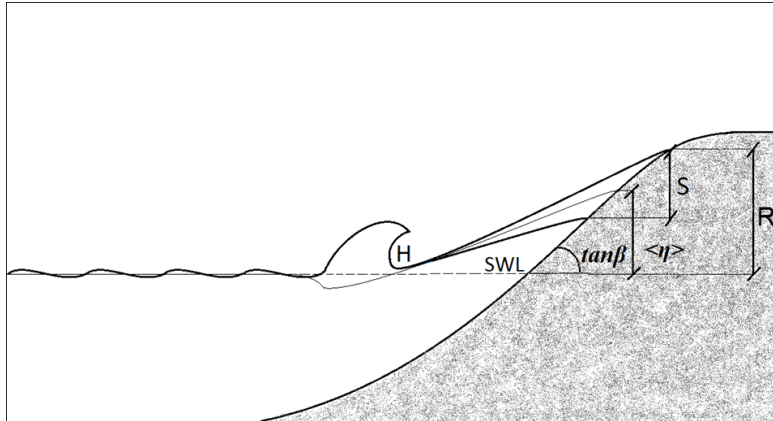


Figure 1.1: Runup components setup ($\langle \eta \rangle$), swash (S) and important parameters wave height (H), beach slope ($\tan\beta$) and still water level (SWL)

Runup oscillations are responsible for a considerable part of the sediment exchange between subaerial and submerged beach profile. (Masselink and Puleo, 2006). It plays also a significant role on coastal inundation and dune erosion, especially during extreme conditions when it can reach catastrophic values if summed to elevations induced by tides and surges (Figure 1.2) (Medina and Méndez, 2006; Sallenger, 2000). Based on that runup statistics are often used as criterion for coastal erosion and flooding risk analysis.

Due to the complexity of nearshore processes, most runup studies is based on empirical approaches (parameterizations) which directly relate the runup to the beach slope and offshore wave characteristics (e.g Ruessink et al., 1998; Senechal et al., 2011; Vousdoukas et al., 2009). However, there is still considerable debate about just how runup is related to these environmental parameters, as well as about the range of application of empirical models because of site-specific conditions and processes that may occur between the wave measurement point and the swash zone.

Many of the complex processes that lead to the swash zones oscillations are related to the morphodynamic conditions of the beach. For example, when a wave group reaches the coast, high frequency waves break in the surf zone and dissipate, while the infragravity wave is released. This mechanism of energy transfer from



Figure 1.2: Example of the effects of wave runup, tide and surge during extreme events. A) Niterói - Brazil; B) Haumoana - New Zealand and C) Santander - Spain. (Photos: Grasiela de Oliveira; Alan Blacklock and Eva Minguez)

incident to infragravity band is especially common on dissipative beaches and during storm conditions. The result is the dominance of infragravity swash on dissipative beaches, whereas incident and subharmonic swash tend to dominate the reflective ones (Wright and Short, 1984). Such complexity makes difficult to generate an empirical model valid for different beach types.

This issue is very relevant, for example, when analysing the flooding level in different coasts and beach types. A study was carried in Brazil, in which the variability of the three components of the flooding level (tide, surge and runup) along the coast of the whole country was analysed (Gomes da Silva et al., 2016). Among the three variables, they identified the runup calculated from empirical model as a possible source of error when assessing the flooding level in different beach types, since some site-specific conditions were not contemplated in runup estimations.

Those facts bring to light some research questions:

How well can we predict the runup values with empirical parameterizations in different beach types?

What site-specific information must be added to runup formulas to improve runup predictions?

How can we improve high and low frequency runup estimations by including morphodynamic information?

Is it possible to provide a parameterization that accomplish the runup estimation in all morphodynamic conditions?

Given the importance of the runup estimations in coastal studies, coastal management tasks and engineering practices, this thesis was developed aiming to answer the above cited questions. The objective was to go deeper on the knowledge of the runup process and to provide empirical parameterizations that improve the runup estimations in all morphodynamic conditions.

1.2. State of the Art

Many effort was made in the past to explain the surf and swash zone processes and their relation with the instantaneous and mean position of the coastline. The role of the wave energy, wave-wave interaction, tides and site-specific geomorphologic characteristics of the beach was deeply discussed. The most relevant findings

regarding empirical predictions of runup and swash values will be shown in this section, highlighting gaps that need to be further explored.

1.2.1. Empirical runup parameterizations

One of the earliest efforts to parametrize wave runup was presented by Hunt (1959). Based on laboratory experiments with monochromatic waves reaching structures, the author tested a number of composed parameters and demonstrated that the normalized runup value scales quite well with the surf similarity parameter (eq. 1.1), also known as Iribarren number ξ - eq. 1.2 (Battjes, 1975; Iribarren, 1949):

$$\frac{R}{H} = K\xi \quad (1.1)$$

$$\xi = \frac{\tan\beta}{\sqrt{\frac{H}{L}}} \quad (1.2)$$

where R is the runup value of each wave, K is a constant, $\tan\beta$, in this case, represents the slope of the structure and H and L are the wave height and length, respectively.

Since then, much effort has been dedicated attempting to demonstrate that ξ could also be used to describe the runup distribution of random waves in natural beaches (Holman and Sallenger, 1985; Senechal et al., 2011; Vousdoukas et al., 2009). Correlations found in previous works using ξ_0 (Iribarren number calculated using the deep-water wave height) may indicate the effect of surf zone processes and beach characteristics on runup values (Holman and Sallenger, 1985; Poate et al., 2016), since it is a parameter commonly used to describe and parameterize wave-breaking, the amount of reflection, and the beach morphodynamic state, among others processes. Miche (1951) suggested that in situations of high ξ_0 the dissipation due to wave-breaking is low and waves reflect on the coast, resulting in high swash amplitudes. When ξ_0 is low, wave-breaking leads to the dissipation of the wave energy

and saturation is expected on the shoreline. The saturation of the shoreline oscillations implies, then, that incident swash reaches a maximum while the infragravity swash keeps increasing according to the incident wave height (Guza and Thornton, 1982). Swash saturation is typically observed on beaches with dissipative characteristics, where wave breaking is an important dissipative process. Distinction on the swash behavior according to the morphodynamic characteristics was presented by Wright and Short (1984), who proposed a classification of the morphodynamic beach state based on the non-dimensional fall velocity parameter (eq. 1.3) (Dean, 1973; Gourlay and Meulen, 1968) and showed details about the amount of swash energy in each frequency band according to the beach state.

$$\Omega = \frac{H_s}{\omega_s T_p} \quad (1.3)$$

H_s is the significant wave height, T_p is the peak period and ω_s is the dimensional fall velocity parameter. As stated in that work, the swash zone of dissipative beaches ($\Omega > 5.5$, fine sediment, high wave energy and low-sloping foreshore) presents dominantly infragravity oscillations, while on reflective beaches ($\Omega < 1.5$, coarse sediment, low wave energy and steeper foreshore) high frequencies oscillations are dominant. Hughes et al. (2014) emphasized this difference in the amount of energy under different morphodynamic conditions through a conceptual model based on the evolutionary characteristics of the swash's spectral signature (Figure 1.3). The model shows that the ratio of swash energy in the high and low frequency bands differs significantly from dissipative to reflective conditions and that the shape of the swash spectrum evolves from the first beach state to the later (and the opposite), through intermediate beach states.

The different response of infragravity and incident oscillations during diverse morphodynamic conditions led some studies to differentiate the parameterizations for distinct morphodynamic states. Nielsen and Hanslow (1991) measured runup distribution in six Australian beaches with different morphodynamic characteristics. The runup was then contrasted with the Hunt scaling of $\tan\beta(H_0L_0)^{0.5}$ and

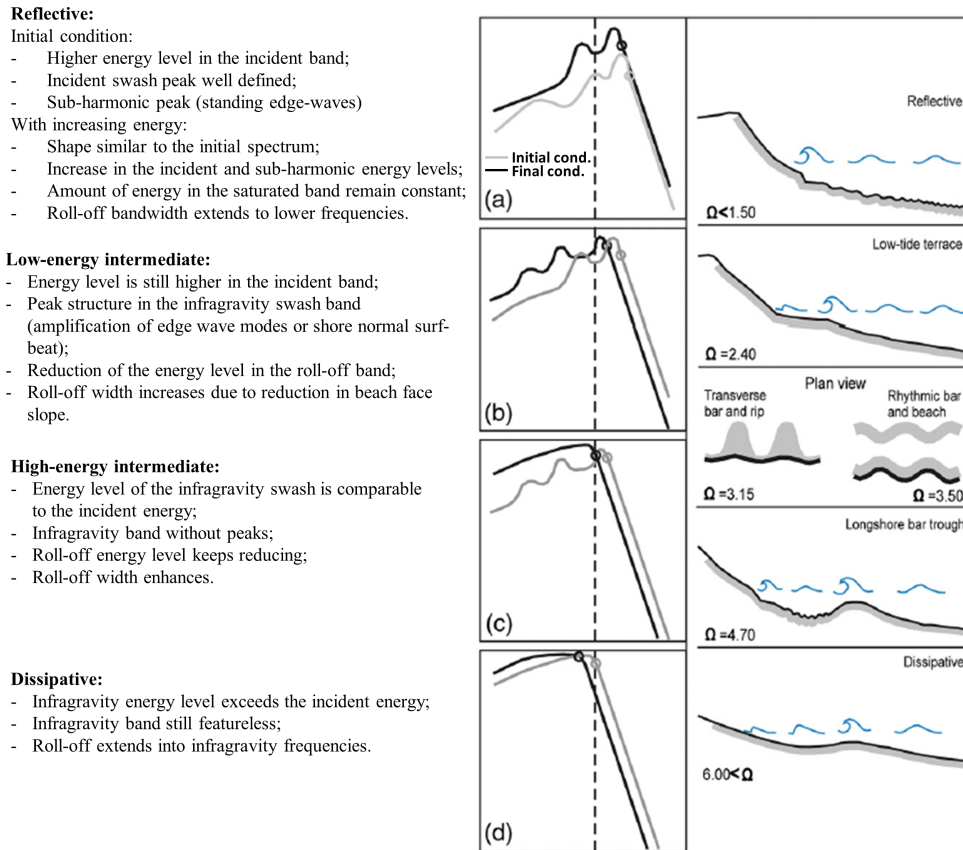


Figure 1.3: Spectral signature of swash according to the morphodynamic beach state. The dashed line represents the boundary between infragravity and incident frequencies (figure adapted from Hughes et al., 2012).

different empirical parameterizations of runup distribution were proposed depending on the foreshore slope (eq. 1.4 to eq. 1.6).

$$R_2 = SWL + 1.98L_{zwm} \quad (1.4)$$

where R_2 is the runup exceeded by 2% of the waves, SWL is the still water level and L_{zwm} is the vertical scale of the runup based on a Rayleigh distribution, given by:

$$L_{zwm} = 0.6(H_{0rms}L_0)^{0.5}\tan\beta \quad (1.5)$$

for $\tan\beta \geq 0.1$, and

$$L_{zwm} = 0.05(H_{0rms}L_0)^{0.5} \quad (1.6)$$

for $\tan\beta < 0.1$.

H_{0rms} is the root mean square wave height at 80 m depth and L_0 is the wave length at the same point. Note that, according to these formulas, low-sloping beaches ($\tan\beta < 0.1$) show no dependence on the foreshore slope. It is also suggested in their work that a distinction between the formulas for low-sloping and steeper beaches can still be made in terms of the non-dimensional fall velocity parameter (eq. 1.3). In this case, the steep behavior would be observed for $\Omega < 6$ and the flat behavior for $\Omega > 6$. The use of parameters like Ω had already been raised by Holman (1986) and Nielsen (1988) and it seems to provide a way to include the morphodynamic component in empirical runup equations.

Following the approach of previous works, Stockdon et al. (2006) (hereinafter S2006) combined information obtained during ten field experiments and constituted the most extensive analysis of wave runup until now (eq. 1.7 to eq. 1.10). The authors fitted the R_2 , obtained from the runup video series, to the beach slope and wave parameters deshoaled to a depth of 80 m. A runup equation was then proposed in which the setup ($\langle \eta \rangle$), infragravity (S_{ig}) and incident swash (S_{inc}) were all parametrized separately. The three values were related to the parameter $\tan\beta(H_0L_0)^{0.5}$. As stated by Nielsen and Hanslow (1991), the S_{ig} , usually dominant in low sloping beaches, showed no correlation with the foreshore slope (eq. 1.10).

$$R_2 = 1.1 \left(\langle \eta \rangle + \frac{\sqrt{S_{inc}^2 + S_{ig}^2}}{2} \right) \quad (1.7)$$

$$\langle \eta \rangle = 0.35(H_0L_0)^{0.5}\tan\beta \quad (1.8)$$

$$S_{inc} = 0.75(H_0L_0)^{0.5}\tan\beta \quad (1.9)$$

$$S_{ig} = 0.06(H_0L_0)^{0.5} \quad (1.10)$$

Aggregating each runup component formula to eq. 1.7, they reached the general formula (eq. 1.11):

$$R_2 = 1.1 \left(0.35(H_0L_0)^{0.5} \tan\beta + \frac{[H_0L_0(0.563 \tan\beta^2 + 0.004)]^{0.5}}{2} \right) \quad (1.11)$$

Numerous works have subsequently proven the validity of Stockdon et al. (2006) equation in the most diverse coasts (e.g Park and Cox, 2016; Ruju et al., 2014; Stockdon et al., 2014; Vousdoukas et al., 2009, 2012). However, despite its demonstrated skill in predicting runup on sandy beaches, S2006 can still present significant scatter (Guza and Feddersen, 2012) and improvements may be achieved by including, for example, the effect of very high-energy events or the influence of different sediment (Poate et al., 2016; Stockdon et al., 2014).

According to S2006, the vertical component of the infragravity swash is best parametrized by $(H_0L_0)^{0.5}$ and the authors defined it as being linearly independent of the beach slope (i.e. neither the foreshore nor the surf zone slope improved their fit). However, that relation means that beach profiles under the same wave conditions but with different morphologic characteristics will present the same infragravity swash (red circles in Figure 1.4). The application of eq. 1.10 would result, for example, in equal infragravity swash on beaches composed of gravel and on beaches with very fine sediment. Such equivalence between different beach types does not represent the reality of the swash process. For a given sea state, fine grain beaches tend to present higher dissipative conditions than gravel ones; the dissipation from wave-breaking is more significant and a larger amount of infragravity energy would be expected at the shoreline (Wright and Short, 1984).

The role of the beach slope in runup parameterizations was discussed by Ruessink et al. (1998), who analyzed the infragravity runup at Terschelling beach and found no correlation with the foreshore slope. Nevertheless, their result was influenced

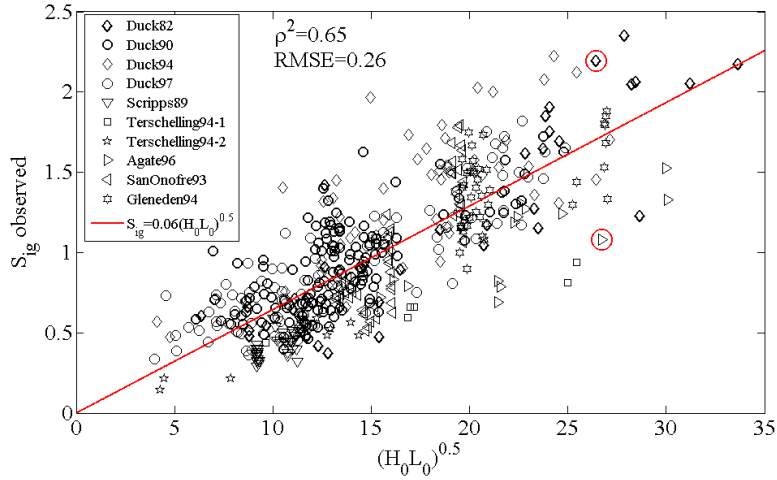


Figure 1.4: Linear regression between S_{ig} and S2006 parameter $(H_0 L_0)^{0.5}$. Symbols represent each experiment analysed by S2006. Red circles indicate an example of S_{ig} calculated under similar sea state in a dissipative (Agate) and a reflective (Duck) beach.

by the small range of $\tan\beta$ in their dataset. Ruggiero et al. (2001) analysed data from Oregon dissipative beaches and verified a direct relation between R_2 and H_s (eq. 1.12).

$$R_2 = 0.5H_0 - 0.22 \quad (1.12)$$

$$R_2 = 0.27(\tan\beta H_0 L_0)^{0.5} \quad (1.13)$$

In that work, the tendency observed for dissipative beaches seemed to be reasonable to explain also the dataset from the Duck reflective beach (North Carolina) (Figure 1.5 - left). However, an offset was verified between the data from these two dynamically different systems. Convergence was only possible, when they included the beach slope and wave length, as shown in eq. 1.13 (Figure 1.5 - right).

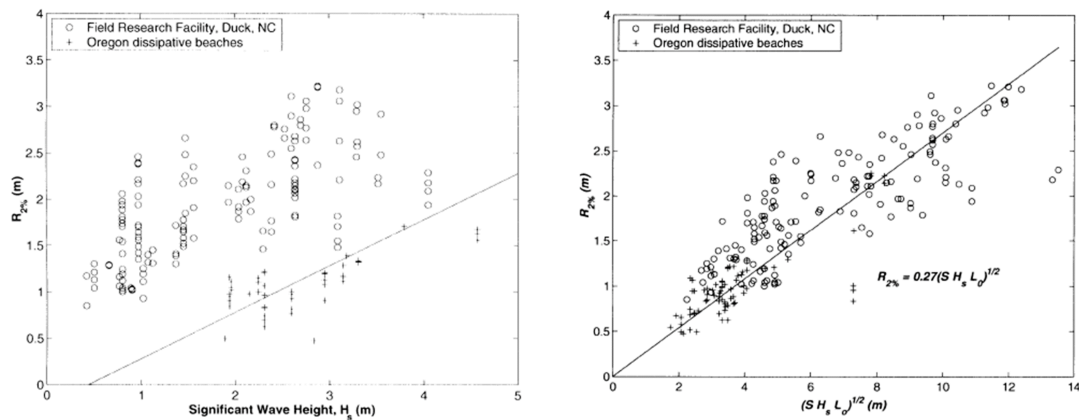


Figure 1.5: Regression fit between the R_2 and H (left) and between R_2 and the parameter including the beach slope (S) and L (right). (Adapted from Ruggiero et al, 2001)

1.2.2. Wave runup and wave reflection on the coast

If the wave steepness is low across the surf zone, the waves may reach the coast without dissipating all the energy by breaking. Long waves, steep slopes and small amplitudes can lead to such conditions. If this is the case, the waves are totally or partially reflected at the shoreline and the runup will depend on the amount of reflection at the coast. In cases of high wave reflection, an amplification of the swash values may be observed due to the presence of a standing wave (Méhauté et al., 1968).

Miche (1951) hypothesized that the amplitude of the swash of a monochromatic wave is proportional to the amount of reflection at the coast and, so, the runup is proportional to the standing wave amplitude. Besides, the author stated that the runup will increase according to wave height until a maximum value reached with H just high enough to break. Any additional energy will be dissipated by breaking, the swash will be saturated and no dependence on the wave height will be observed. The limit between both regimes (saturated and reflective) was given by the parameter M :

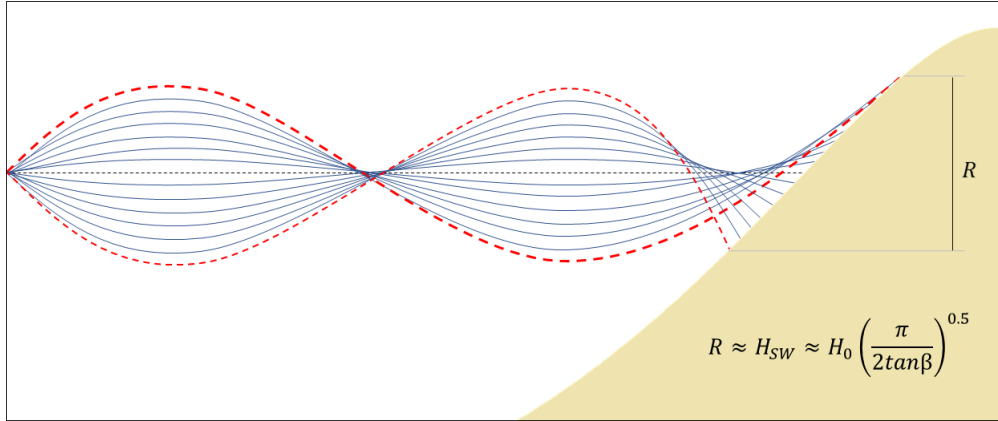


Figure 1.6: The wave runup as an approximation of the standing wave height at the shoreline.

$$M = \begin{cases} \frac{16g^2 \tan^5 \beta}{2\pi^5 H^2 f^4} & \text{if } M < 1 \text{ (reflection)} \\ 1 & \text{if } M \geq 1 \text{ (saturation)} \end{cases} \quad (1.14)$$

where g is the acceleration due to the gravity and f is the wave frequency.

Using monochromatic wave data, Guza and Bowen (1976) verified that for conditions in which the reflection coefficient (K_r^2) is higher than 0.3, the linear theory can be applied to describe the wave evolution across the surf zone. They related the wave runup to the height of the standing wave at the vicinity of the shoreline (H_{SW}) as shown in eq. 1.15 and Figure 1.6.

$$R = H_{SW} = H_0 \left(\frac{\pi}{2 \tan \beta} \right)^{1/2} \quad (1.15)$$

The same concept was applied by Muttray et al. (2006) when approaching the wave runup on sloping structures. Assuming the hypothesis that the wave runup and rundown on the breakwater slope can be interpreted as a slightly distorted anti-knot of the partial standing wave system. Thus, the runup height could be calculated from the standing wave height, as a function of the reflection coefficient (K_r^2) as:

$$R = aH_i + H_r = aH_i(1 + K_r^2) \quad (1.16)$$

where a is a constant and H_i and H_r are the incident and the reflected wave height.

Carrier and Greenspan (1958) demonstrated that, for monochromatic waves over a planar beach, a standing wave solution exists when (according to inviscid nonlinear shallow water solution):

$$\epsilon_s = \frac{A_s \sigma^2}{g \tan \beta^2} \leq 1 \quad (1.17)$$

where ϵ_s is the nondimensional term that describes the swash, $2A_s$ represents the vertical excursion of the swash (S) and σ is the radian frequency ($\sigma = 2\pi/T$).

Meyer and Taylor (1972) determined the offshore criterion for total reflection on the coast:

$$\epsilon_i = \frac{A_0 \sigma^2}{g} (2\pi)^{1/2} \tan^{-5/2} \beta \leq 1 \quad (1.18)$$

where ϵ_i is the nondimensional wave parameter and A_0 is the deep water wave amplitude.

Combining both limits (eq. 1.17 and eq. 1.18) with Miche's hypothesis (Guza et al., 1984), the solution to the relative swash becomes:

$$\frac{S}{H} = \begin{cases} \epsilon_i, & \text{if } \epsilon_i \leq 1 \text{ (saturated)} \\ 1, & \text{if } \epsilon_i > 1 \text{ (reflective)} \end{cases} \quad (1.19)$$

The relation described above in terms of the Iribarren number is:

$$\frac{S}{H} = \begin{cases} \left(\frac{\pi}{2 \tan \beta}\right)^{1/2} & \text{if } \xi_0 \geq \xi_c \text{ (reflective)} \\ \frac{\xi_0^2}{\pi} & \text{if } \xi_0 < \xi_c \text{ (saturated)} \end{cases} \quad (1.20)$$

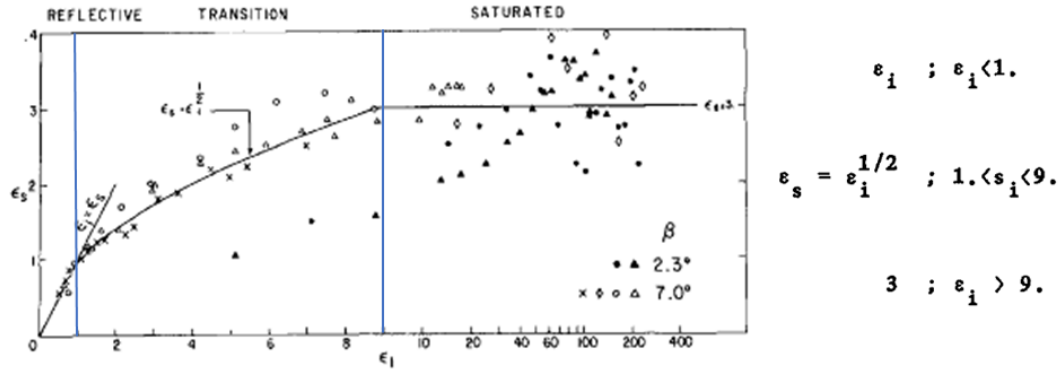


Figure 1.7: Guza et al. (1984) dataset along the three conditions observed.
(Adapted from Guza et al, 1984)

where $\xi_c = \left| \frac{\pi^3}{2 \tan \beta} \right|^{1/4}$ is the minimum value for complete reflection. It is worth noting that large waves result in high ϵ_i and low ξ_0 .

Based on the relation presented in eq. 1.20 and using the dataset from Guza and Bowen (1976), Guza et al. (1984) tested Miche's hypothesis and observed that the swash of monochromatic waves actually responds to three conditions: i) complete reflection, ii) spilling wave condition and iii) a transitional condition between the other two (Figure 1.7).

The reflective condition correspond to fully reflected waves and follow the standing wave solution (eq. 1.15). The spilling condition represents the saturation of the swash due to energy dissipation in the surf zone and in this case, as stated by Miche, the swash have no influence of the wave height. However, the threshold of M above which saturation occur was higher (≈ 3). Finally, the transitional condition represents the waves that are partially reflected at the coast. The formula for transitional regime was obtained by fitting the dataset and has no physical meaning. Based on that, the ratio of the vertical swash excursion to H in monochromatic conditions was finally represented by:

$$\frac{S}{H} = \begin{cases} 3\xi_0^2/\pi & \text{if } \xi_0 < \xi_c \text{ (saturated)} \\ (2\pi\beta)^{-1/4}\xi_0 & \text{if } \xi_c/3 < \xi_0 < \xi_c \text{ (transition)} \\ (\pi/2\tan\beta)^{1/2} & \text{if } \xi_c < \xi_0 \text{ (reflective)} \end{cases} \quad (1.21)$$

The need for different expressions brings up the issue of using one single formula for predicting the swash on beaches under different morphodynamic conditions.

Eq. 1.21 can be applied to idealized conditions and some aspects of it have been qualitatively verified for random waves (Raubenheimer and Guza, 1996). However, a standard fit has not been established for pragmatic application on natural beaches.

Miche's hypothesis was also used to explain the amount of reflection on natural beaches. Assuming saturation and total reflection, the square reflection coefficient can be described as:

$$K_r^2 = \begin{cases} M & \text{if } \xi_0 \geq \xi_c \\ 1 & \text{if } \xi_0 < \xi_c \end{cases} \quad (1.22)$$

Only few studies have been carried out with the aim of measuring the wave reflection on natural beaches. Some of them have tested the relation between M and the amount of reflection from the coast and the relation presented in eq. 1.22 showed to represent well the tendency of the reflection coefficients measured in situ (e.g Arduin and Roland, 2012; Elgar et al., 1994; Raubenheimer and Guza, 1996), although a quantitative parameterization have not been established.

1.3. Thesis Objectives

Previous works have shown the importance of the wave transformation in the surf zone on the swash excursion at the shoreline. Beach morphology and energy dissipation are important characteristics that have influence in the swash zone

oscillations (Guza et al., 1984; Miche, 1951; Ruggiero et al., 2001). Such characteristics change from one beach type to the other and so, swash values are closely related to morphodynamic condition (Wright et al., 1985). The existent literature presented in the State of the Art, suggest that improvement in both incident and infragravity swash predictions can be achieved by using additional information about the beach morphodynamic state on swash parameterization.

Based on that, the main goal of this thesis is to broad the knowledge on swash zone processes and to improve empirical swash parametrizations by considering the beach morphodynamic conditions. To achieve this goal the following specific objectives were proposed:

1. To analyze wave and swash processes at Somo and El Puntal beaches based on field measurements.
2. To analyze the role of the profile shape and the morphodynamic conditions on the infragravity swash values.
3. To assess the effect of the morphodynamic beach state and the amount of reflection on the high frequency swash.
4. To ascertain the improvement on runup predictions when using the swash parameterizations proposed in this work.

1.4. Outline

The content of this thesis is organized as follows:

Chapter 2 describes the field campaigns carried out on Somo and el Puntal beaches. The main results of the measured dataset are also presented in this section.

Chapter 3 presents the infragravity swash analysis and parameterization.

Chapter 4 presents the incident swash analysis and parameterization.

Chapter 5 demonstrates the impact of the swash parameterization presented in previous chapters on the runup values.

Chapter 6 presents the general conclusions of the work, the main contributions of the research and some suggestions for future research lines.

Chapters 2 to 5 correspond to the objectives 1 to 4 of this work, respectively.

Chapter 2

Field experiments

2.1. Introduction

To accomplish the purpose of this thesis, field measurements were carried out in Somo-El Puntal beaches (Santander, Spain) during the ¹MUSCLE-Beach project experiments on 2016 and 2017. The measured data were used to elucidate the processes occurring in the surf and swash zones that lead to runup oscillations. The dataset obtained from these measurements was later added to a large database obtained from previous works to develop the new swash parameterizations.

This chapter is dedicated to describe the two field campaigns, the data process and the results obtained from the measurements. A resume of the environmental conditions and runup parameters statistics from the experiments is presented in Appendix 1 (Table A.1 to Table A.3). Environmental parameters obtained from MUSCLE-Beach experiments and used in this work are available in Gomes da Silva et al. (2017).

¹The Multiscale Climate analysis of flooding and Erosion at Beaches project (MUSCLE-Beach) was carried out by UNICAN with the support of the Spanish “Ministerio de Economía y Competitividad” under Grant BIA2014-59643-R.

2.2. Field Site - Somo Beach

The Somo and El Puntal beaches are part of a sandy spit located at the entrance to Santander Bay, on the Northern coast of Spain (Figure 2.1). To simplify the description, the stretch of coast comprising Somo and El Puntal will be hereinafter referred to as Somo beach.

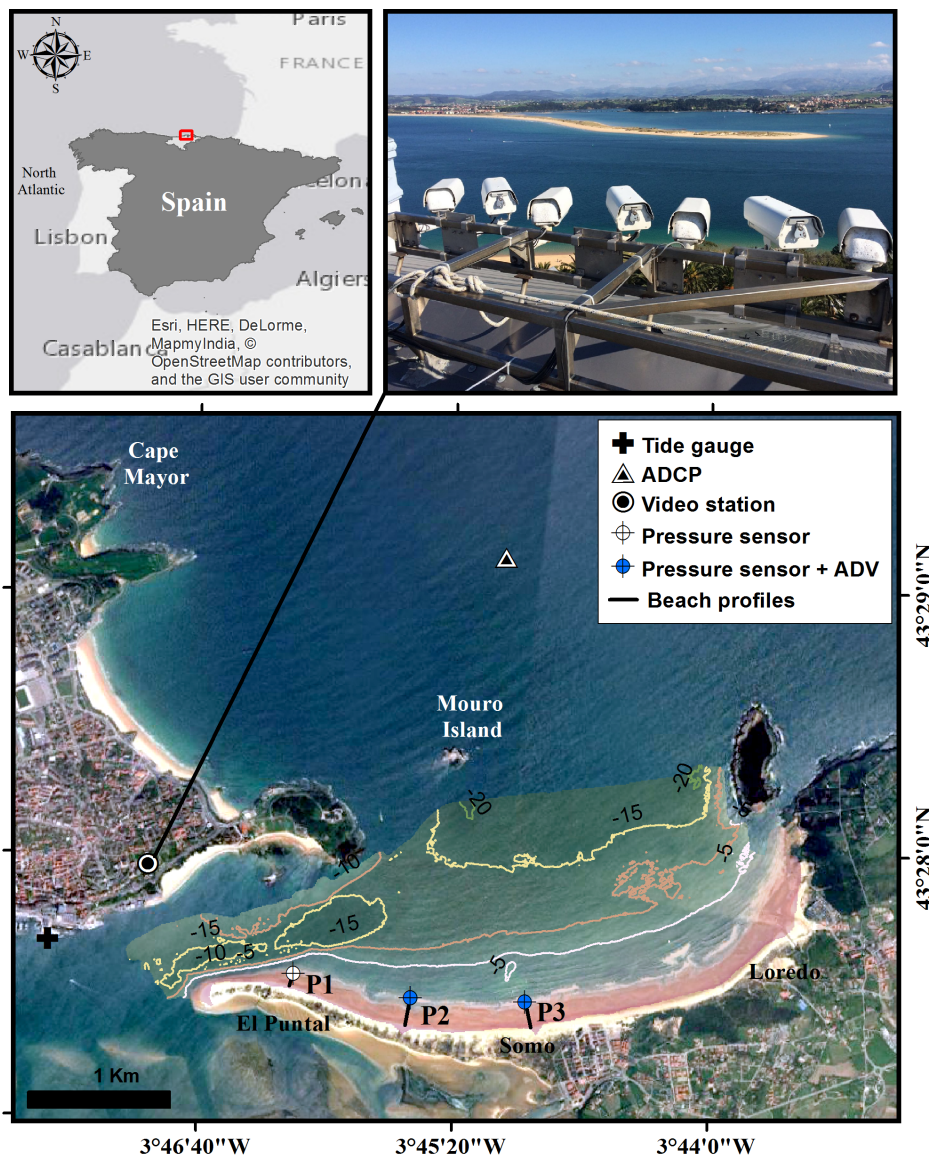


Figure 2.1: Location of the field experiment and measurements position. In detail, the view from the video station.

Dominant NNW swells and less frequent small wave amplitude seas (order of 0.5 m) coming from NNE typically characterize the wave regime in this area. The

annual average significant wave height is about 1 m with storm waves in the order of 4 m. The average sediment size is typically 0.3 mm; however, a significant longshore grain size distribution exists (Losada et al., 1991). An important characteristic of this site is the longitudinal wave gradient along the spit, where different morphodynamic characteristics can be verified: reflective conditions are observed in the sheltered western area of the spit, in front of the navigation channel; intermediate profiles with complex and dynamic bar systems exist in the central part of the beach, and fully dissipative conditions are dominant in the exposed zone, near to Loredo beach. This fact motivated the staging of a field campaign in this area, making the data acquisition from a variety of beach profiles possible during a single experiment.

2.3. Experiments set-up

2.3.1. MUSCLE-Beach experiment (2016)

Wave, current and runup series, topography, bathymetry data and sediment were collected in three profiles (named P1, P2 and P3) in 4th May 2016. Wave data was also obtained at 25 m depth in the middle of the Sardinero bay. The measurements locations are represented in Figure 2.1.

The topography along those cross-shore profiles was measured using real time kinematic performance GPS systems with a precision of 15 mm (planimetry) and 25mm (altimetry). Measurements were taken along the profiles, from the top of the foredune to the coastline, during low tide when the largest part of the beach was exposed. Topographic data were used to obtain the vertical runup level from video images and to calculate the foreshore slope $\tan\beta$.

An Acoustic Doppler Current Profiler (ADCP) AWAC with Acoustic Surface Tracking (AST) was moored at 25 m depth (see ADCP position in Figure 2.1) and collected data from 28th April to 4th June 2016. The ADCP measured the free surface with a frequency of 2 Hz (AST measurements) during 17-min bursts

taken every 20 min (3 min for current measurements). Near the coastline, three pressure sensors installed at the most seaward part of the beach profiles (one per profile) measured free surface elevations with a sampling frequency of 4 Hz. Additionally, two Acoustic Doppler Velocimeter (ADV) were installed at P2 and P3 and acquired velocity data with 10 Hz frequency. Installation of the equipment was done during low tide, while measurements were taken during high tide, when the sensors were submerged (Figure 2.2).

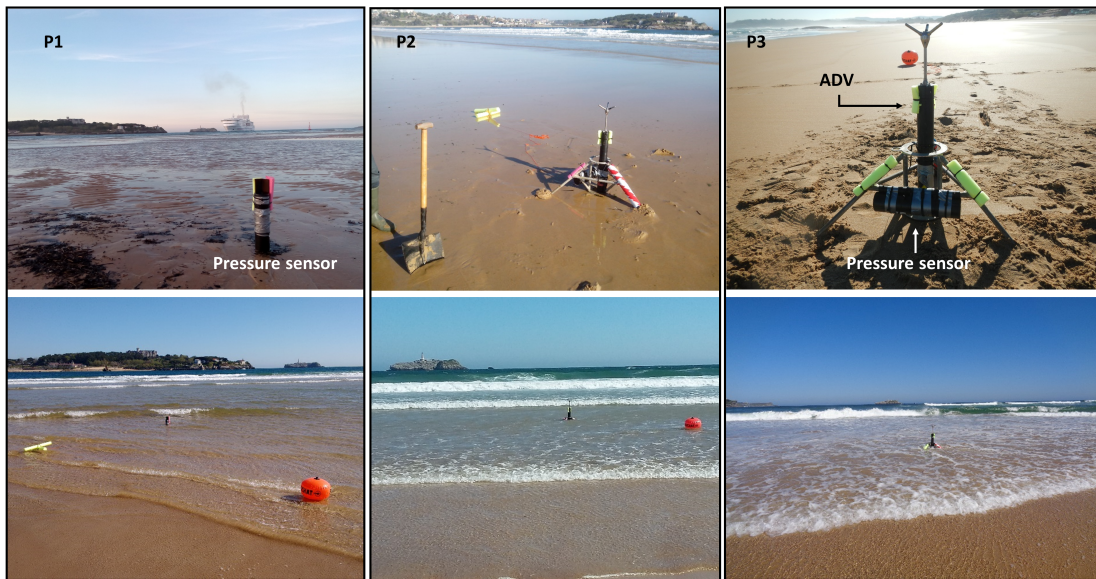


Figure 2.2: Pressure Sensors and ADV installed at low tide (up) and been submerged during the flooding tide (down).

Continuous time series of wave runup oscillations were collected using video imagery techniques during the day of the field campaign. Three cameras, mounted at the opposite side of the bay on the roof of a building facing the spit (see Figure 2.1), collected images of the beach profiles at a sampling rate of 4 Hz. The height of the video station was about 140 m above the mean sea level and the distance from the profiles P1, P2 and P3 was 1200 m, 2100 m and 2800 m, respectively. Pixel resolution varied between 4 and 16 cm in the vertical (Z) plane and 43–63 cm in the horizontal (cross-shore). Cross-shore transects of pixel intensity were obtained from the images. The identification of the pixels that correspond to the profiles was done by displaying square canvas sheets along the transects and measuring the corners with the GPS. The corners were identified in the images and the

respective X, Y and Z values were attributed to the corresponding pixels (Figure 2.3).



Figure 2.3: Example of the process carried out to identify the pixels correspondent to the profiles on images.

The maximum wave runup reached by each wave was measured with GPS during a short period of time (20 min during flooding tide and ≈ 1 h during high/ebb tide) (Figure 2.4), using the same methodology applied by Vieira da Silva et al. (2017). These data were used to verify the accuracy of video measurements during different tidal moments.

An important point to be highlighted regarding the runup measurement technique from images is that the method applied here is a little bit different from those applied in previous works (e.g. Holman and Sallenger, 1985). To ensure better resolution, the cameras were focused only in the three profiles of interest. There were three cameras, one camera pointing to each profile. Since there was no interest in monitoring the rest of the beach, the zoom was established according to the need for resolution. This allowed to have accuracy spite of the distance. Besides, the images did not need to be rectified, what usually results in additional errors.

Sediment samples were collected in the intertidal zone of the beach profiles. Median sediment size and wave parameters were used to define the morphodynamic state of the profiles, through the non-dimensional fall velocity parameter ($\Omega = H_0/wT_p$).

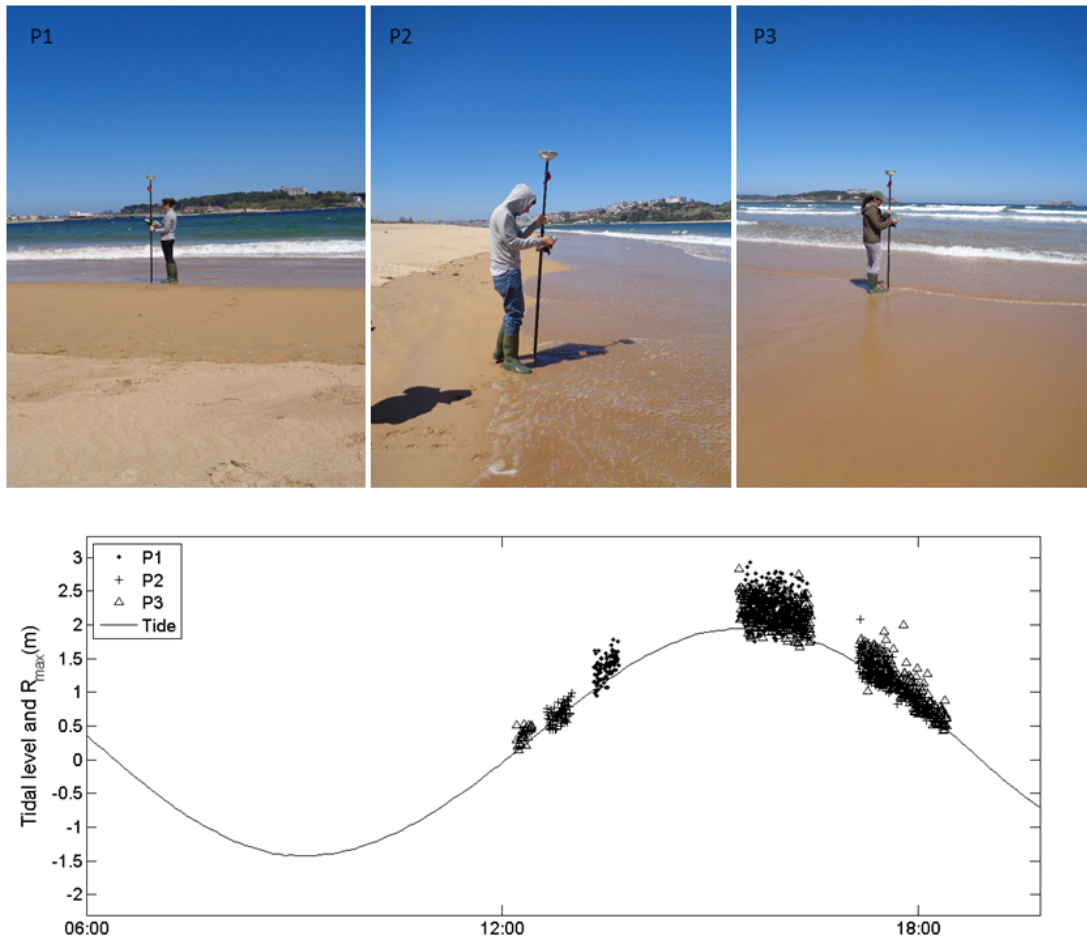


Figure 2.4: Runup measurement with GPS in the three profiles (up) and measured values over the tide series (down).

Finally, topobathymetry data was measured between the 21st and the 23rd of April, 2016 using multibeam echosounder equipment. Depth measurements were taken until 15 m depth with 1m resolution, covering an area of 4.7 Km² (coloured area in Figure 2.1). These data were used as input for later numerical analysis.

2.3.2. MUSCLE-Beach experiment (2017)

The second experiment was undertaken on 19th and 21st September 2017. With the aim of understanding the wave transformation along the surf zone, 7 pressures sensors (3 synchronized pressure sensors) and 2 ADV were disposed over profile P2 (Figure 2.5).



Figure 2.5: Equipments installed at P2 at different tidal moments.

Topography, sediment and runup were measured as made in the previous campaign and an ADCP was installed at the same position (at about 25 m depth). The ADCP measured the free surface elevation from 23rd August (27 days before the field campaign at the beach) to 7th October 2017. In this second field work, topobathymetry measurements were taken over a smaller zone, around the beach profile of interest (Figure 2.6), covering an area of about 2.3 Km². Measurements were carried out between the 6th and the 10th October 2017. Again, this data was used as input to later numerical modeling of the beach.



Figure 2.6: Topobathymetry measured on October 2017.

2.4. Data process

Waves

A moving-average filter was used to obtain the low frequency tidal signal from the free surface oscillation time series measured by the ADCP. The records were compared with tidal data obtained from the tide gauge located at the entrance of the bay (dataset provided by the Puertos del Estado Agency) to set the time of the series. After that process, a Fourier transform was applied to the original signal to analyse it in the frequency domain and the wave parameters were thereby obtained.

A similar process was applied to the series obtained from the pressure sensors at the beach. The time series from the sensors were divided into 10 min records to which a Fourier transform was applied in order to calculate the wave spectra. Finally, the wave parameters were obtained. To establish a relation with the results presented by Stockdon et al. (2006) and other works, the significant wave heights and lengths obtained from the pressure sensor measurements were deshoaled to a depth of 80 m using linear wave theory and considering a shore-normal approach. For the second experiment, when many sensors were displayed across the profile, the most seaward one was used to obtain de deshoaled H_0 .

Swash

10-min timestacks images (time sequence of pixel transects) were generated aiming to obtain runup statistics during periods considered to be tidal constants. Each timestack was manually digitalized using the GUI Timestack interface (Vousedoukas et al., 2012), in which the runup was identified as the white moving edge in the swash zone (Figure 2.7).

The same procedure carried out by Stockdon et al. (2006) to obtain runup, setup and swash statistics was applied to the runup series digitalized from the timestacks.

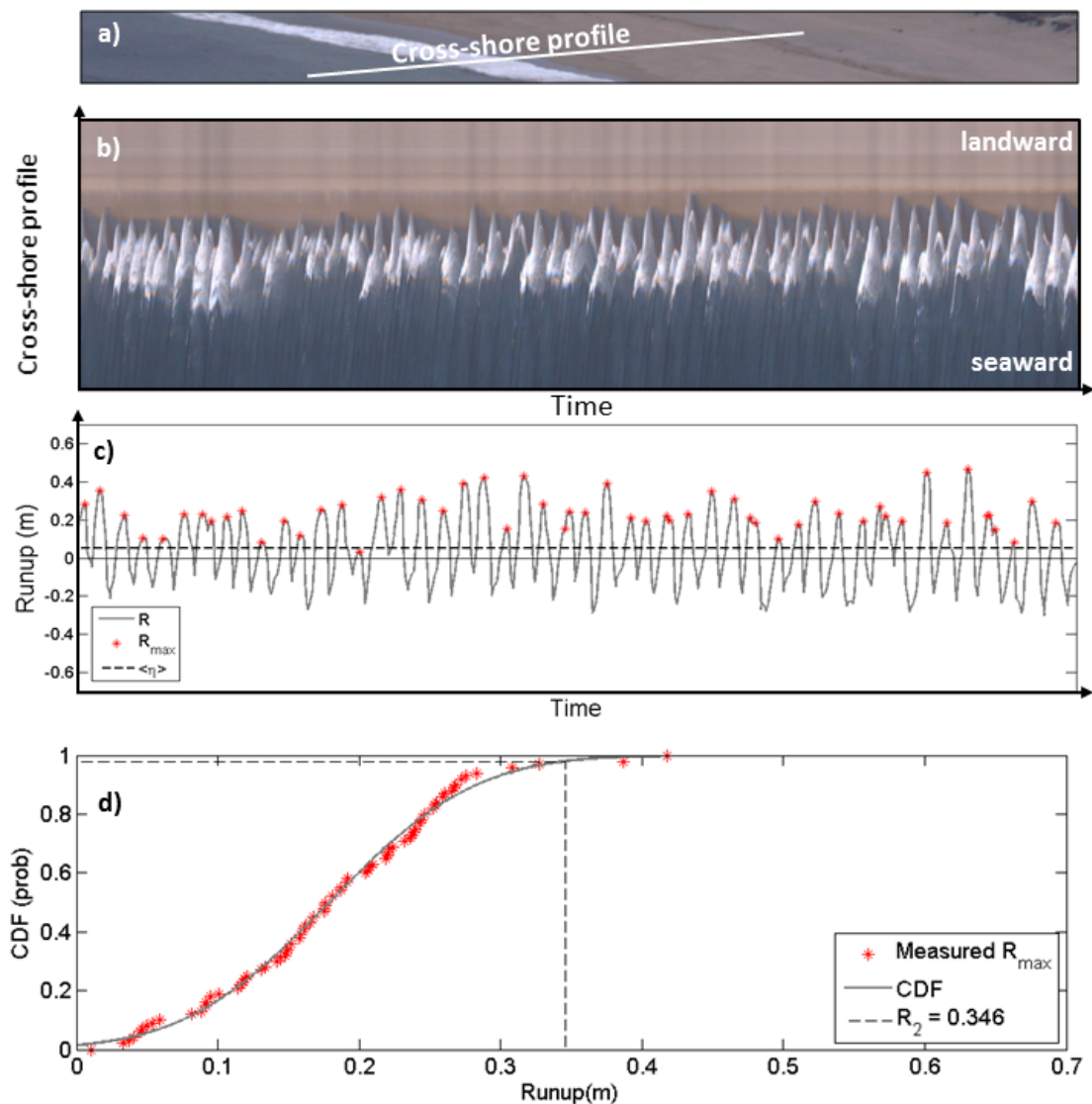


Figure 2.7: Generation of timestacks from the images: a) image obtained from the video camera – the white line represents the transect over which the pixels were extracted; b) runup timestack generated with the time sequence of cross-shore pixels and c) runup time series digitalized from timestack image; d) fit to a cumulative distribution function (CDF) to obtain the R_2 .

After removing the tidal signal, the maximum runup (R_{max}) was obtained as the maximum elevation over the SWL. These values were fitted to a Gaussian distribution and R_2 values were obtained from the Cumulative Distribution Function - CDF (as shown in Figure 2.7). Some studies have suggested that the wave runup have positive skewness and, because of that, may fit better to a Rayleigh distribution (Nielsen and Hanslow, 1991; Power et al., 2013). Nevertheless, recent works have shown that runup distributions are consistently represented by a normal

fit (Hughes et al., 2010; Vousdoukas, 2014), what support the method applied by S2006. Besides, the dataset measured at Somo beach showed to be well represented by the Gaussian distribution (Figure 2.7d).

To obtain the swash series, the static setup $\langle \eta \rangle$ (not considering breakpoint oscillation), calculated as the average of the 10-min record, was subtracted from the series of runup oscillation; then the significant swash was calculated as:

$$S = 4\sqrt{PSD(f)df} \quad (2.1)$$

where $PSD(f)$ is Power Spectral Density in each frequency. S_{inc} and S_{ig} values were obtained by summing PSD only over the respective frequency bands.

Forshores slope and morphodynamic beach state

The foreshore slope $\tan\beta$ was calculated for each 10-min time series as the slope of the profile section with elevations (Z) ranging between $Z = SWL \pm 2std(R)$, where SWL is the still water level and $std(R)$ expresses the standard deviation of the runup values. The morphodynamic beach state was assessed through the parameter Ω (eq. 1.3).

2.5. Results

2.5.1. MUSCLE-Beach experiment 2016

Evaluation of wave runup measurement technique

To ensure that the runup values obtained by the images were in accordance to those observed *in situ*, comparison analysis between the runup from timestacks and those obtained with the GPS during the first field experiment were carried

out. The maximum runup values (R_{max}) measured with the GPS was fitted to a Gaussian distribution from which the R_2 for each 10 min series was obtained. R_2 values obtained from GPS and those from the timestack were then contrasted.

Comparison of data measured during high tide showed maximum differences around 0.1 m (on R_2 values of about 0.8 m). During the ebb/flooding tide, the values were still in good agreement at P1 and P2, with maximum differences of about 0.15 m. However, a large underestimation was observed at P3 (maximum difference of 0.7 m). The same issue was verified in previous studies when applying video techniques to measure runup in places of important tidal amplitudes (Andriolo and Sánchez-García, 2016). High water saturation of the intertidal profile leads to difficulties on identifying the white edge that represents the runup in the timestacks. In this cases, it is recommended to limit the analysis to the values obtained during high tide.

Waves

H_s values measured with the ADCP ranged between 1.43 m to 1.69 m with T_p values from 10.67 s to 12.8 s. During the experiment, a NNW ($\approx 340^\circ$) swell was predominant, with a less energetic sea from the NNE ($\approx 35^\circ$). Wave spectra obtained from the ADCP and from the three pressure sensors are presented in Figure 2.8. Differences are evident between the spectrum measured in each location and represent the wave transformation along the beach. The amount of wave energy decreases from east (P3) to west (P1) in both, the incident and infragravity bands, in agreement with the wave exposure of each sector. Wave transformation along the beach is also clear in H_s series obtained from the 10-min wave spectra measured at P1, P2 and P3 (Figure 2.9). Lower values were observed at P1 that is located in the most sheltered area, ranging from 0.41 m to 0.49 m. P2 and P3 presented similar H_s values ranging from 0.67 m to 0.95 m at P2 and 0.69 m to 1.07 m at P3. Wave peak period reached 12.8 s at the three profiles.

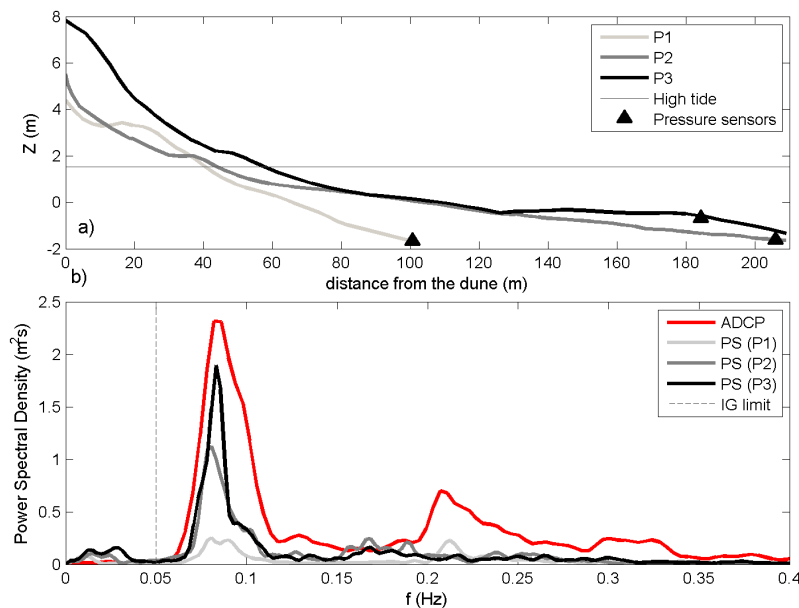


Figure 2.8: Topography of Somo profiles (a) and examples of wave spectra obtained by the pressure sensors (PS) at P1, P2, P3 and at ADCP position (b). See equipment and profile position in Figure 2.1.

A secondary energy peak was registered by the ADCP in frequencies of about 0.22 Hz. The energy on that frequency range was not observed on the measurements at P2 and P3 and only a small quantity was observed in the wave spectra measured in profile P1. It was verified that the amount of energy in these frequencies is related to NNE seas that does not reach the eastern part of the beach due to the presence of Santa Marina Island.

Swash

Swash values ranged between 0.89 m to 1.11 m at P1, from 0.75 m to 1.35 m at P2 and from 0.75 m to 1.10 m at P3. The shape of the swash spectrum at the three measurement points is presented in Figure 2.10. P2 and P3 presented higher amount of energy within the infragravity band, while incident frequency energy was dominant at P1.

In all swash spectra there was a saturated region within high frequencies band where the energy density was proportional (in the log-log scale) to f^{-3} , an spectral

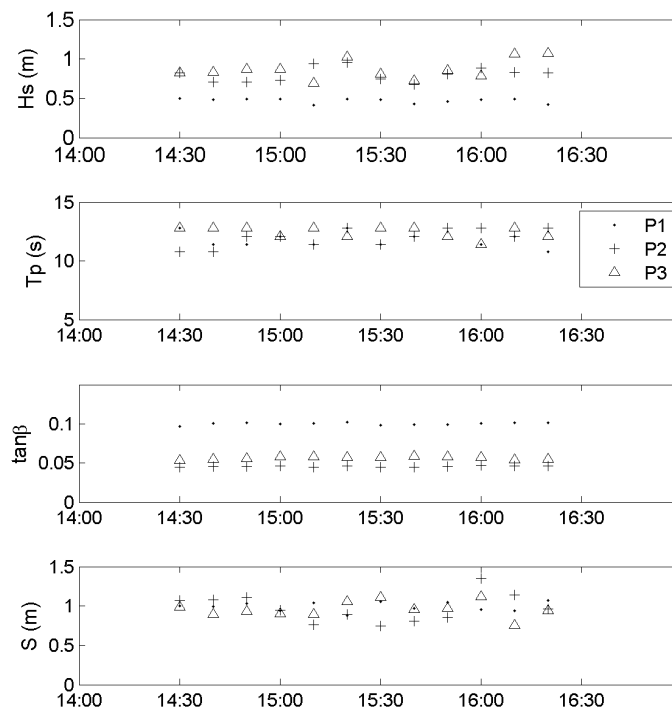


Figure 2.9: Wave parameters, $\tan\beta$ and swash values obtained at the three profiles during the high tide.

decay consistent with the field experiments of Guza and Thornton (1982) and Ruessink et al. (1998); and modeled data from Ruju et al. (2014).

Beach profiles and morphodynamic beach state

Median grain size (D_{50}) was 0.28 mm, 0.34 mm and 0.35 mm at P1, P2 and P3, respectively. D_{50} , wave parameters and $\tan\beta$ were used to verify the morphodynamic state of each profile (see Ω values in Table A1, Appendix 1). According to the classification proposed by Wright and Short (1984), the values of Ω indicated reflective conditions ($\Omega_{reflective} < 1.5$) at the three profiles during the experiment, ranging from 0.67 to 0.84 at P1, from 0.87 to 1.34 at P2 and from 0.78 to 1.31 at P3.

The shape of the swash spectra showed in Figure 2.10 indicate different amount of energy in the infragravity and incident band at the three profiles. According to the

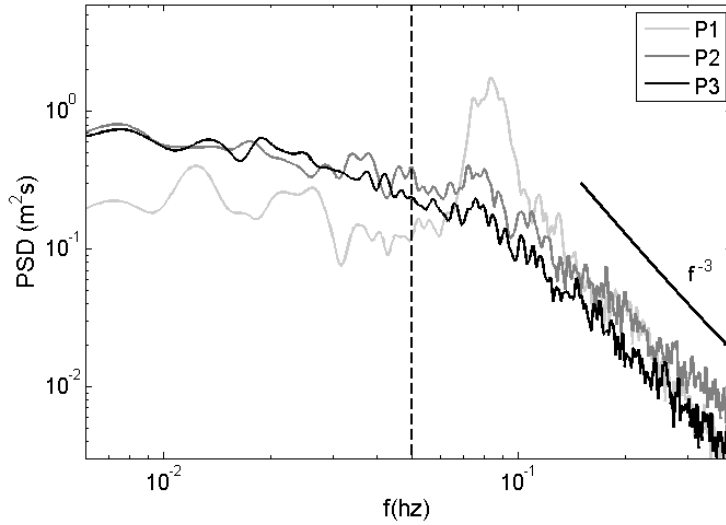


Figure 2.10: Total swash spectra obtained at Somo beach profiles P1, P2 and P3. The vertical dashed line represents the limit between infragravity and incident bands ($f = 0.05$ Hz). Diagonal black line shows the f^{-3} dependence of swash energy.

conceptual model proposed by Hughes et al. (2014) (see Figure 1.3, Chapter 1), under reflective conditions, the swash is dominated by high frequency oscillations and the shape of the swash spectrum is characterized by peaks within the incident frequency band. Beach profiles under intermediate conditions (low-tide terrace, transverse bar and rip, rhythmic bar and beach and longshore bar and through) present energy peaks also in the low frequencies, with more energy in the infragravity band as long as the profile becomes more dissipative. Finally, under totally dissipative conditions, the swash spectrum shows no peaks and the infragravity energy is dominant. Based on that, one should expect an intermediate beach state at P2 and P3, that presents peaks in both incident and infragravity frequencies. The shape of the profiles measured in situ also reflected those conditions: P1 was shorter ($\approx 100m$) and presented higher slopes ($\overline{\tan\beta} = 0.1$), while P2 and P3 were longer ($> 200m$) and flatter ($\overline{\tan\beta} = 0.04$ and 0.06 , respectively). Moreover, captured images revealed patterns of wave breaking and rips indicative of intermediate beach state at P2 and P3. In spite of this, the average non-dimensional fall velocity parameter indicated reflective conditions in all Somo beach profiles (Table A.1 - Appendix 1).

The influence of previous sea states on the current profile shapes at P2 and P3 may be the reason for the contrast between the in situ observations and the calculated values of Ω . Figure 2.11 presents the wave series measured by the Virgen del Mar Waverider buoy (moored 35 Km to the north of Cape Mayor, at a depth of 30 m) in the period that preceded the measurements at Somo beach. The register shows that four energetic swells hit the Santander coast in the month before the experiment. On the 30th April, significant wave heights of 3m were registered by the Virgen del Mar buoy, double the wave height registered by the same equipment during the field work. Three other energetic events were recorded earlier in that month on the 7th, 10th and 19th April, with wave heights reaching values of 3.97 m, 5.24 m and 1.86 m, respectively. These energetic events were followed by periods of calm conditions with low wave heights (<1 m). That sequence of events implies that the morphodynamic conditions of the beach during the experiment still had some inheritance from the recent storms.

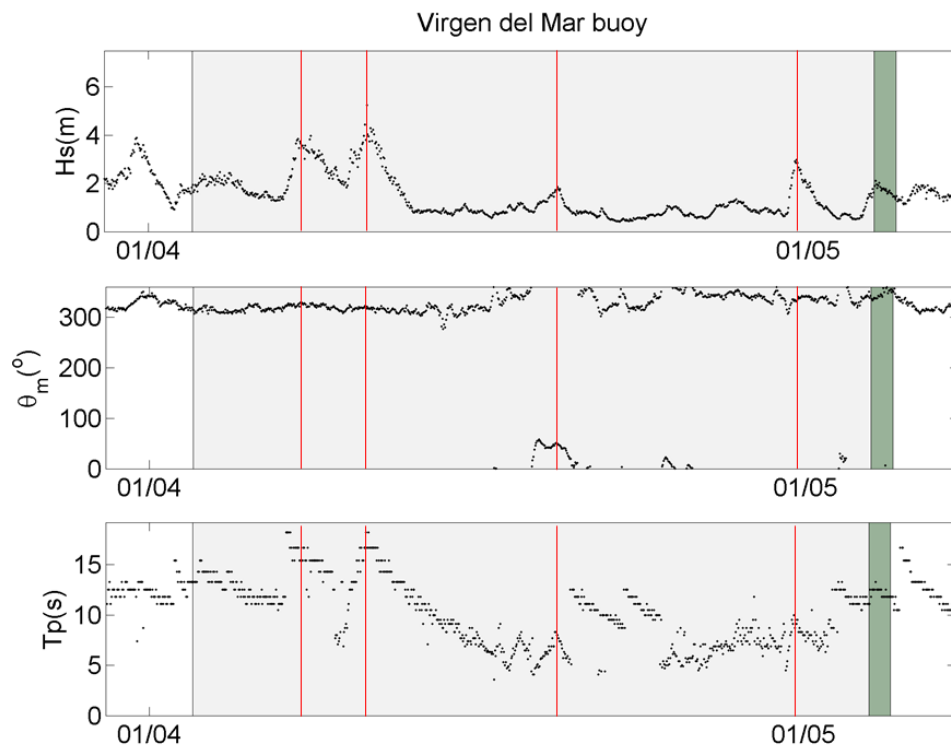


Figure 2.11: Wave parameters time series measured by the Virgen del Mar Waverider buoy. The green shaded area represents the day of the experiment, while the gray shaded area represents the previous 30-days period used to calculate the beach state according to previous wave condition. Red lines indicate the energetic events that preceded the field experiment.

Given the importance of properly determining the morphodynamic beach state in this work, the relevance of the previous sea conditions when determining the beach type was assessed through the parameter Ω^* (eq. 2.2) which indicates the morphodynamic beach state, taking into account not only the current wave conditions, but also the previous sea states (called here 'beach memory'). Ω^* was calculated for the three profiles at Somo beach, according to the methodology proposed by Wright et al. (1985).

$$\Omega^* = \left[\sum_{n=1}^D D^{-i/\phi} \right]^{-1} \sum_{n=1}^D \Omega_i 10^{-i/\phi} \quad (2.2)$$

where $i = 1$ on the day of the experiment and $i = D$ on D days prior to the observations. ϕ is the decay rate in days such that the weighting factor reaches 10 percent after ϕ days. To calculate the morphodynamic state of the Somo beach profiles taking into account the inheritance from previous sea states, a five-step method was applied (see also Figure 2.12):

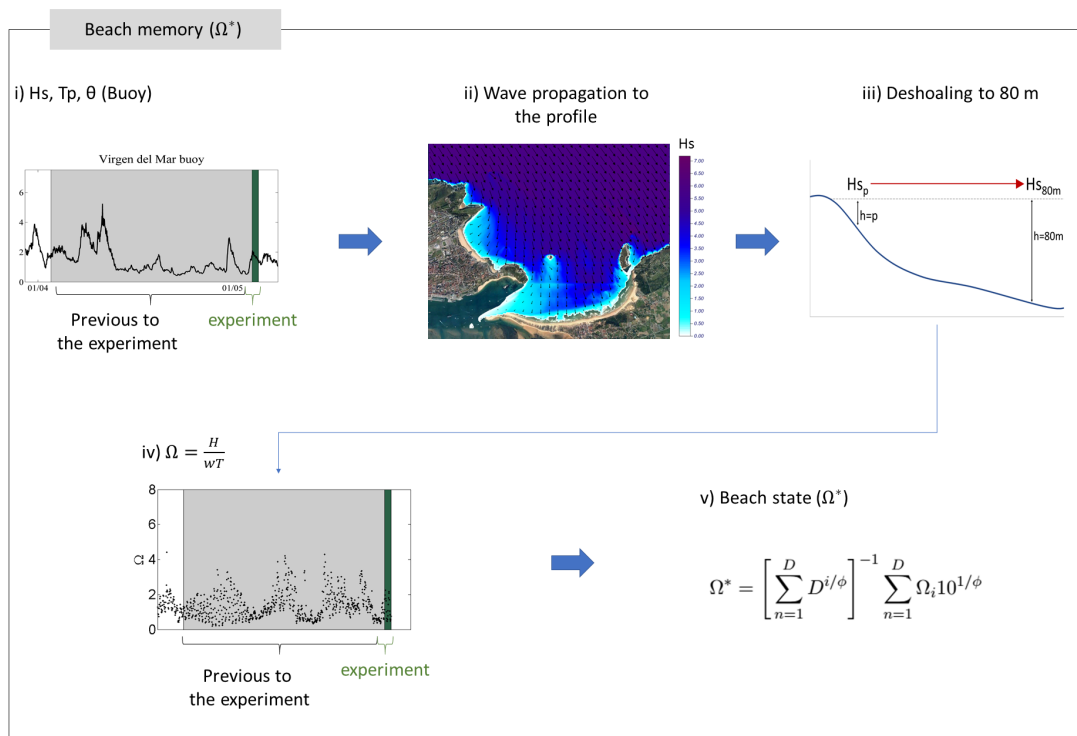


Figure 2.12: Methodology applied to calculate the beach state taking into account the beach memory.

- I. validation of the wave model OLUCA-SP (González et al., 2007) with data from the experiment;
- II. propagation of the wave parameters from the Virgen del Mar buoy time series up to the points where the pressure sensors were installed;
- III. deshoaling of the wave parameters from the positions of the pressure sensors to a depth of 80 m to obtain H_0 time series;
- IV. calculation of the instantaneous Ω for the period just prior to the experiment using H_0 in eq. 1.3 and
- V. calculation of the Ω^* (eq. 2.2) based on the time series of daily average Ω and using $D=30$ days and $\phi=5$ days, as suggested by Wright et al. (1985).

The analysis of the beach state according to the previous wave conditions resulted in Ω^* values equals to 1.41, 2.39 and 2.32, at P1, P2 and P3, respectively. The values obtained at P2 and P3 correspond to the low tide terrace state in the beach state classification proposed by Wright and Short (1984) and are in accordance with the morphodynamic conditions verified in situ.

2.5.2. MUSCLE-Beach experiment 2017

Waves

During the second experiment, a NNW (340°) swell was predominant all the time. Wave spectra from ADCP measurements can be verified in Figure 2.13. H_s values measured by the ADCP ranged between 0.37 m to 0.52 m on the 19th and from 0.3 m to 0.84 m on the 21st. Wave peak period during high tide was 7.7 s on the first day and 10.39 s on the second day of measurements. Near the coast, the most seaward pressure sensure registered sea states with H_s ranging from 0.19 m to 0.24 m on the first day, and from 0.29 m to 0.40 m on the second day (Figure 2.14).

Swash

Swash values were higher on the 21st, from 0.45 m to 1.10 m, while on the 19th swash series ranged from 0.34 m to 0.68 m. Example of the swash spectrum obtained in each measurement day is presented in Figure 2.15. A peak of high energy in the incident frequency and small peaks that enters the infragravity band were observed. Again, the saturated band of the swash spectrum showed a roll-off of f^{-3} in both days of the field work, same dependence observed at the three profiles of the experiment of 2016. The amount of energy in the saturated frequencies was slightly higher during the second day of campaign.

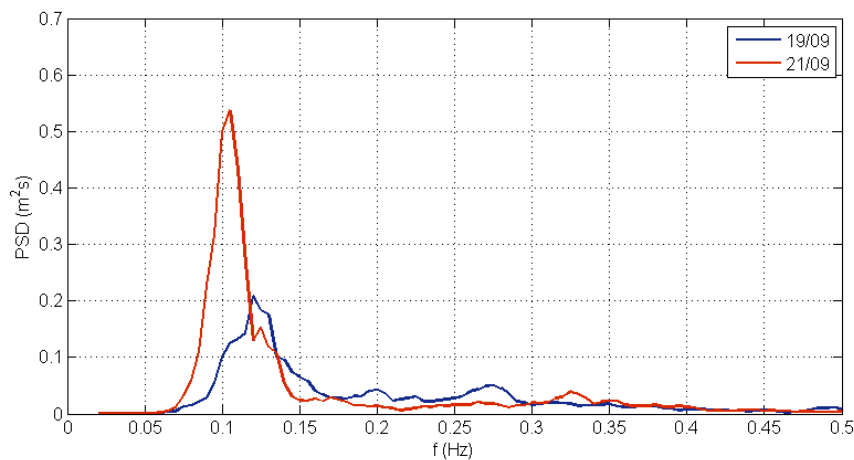


Figure 2.13: Wave spectra measured at the ADCP position on 19th and 21st September.

Beach profiles and morphodynamic beach state

Median grain size (D50) was 0.29 mm in the intertidal zone. Sediment size was used to calculate the morphodynamic beach state through Ω^* (eq. 2.2), taking into account the previous state. The same procedure taken in the first experiment to achieve Ω^* value was applied. By this time, wave series used as input to the wave model were obtained from the ADCP measurements. The results revealed Ω^* values equal to 1.85 and 1.90 on the 19th and the 21st, respectively, what indicates that the profiles are under Low Tide Terrace conditions. Figure 2.16 and Figure 2.17 show the profile shape and wave spectral evolution along the profiles

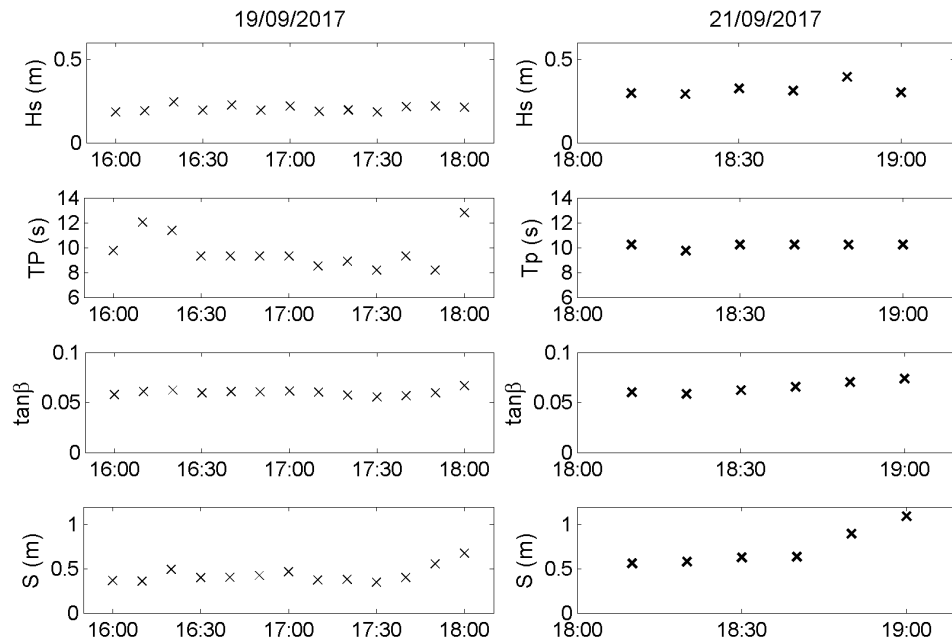


Figure 2.14: Wave parameters, foreshore slope and swash values obtained during the 2017 experiment.

at high tide. Measured topography showed long profiles with steep foreshore and a pronounced bar in the intertidal zone, on both days. The shape of profile P2 is clearly different from the one measured on 2016 which was observed to be flatter and with no clear features in the intertidal zone. The low energy combined with steep foreshore resulted in more reflective conditions if compared to the previous experiment.

Wave reflection and standing waves

High and low wave energy alternating along the beach profile was observed during the second day of the experiment, what may indicate the presence of a partial standing wave, as result of the reflection at the beach (Figure 2.17). Higher energy spectra indicate sensors positioned at anti-nodes of the standing wave, while lower energy spectra represent pressure sensors at nodes position. This behaviour was not evident at the first day of measurements, what may indicate that no nodal

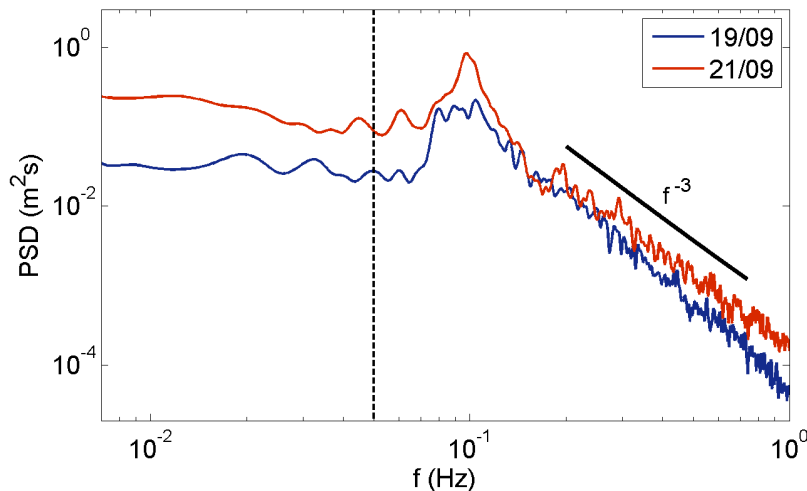


Figure 2.15: Total swash spectra measured at profile P2 on the 19th and 21st September. The vertical dashed line represents the limit between infragravity and incident bands ($f = 0.05$ Hz). Diagonal black line shows the f^{-3} dependence of swash energy.

structure was occurring or simply that the sensors were not located at nodal/anti-nodal position. This can be an important point to be taken into account when assessing the swash values since the presence of a standing wave can lead to an amplification of the swash oscillation at the beach. This issue will be further explored on next chapters, when assessing the infragravity and the incident swash.

2.6. Summary and Conclusions

Two field experiments were undertaken at Somo beach (North Spain) on May 2016 and on September 2017. In the first experiment (MUSCLE-Bach 2016), pressure sensors and ADV installed at a point outside the surfzone measured waves and velocity in three morphodynamically different beach profiles. The results from that experiment indicate different swash behaviour under different morphodynamic conditions, what support the first hypothesis of this thesis. The morphodynamic condition of the three profiles was verified through the non dimensional fall velocity parameter (Ω^*) and showed to be influenced by the previous sea states.

The second experiment (MUSCLE-Beach 2017) was carried out under more reflective conditions, on September 2017. With the aim of verifying the evolution of waves and currents across the beach, an array of pressure sensors and ADV measured data along one beach profile. Initial results indicate the presence of a standing (partial) wave across the surf zone. This kind of nodal structure may have influence over the swash values, since amplification of the wave amplitude is expected in the coastline. This issue will be further analysed on the next chapters.

All swash spectra showed a dependence of f^{-3} in the saturated region. Saturation was always restricted to high frequencies, and peaks of energy could still be observed in the incident bands. This indicates that the lower frequencies of incident band were not saturated. This behaviour is typical from transition conditions between reflective and fully saturated swash.

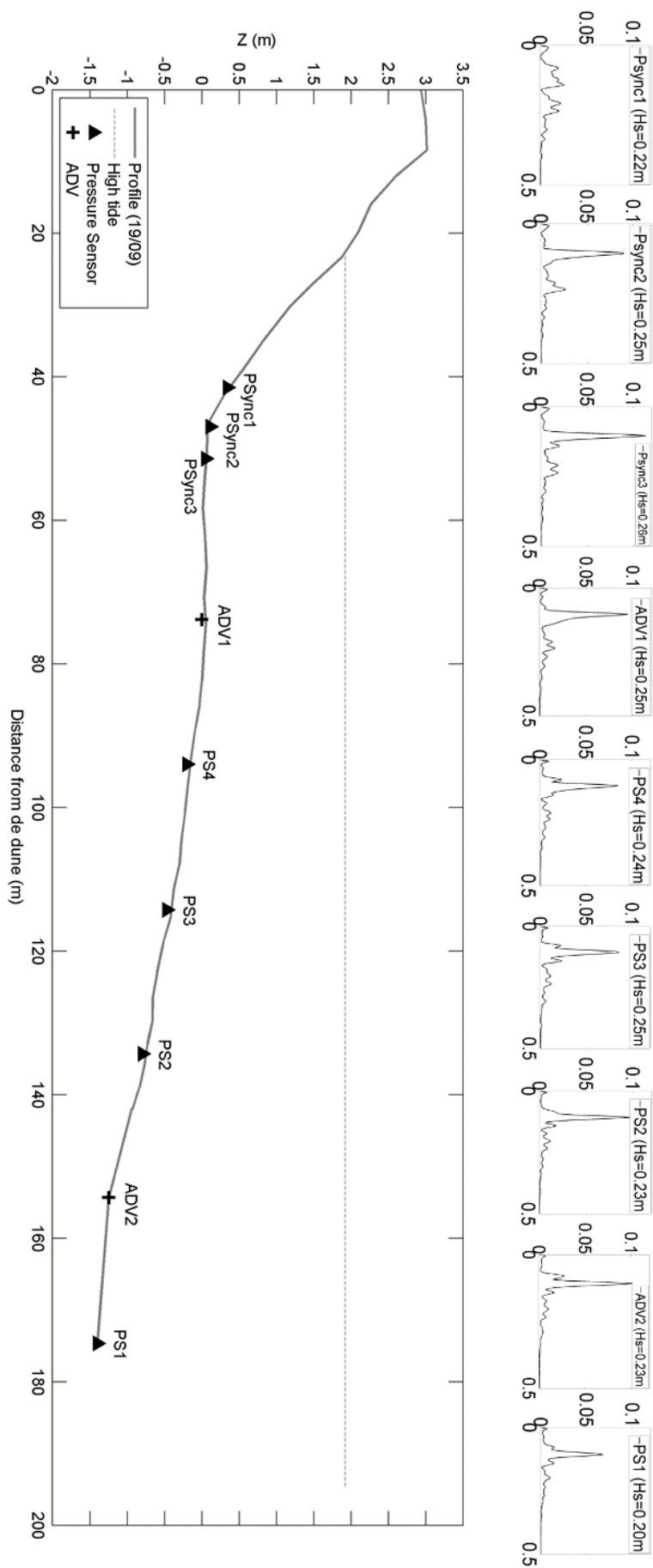


Figure 2.16: Topography of the profile P2 measured at 19/09/2017 and wave spectra obtained from each of the 9 sensors.

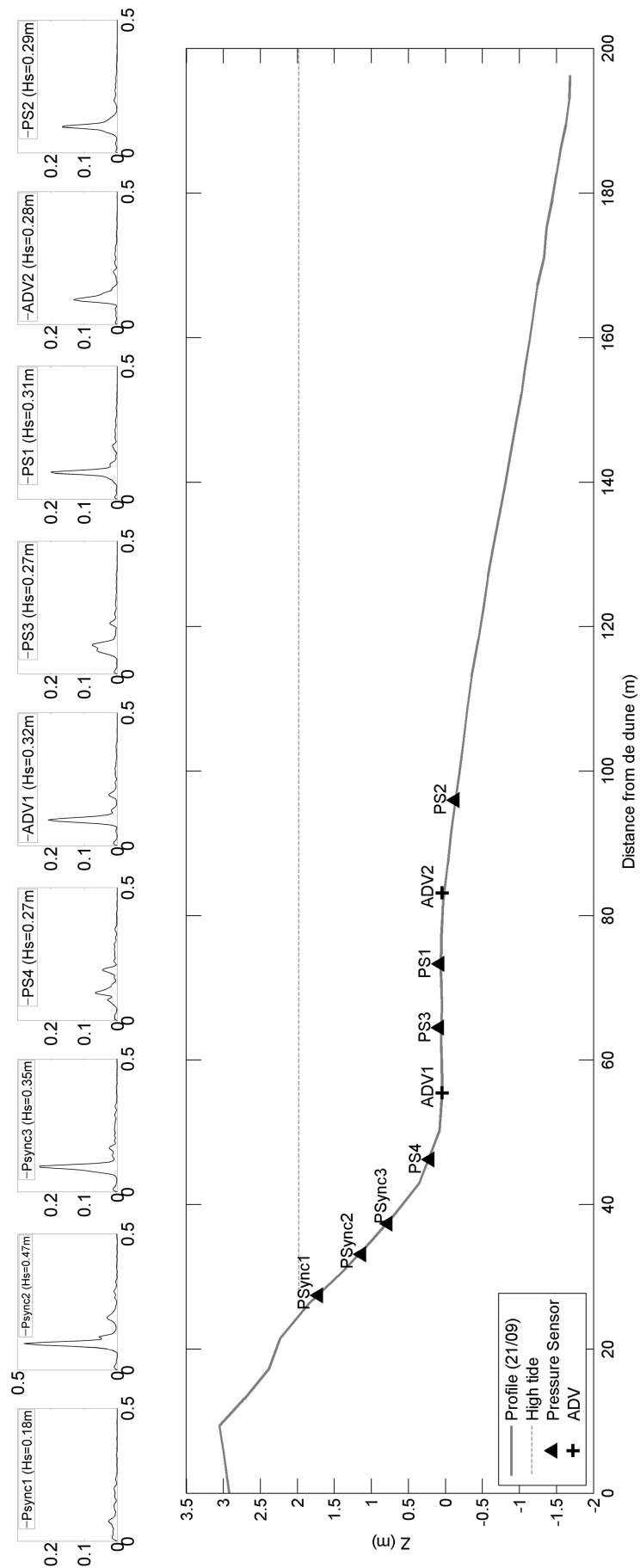


Figure 2.17: Topography of the profile P2 measured at 21/09/2017 and wave spectra obtained from each of the 9 sensors.

Chapter 3

Infragravity swash analysis and parameterization

3.1. Introduction

As stated in Chapter 1, according to Stockdon et al. (2006), the vertical component of the infragravity swash is best parametrized by:

$$S_{ig} = 0.06(H_0L_0)^{0.5} \quad (3.1)$$

However, the use of parameter $(H_0L_0)^{0.5}$ does not allow to differentiate the infragravity swash on beaches under different morphodynamic conditions, since neither profile slope nor sediment size are included in the above parameterization (see also Figure 1.4). On the other hand, Ruggiero et al. (2001) (hereinafter R2001) showed that low frequency runup can be represented on reflective and dissipative beaches through the following relation:

$$R_{ig} = 0.27(\tan\beta H_0L_0)^{0.5} \quad (3.2)$$

Good correlation when using $(\tan\beta H_0 L_0)^{0.5}$ indicate the need for additional parameters that include morphodynamic information of the beach. The aforementioned fact was used as main guideline for the analysis carried out in this work when approaching the low frequency swash oscillations. Taking the studies presented by S2006 and R2001 as a starting point, data obtained from the field measurements (MUSCLE-Beach 2016) and the dataset from previously published works were used to analyse the effect of the beach slope and the morphodynamic state on the infragravity swash. Based on those analysis, a new parametrization for predicting infragravity swash on beaches was developed.

3.2. Methods

The dataset obtained from the measurements at Somo Beach was used to elucidate the processes that lead to low frequency oscillation at the beach. Besides those data, a recompilation of data published on previous studies was carried out. This additional dataset, allowed to enlarge the database used to stablish the infragravity swash parameterization.

3.2.1. Previous studies dataset

Data published by S2006 and Senechal et al. (2011) were obtained to be used in the empirical model of the infragravity swash. The location of the experiments from both works is presented in Figure 3.1.

The dataset compiled by S2006 and used to stablish their runup, setup and swash parameterizations is available online (Stockdon and Holman, 2011). It consists of data from 10 field campaigns undertaken in 6 beaches along the east and west coasts of the USA, and on the coast of the Netherlands. The set of data post-processed by S2006 is composed of R_2 , setup ($< \eta >$), total swash (S), incident swash (S_{inc}), infragravity swash (S_{ig}), H_0 , T_p and $\tan\beta$. Additional information about sediment grain size was obtained from the papers and reports describing

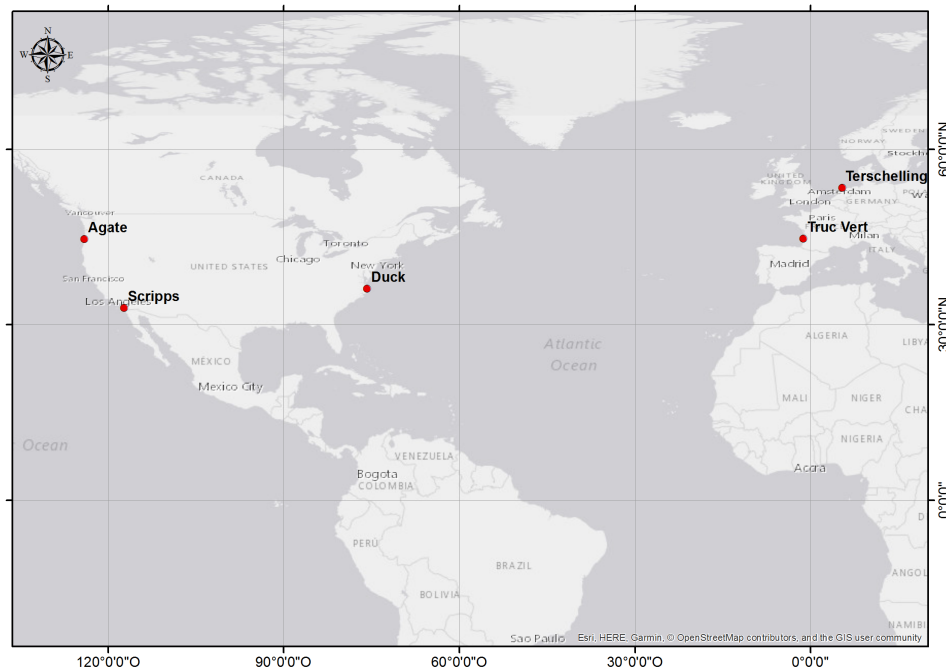


Figure 3.1: Location of the experiments presented by Stockdon et al (2006) and Senechal et al (2011).

the experiments. As it was not possible to obtain sediment grain size from two of the studies, only 8 of the 10 experiments were used:

- Duck, USA -1982 (Holman, 1986; Holman and Sallenger, 1985);
- Duck, 1990 (<http://frf.usace.army.mil/delilah/start>);
- Duck, 1994 (Holland and Holman, 1996; Staubke and Cialone, 1996);
- Duck, 1997 (www.frf.usace.army.mil/SandyDuck/SandyDuck);
- Scripps Beach, USA .1989 (Holland et al., 1995; Raubenheimer et al., 1995);
- Terschelling, the Netherlands -1992 (APR/OCT) (Ruessink et al., 1998);
- Agate Beach, USA .1996 (Ruggiero et al., 2001, 2004).

The dataset comprises the full range of Ω and ξ_0 (see Table A.2 in Appendix 1, with Agate Beach and Terschelling corresponding to the most dissipative ($\Omega > 5.5$ and $\xi_0 < 0.3$) and the Duck experiments (1982 and 1997) corresponding to the most

reflective conditions ($\Omega < 2$ and $\xi_0 > 1$). Wave data were obtained at different depths in each experiment (between 7 m and 64 m) and, to enable comparisons to be made between datasets, S2006 deshoaled the wave height and length to a depth of 80 m using linear wave theory and assuming a shore-normal approach.

Senechal et al. (2011) published part of the results of the ECORS TrucVert-08 experiment, which was conducted out on the French Atlantic coastline on March 2008. Statistical parameters representing the environmental conditions and swash values are available in the published paper. The experiment was carried out at Truc Vert, a macrotidal beach, during very particular conditions when an extreme storm event representative of the 10-year return period coincided with large tidal amplitudes (>4 m). This led to the landward displacement of the swash zone to areas with steeper slopes (>0.06) due to the presence of embryonic dunes. As a consequence, despite the energetic wave condition verified in the surf zone, the morphodynamic beach state remained in the range of intermediate to reflective, the Iribarren number was high (between 0.47 and 0.87) and the resultant horizontal excursion of the runup was relatively short (<50 m). A Waverider buoy moored at a depth of 20 m measured sea state conditions. During the field campaign, the H_s reached 6.4 m and the T_p ranged between 11.2 s and 16.4 s. The available dataset is composed of infragravity swash (S_{ig}), H_s , T_p and $\tan\beta$. To standardize the dataset for use in the present work, wave parameters obtained from Senechal et al. (2011) were deshoaled to a depth of 80 m, as done in S2006.

3.2.2. Data analysis methodology

The analysis and parameterization of the low frequency swash followed the steps listed below:

- i) the validity of S2006 and R2001 was tested to verify the performance of previous proposed formulas;
- ii) a set of parameters was chosen to verify the relation with the infragravity swash;

TABLE 3.1: Performance evaluation of the infragravity swash parameterization for each experiment, using S2006 (eq. 3.1) and R2001 (eq. 3.2) parameterizations

Experiment	Measured	R2001		S2006	
	$\overline{S_{ig}}(m)$	$\overline{S_{igc}}(m)$	RMSE(m)	$\overline{S_{igc}}(m)$	RMSE(m)
Duck82	1.18	1.74	0.63	1.11	0.30
Duck90	0.91	1.08	0.28	0.80	0.23
Duck94	1.35	1.30	0.31	1.03	0.43
Duck97	0.88	1.08	0.31	0.79	0.21
Scripps89	0.44	0.54	0.11	0.62	0.19
Terschelling94/1	0.68	0.70	0.10	1.11	0.46
Terschelling94/2	0.40	0.31	0.11	0.62	0.24
Agate96	1.06	0.76	0.34	1.35	0.34
TrucVert08	1.33	1.66	0.46	1.51	0.27
P1Somo2016	0.34	0.65	0.32	0.46	0.14
P2Somo2016	0.62	0.61	0.14	0.64	0.15
P3Somo2016	0.68	0.72	0.11	0.68	0.11
All data	0.97	1.15	0.35	0.95	0.27

iii) the relation between the infragravity swash (horizontal/cross-shore and vertical excursion) and the selected parameters was verified through regression analysis;

iv) the slope of the best fit obtained from the previous analysis was related to the morphodynamic beach state;

v) the results were compared to those obtained with the previous formulas.

3.3. Results

3.3.1. Infragravity swash estimation using the R2001 and S2006 formulas

The performance of R2001 and S2006 parameterizations was evaluated both, in terms of the entire dataset (*all data*) and in terms of individual experiments. Given the different beach state characteristics of the Somo profiles, P1, P2 and P3 were considered separately in the analysis. Statistical parameters obtained from the comparison between measured (S_{ig}) and calculated (S_{igc}) data from both models are presented in Table 3.1. The linear regression fit is represented in Figure 3.2.

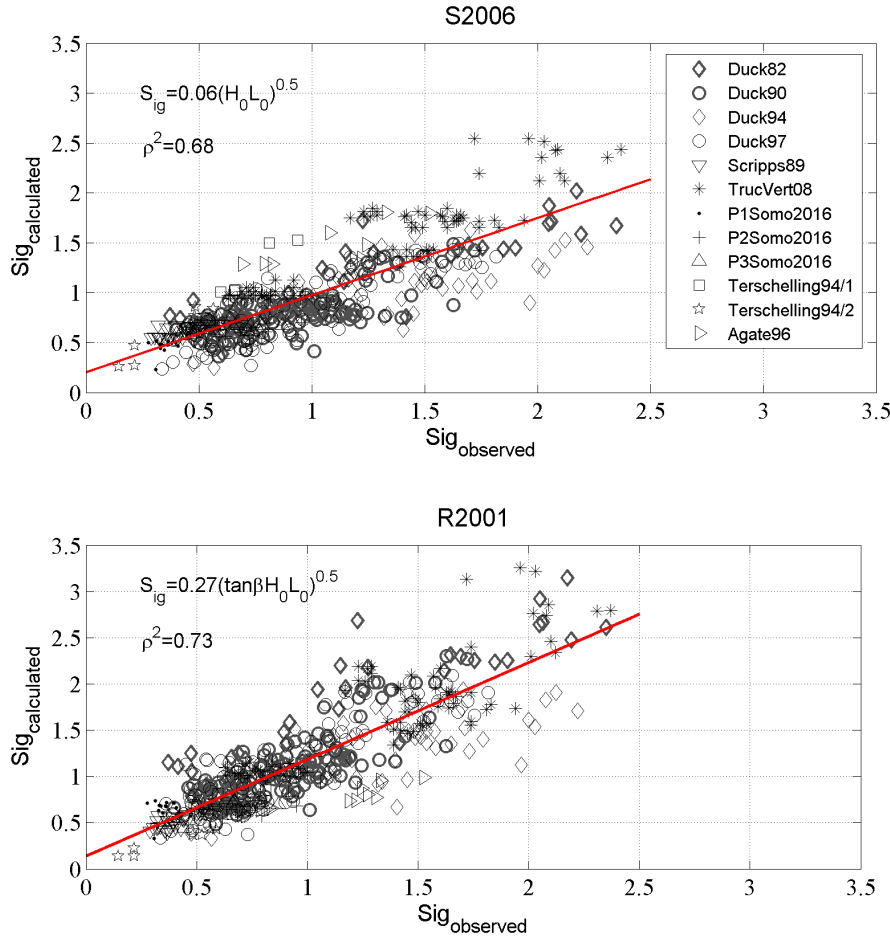


Figure 3.2: Linear regression between S_{ig} observed and calculated with S2006 (up) and R2001 (down) parameterizations.

When analyzing the experiments individually, R2001 presented the higher RMSE, reaching 0.63m for Duck82, while the maximum RMSE value obtained using S2006 was 0.46m for Terschelling 94/2. On the other hand, for Duck82, Duck94; Scripps89, Terschelling94, P2 and P3, R2001 showed to predict better the infragravity swash. S2006 resulted in lower RMSE for the other experiments: Duck82, Duck90, Duck97, TrucVert08 and P1.

The R2001 model showed better correlation fit when analyzing *all data*, with ρ^2 equals to 0.73 when compared to ρ^2 equals to 0.68 from the analysis using S2006. Even though, RMSE obtained from S2006 model (0.27 m) was slightly lower than that obtained with R2001 (0.35 m). This may indicate that, R2001 describes better the tendency of the correlation, but the scatter verified when using this model is higher. In general, however, high ρ^2 and low RMSE obtained from the

TABLE 3.2: Results of the linear regression ($y = Kx$) between the measured S_{ig} and different parameters.

Relation	Slope(K)	ρ^2
$S_{ig} \times H_0$	0.55	0.30
$S_{ig} \times L_0$	0.01	0.24
$S_{ig} \times T_0$	0.09	0.31
$S_{ig} \times \tan\beta$	11.3	-0.30
$S_{ig} \times \tan\beta^{-0.5}$	0.22	0.65
$S_{ig} \times \xi_0$	0.80	-1.18
$S_{ig} \times \Omega$	0.19	-1.28
$S_{ig} \times (H_0L_0)^{0.5}$	0.06	0.67
$S_{ig} \times \tan\beta(H_0L_0)^{0.5}$	0.73	0.44
$S_{ig} \times (\tan\beta H_0L_0)^{0.5}$	0.22	0.71
$S_{ig} \times (H_0L_0/\tan\beta)^{0.5}$	0.01	-0.09

analysis with all data, reflects the good predictive capability of S2006 and R2001 when calculating the infragravity swash.

3.3.2. Infragravity swash parameterization

Several parameters containing information about beach morphology were tested to verify their relation to the infragravity swash. The results are presented in Table 3.2.

The best correlation was found when relating the infragravity swash to the parameter $(\tan\beta H_0L_0)^{0.5}$ ($\rho^2 = 0.71$) proposed in R2001, followed by the $(H_0L_0)^{0.5}$ ($\rho^2 = 0.67$) from S2006. The slope observed in the relation with the R2001 parameter was equal to 0.22, slightly lower than the value obtained by Ruggiero et al. (2001) who found $K = 0.27$. High correlation was also verified with the $\tan\beta^{-0.5}$ ($\rho^2 = 0.65$). This parameter was then tested in a composition with other parameters and an interesting pattern was verified when plotting the infragravity swash from all experiments respect to $(H_0L_0/\tan\beta)^{0.5}$. The results obtained from that relation clearly show three groups of beaches that present the same behaviour regarding S_{ig} values (Figure 3.3). Different regression slopes were obtained when the groups were fitted separately, and the beaches comprised in each group presented similar characteristics:

- Group 1: the first group comprised the data from the Duck experiments. These data represent the most reflective conditions (higher ξ_0 and lower Ω) with coarser sediment size ($D_{50} > 0.36$ mm).
- Group 2: the second group included Scripps beach, Truc Vert beach, and the Somo profiles. These beaches presented reflective to intermediate states according to the instantaneous ξ_0 and Ω values during the experiments, with D_{50} values ranging between 0.28mm and 0.35 mm.
- Group 3: the third group comprised the dissipative experiments at the Agate and Terschelling beaches. In this case, the D_{50} in both beaches was around 0.2 mm.

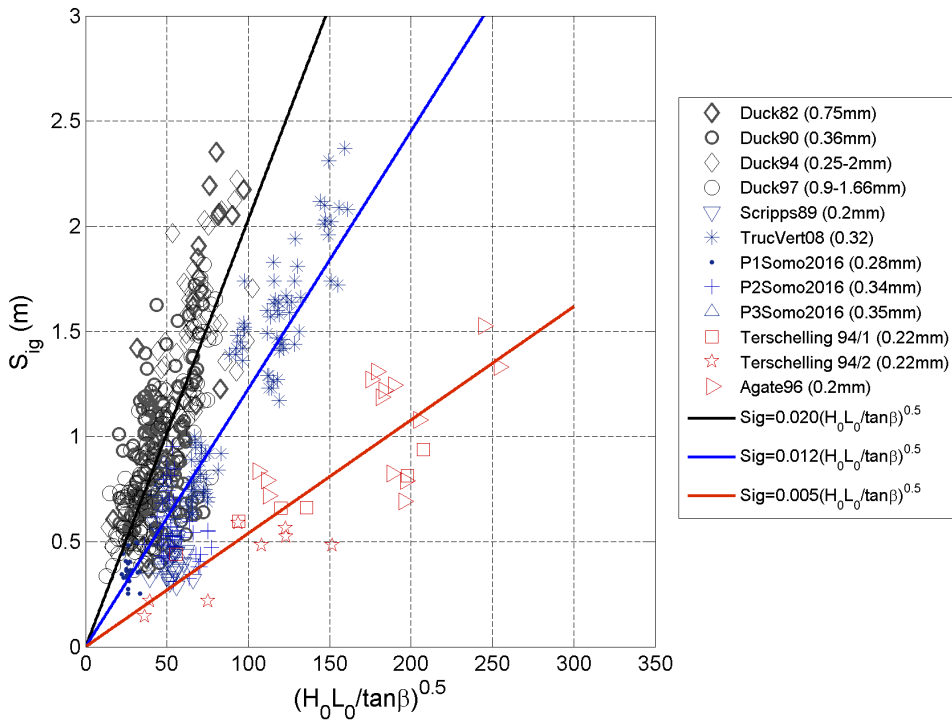


Figure 3.3: Linear regression between S_{ig} y $(H_0 L_0 / \tan \beta)^{0.5}$ (passing through the origin). Colors represent three groups of beaches: coarse sediment beaches (black), beaches with intermediate sediment size (blue) and fine sediment beaches (red).

The distinction of groups with different sediment underscores the need for evaluating the swash in terms of morphodynamic parameters like the foreshore slope and

grain size. The sediment size is partially responsible for the slope of the profile. Besides, it determines the capacity of the seabed to allow water percolation during the uprush and backwash, and may be relevant for swash predictions.

The use of $(H_0L_0/\tan\beta)^{0.5}$ is equivalent to the horizontal (cross-shore) excursion of the infragravity swash when using the R2001 parameter (i.e. $S_{igH} = S_{ig}/\tan\beta$). Hence, the correlation between the horizontal swash S_{igH} and the parameter $(H_0L_0/\tan\beta)^{0.5}$ was assessed as:

$$S_{igH} = K \left(\frac{H_0L_0}{\tan\beta} \right)^{0.5} \quad (3.3)$$

where K is the slope of the linear regression. The regression fit is presented in Figure 3.4. The parameterization using the horizontal swash and the parameter $(H_0L_0/\tan\beta)^{0.5}$ resulted in $\rho^2 = 0.79$, what represents a 12% and 8% improvement if compared to the correlation with the parameters proposed by S2006 ($\rho^2 = 0.67$) and R2001 ($\rho^2 = 0.71$), respectively. The best fit was obtained with $K = 0.26$:

$$S_{igH} = 0.26 \left(\frac{H_0L_0}{\tan\beta} \right)^{0.5} \quad (3.4)$$

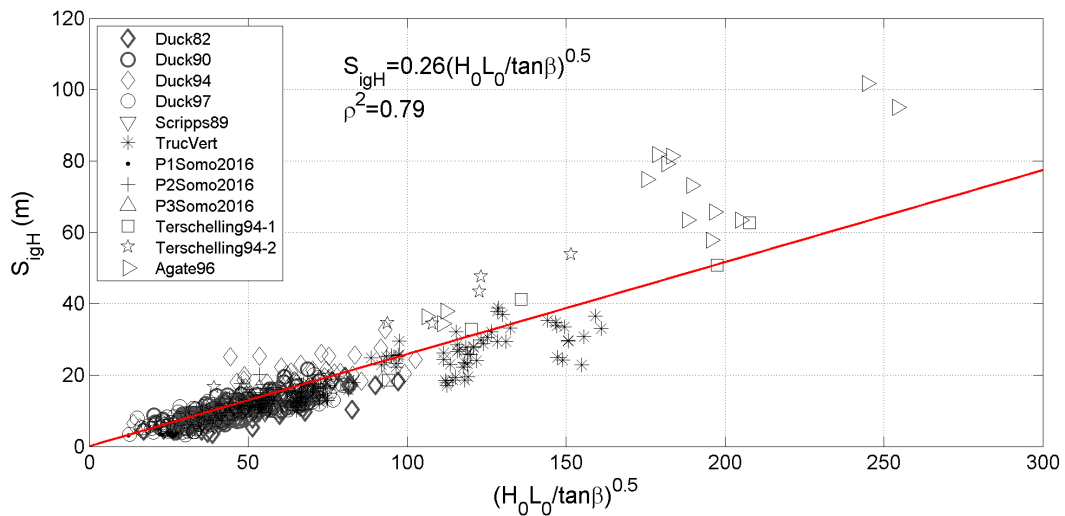


Figure 3.4: Regression fit between S_{igH} and $(H_0L_0/\tan\beta)^{0.5}$.

The improvement in the correlation when using the horizontal excursion instead of the vertical one, may be related to the representation of the swash in low sloping

beaches. In highly dissipative conditions, due to very flat profiles, the vertical excursion of the long wave is minimal, while the horizontal excursion (inundation) is very significant. The detection of vertical swash in these cases is, then, very subjective to errors during measurements and estimations. It seemed intuitive, then, to represent the infragravity swash using the horizontal component rather than the vertical one. Still, the disposition of the data in Figure 3.4 shows some underestimation regarding the values from highly dissipative conditions, which are distributed over the fitted curve (i.e. Terschelling and Agate beach).

3.3.3. The role of the morphodynamic beach state

The tendencies observed in Figure 3.3 and the differences in the model fit presented in Figure 3.4 indicate different infragravity swash behaviour according to the morphodynamic and sediment size characteristics. Based on this, it was assumed the hypothesis that K from eq. 3.3 may not be a constant, but a function of the morphodynamic beach state and the relation between the value of K and the beach state was tested. Given the importance of the previous sea state in the current morphodynamic conditions, the parameters Ω^* was used to establish the relation with K . Data from the Global Ocean Wave (GOW) database (Reguero et al., 2012) obtained from points in front of the beaches (Figure 3.5) were used to calculate Ω^* for each of the experiment from previous works (Ω^* for MUSCLE-Beach experiment was presented on Chapter 2). The wave data were deshoaled (or shoaled) from the GOW depth until a depth equals to 80 m.

With that information, the $\Omega = H_0/\omega_s T_p$ values were established for the D days previous to the field experiment. Finally, Ω^* was established according to eq. 2.2 (Chapter 2) using the parameters $D=30$ days and $\phi=5$ days.

K values, obtained from each experiment dataset as the slope of the linear regression between S_{igH} and $(H_0 L_0 / \tan \beta)^{0.5}$ showed to be related to Ω^* (Figure 3.6).

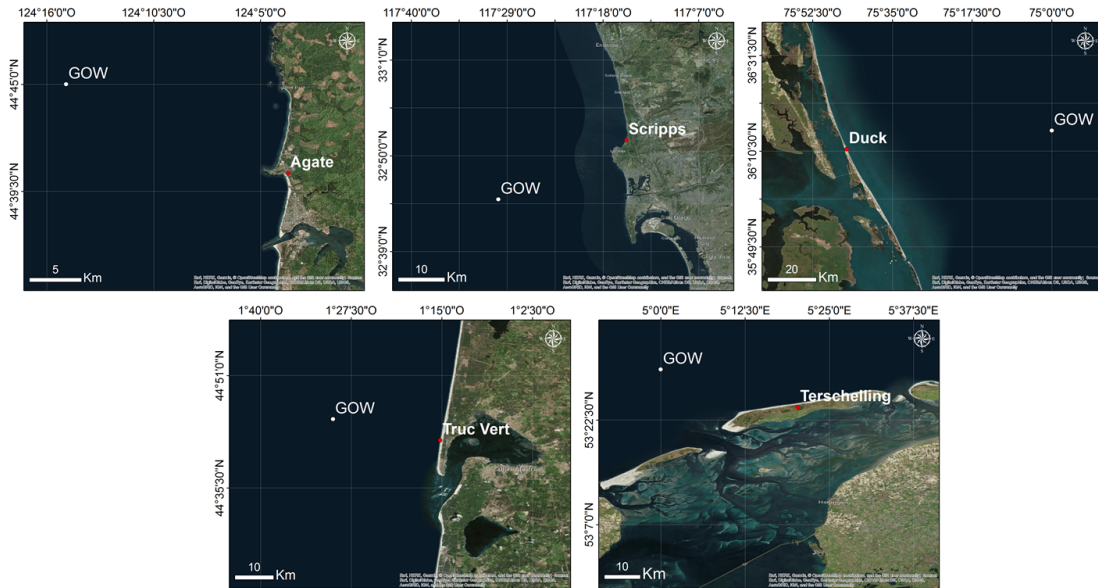


Figure 3.5: Points of the GOW database used to calculate Ω^* for each experiment.

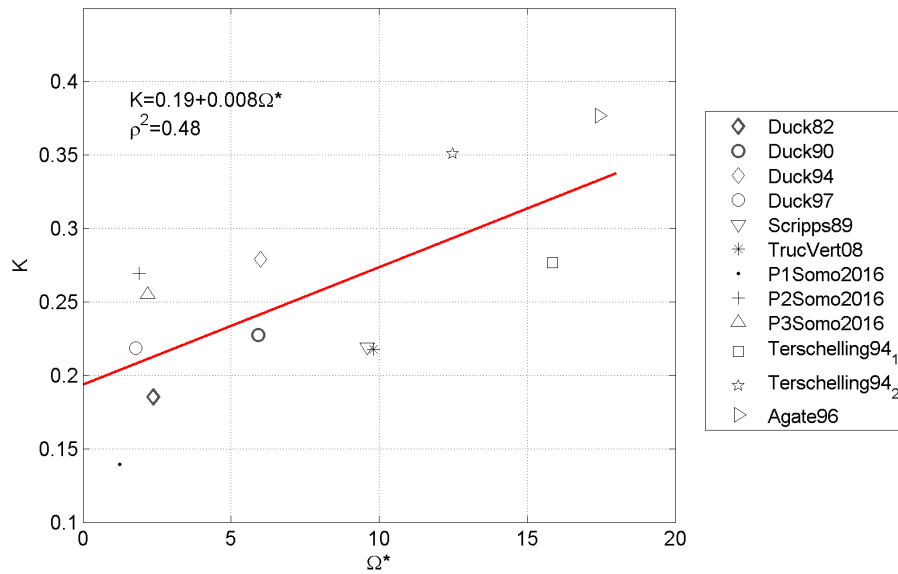


Figure 3.6: Linear regression between K and Ω^* from each experiment. Symbols represent the dataset from each experiment and the red line is the best fit obtained.

Substituting the relation presented in Figure 3.6 [$K = f(\Omega^*)$] into eq. 3.3, the parameterization considering the foreshore slope and the morphodynamic beach state then becomes:

$$S_{igH} = \left(0.19 + 0.008\Omega^*\right) \left(\frac{H_0 L_0}{\tan\beta}\right)^{0.5} \quad (3.5)$$

3.3.4. Evaluation of the infragravity swash parameterization

Statistics obtained from the performance analysis of horizontal infragravity swash parameterization using eq. 3.4 and eq. 3.5 are presented in Table 3.3. It should be noted that vertical and horizontal infragravity swash (Tables 3.1 and Table 3.3, respectively) have different magnitudes and higher values are therefore expected from dimensional statistical errors when analysing the horizontal (cross-shore) variable. Furthermore, magnitudes may vary from one beach type to another. Mean values for measured (S_{igH}) and calculated (S_{igHc}) data are presented to evaluate the significance of statistical errors. A general analysis of all the datasets shows calculated values in good agreement with the measured ones. Performance analysis of eq. 3.5 showed an improvement of the horizontal infragravity swash prediction in comparison to that obtained with constant K (eq. 3.4). ρ^2 increased to 0.87 and RMSE reduced from 5.60m to 4.56m (ρ^2 shown in Figure 3.7 and RMSE shown in Table 3.3).

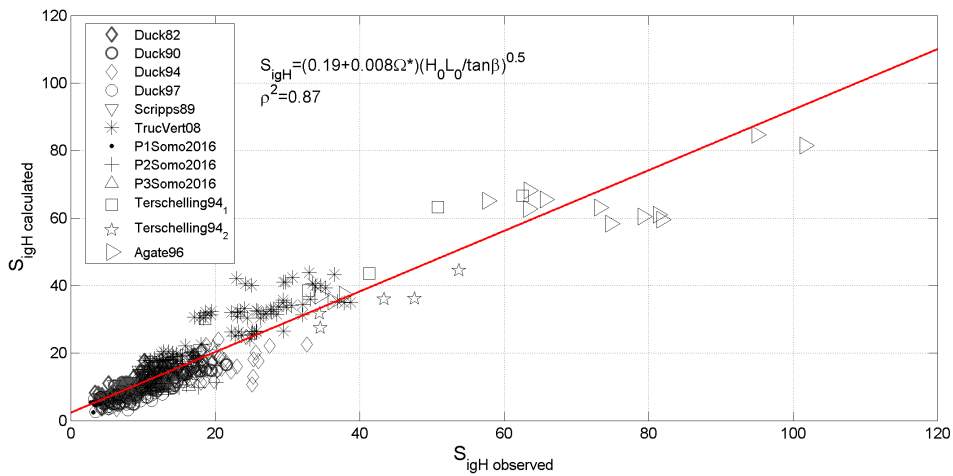


Figure 3.7: Regression fit between measured horizontal infragravity swash S_{igH} and the values calculated S_{igHc} with the parameterization using $K = f(\Omega^*)$.

TABLE 3.3: Performance evaluation of infragravity swash parameterization for each experiment using Eq. 3.4 (K constant) and Eq. 3.5 (K as a function of Ω^*).

Experiment	Measured	Eq. 3.4		Eq. 3.5	
	$\overline{S_{igH}}(m)$	$\overline{S_{igHc}}(m)$	RMSE(m)	$\overline{S_{igHc}}(m)$	RMSE(m)
Duck82	9.75	13.85	4.76	11.43	2.75
Duck90	10.48	11.75	2.54	10.98	2.19
Duck94	17.49	15.90	4.41	14.90	4.83
Duck97	9.65	11.20	2.82	9.03	2.18
Scripps89	11.77	13.83	2.57	14.50	3.14
Terschelling94/1	36.81	34.85	5.12	43.31	7.65
Terschelling94/2	32.57	24.16	10.02	27.51	6.73
Agate96	67.56	46.46	24.06	59.99	12.62
TrucVert08	22.39	26.50	5.88	27.97	7.06
P1Somo2016	3.44	6.22	2.95	4.91	1.67
P2Somo2016	13.50	12.88	3.14	10.43	4.33
P3Somo2016	12.17	12.27	1.94	10.05	2.85
All data	15.28	16.23	5.60	16.03	4.56

TABLE 3.4: Performance evaluation of infragravity swash parameterization for intermediate and dissipative beaches using Eq. 3.4 (K constant) and Eq. 3.5 (K as a function of Ω^*).

Experiment	Measured	Eq. 3.4		Eq. 3.5	
	$\overline{S_{igH}}(m)$	$\overline{S_{igHc}}(m)$	RMSE(m)	$\overline{S_{igHc}}(m)$	RMSE(m)
Intermediate beaches	16.98	16.98	19.85	20.37	5.58
Dissipative beaches	67.56	67.56	46.46	59.99	12.62

The analysis of both equations for each experiment revealed higher RMSE values for Agate and Terschelling, typically dissipative beaches. This can be related to the magnitude of the horizontal swash in that beach type. The average S_{igHc} at these beaches are in the order of dozens of meters, much higher than those verified at the other beaches analyzed.

In order to evaluate the performance of eq. 3.4 and eq. 3.5 when applied to beaches with different morphodynamic characteristics, an analysis for each beach state was carried out. The beaches were classified according the Ω^* values as reflective ($\Omega^* \leq 1.5$), intermediate ($1.5 < \Omega^* \leq 5.5$) and dissipative ($\Omega^* > 5.5$). Since only P1 (Somo) was classified as reflective, the performance regarding this beach state was not assessed. Average $\overline{S_{igH}}$ and RMSE errors obtained from this analysis are presented in Table 3.4 .

The improvement of the predictions from eq. 3.4 to eq. 3.5 in both, intermediate and dissipative beaches, is evident. RMSE error decayed from 19.85 m to 5.58 m in intermediate beaches and from 46.46 m to 12.62 m in dissipative beaches. In order to evaluate the improvement from previous proposed formula, the correlation coefficient obtained from the regression analysis between observed and calculated data for each beach state using R2001, S2006, eq. 3.4 and eq. 3.5 was compared (Figure 3.8). The results obtained from eq. 3.4 and eq. 3.5 showed better correlation if compared to those obtained by R2001 and S2006. The most important difference was verified when analyzing data from dissipative beaches, for which ρ^2 rises from 0.77 and 0.55 using R2001 and S2006 models, to 0.91 and 0.92 using eq. 3.4 and eq. 3.5.

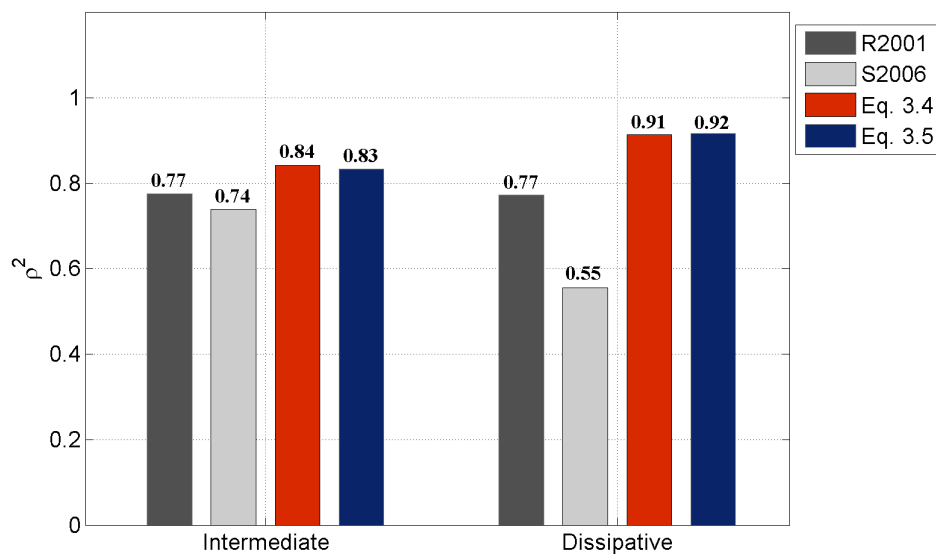


Figure 3.8: Correlation coefficient obtained from the linear regression analysis between measured and calculated infragravity swash for beaches under intermediate and dissipative conditions.

The difference between ρ^2 obtained from R2001 and the value obtained from eq. 3.4 (horizontal version of R2001 parameterization), for both intermediate and dissipative beaches, reflects the importance of using the horizontal excursion of the infragravity swash, instead of the vertical value.

3.4. Discussion

Regression analysis confirmed S2006 results, and no improvement was verified in the correlation with the Hunt scaling $\tan\beta(H_0L_0)^{0.5}$ (Figure 3.9), commonly used in previous works to represent oscillations in the coastline (e.g Hunt, 1959; Nielsen and Hanslow, 1991). ρ^2 was 0.44 in comparison to the 0.67 obtained with the S2006 parameter $(H_0L_0)^{0.5}$ (see parameters analysis in Table 3.2).

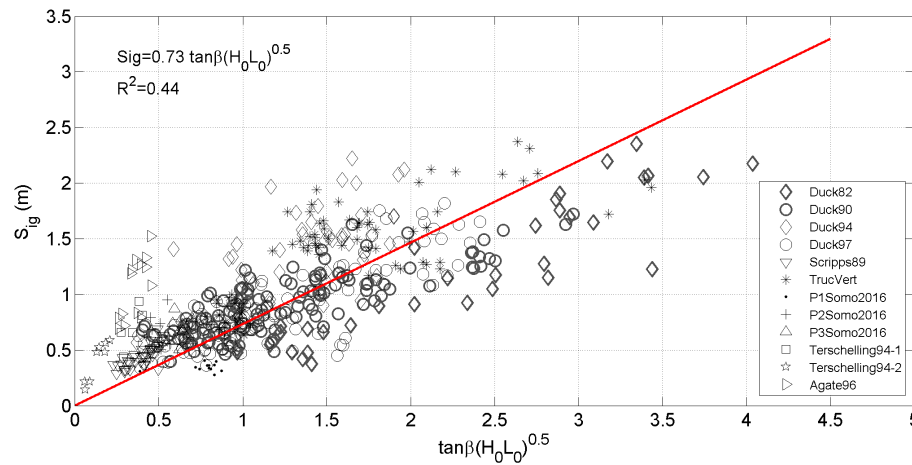


Figure 3.9: Linear regression fit between measured S_{ig} and the Hunt scaling.

Ruessink et al. (1998) analyzed the infragravity runup at Terschelling beach and no correlation with the foreshore slope was verified. Nevertheless, the result was influenced by the small range of $\tan\beta$ in their dataset, obtained from one beach. Atkinson et al. (2017) discussed about the importance of the predominance of data from one beach in S2006 data, since most part of their dataset was composed of measurements made at Duck beach. The data from Duck also represents a great amount of the dataset in the present work (52%). This could explain why there was less correlation when relating the infragravity swash to the Hunt' scaling parameter, since variations of $\tan\beta$ are not expected to be so representative in one single beach. Still, the correlation with $\tan\beta(H_0L_0)^{0.5}$ when not considering Duck data (not shown) resulted in no significant difference from the correlation analysis using the whole dataset (ρ^2 was still 0.44) and this hypothesis was rejected.

The R2001 parameter, that includes $\tan\beta^{0.5}$, on the other hand, showed better correlation than the one verified with S2006 parameter. The improvement in the correlation when adding the square root of the foreshore slope, indicates that there is a link with the gradient of the swash zone, although this relation is not linear. The correlation between S_{igH} and $\tan\beta^{-0.5}$ may be related to the behavior of long waves that are reflected in the coast. Guza et al. (1984) demonstrated that when the wave steepness is low, the waves reflect at the beach and travels back, generating a standing wave system. The oscillations in the swash zone, then, can be described by the standing wave solution of linear theory in which the swash is proportional to $H(\pi/2\tan\beta)^{0.5}$ (see Figure 1.6, in Chapter 1), similar to the relation proposed here. This is particularly true for infragravity waves that present small amplitude in comparison to the wave length. Raubenheimer and Guza (1996) suggested that the infragravity waves in the surf zones often assumes the form of a free cross-shore standing wave that are nearly completely reflected at the shoreline. With exception of very dissipative conditions, the infragravity waves rarely dissipates on swash zone and reflection coefficients are usually around 1, what makes reasonable to apply the standing wave solution parameters to calculate the infragravity swash.

Additional improvement in the model performance was verified when adding Ω^* to the infragravity swash parameterization. The slope K (from eq. 3.3) showed reasonable correlation to Ω^* ($\rho^2 = 0.48$), despite of the scatter verified. This result represents the influence of the morphodynamic characteristics in the low frequencies oscillations at the beach. The relation with Ω^* , not observed with the instantaneous Ω , reflects the importance of the previous wave conditions in the current morphodynamic beach state and, consequently, in the resultant infragravity swash. There is, however, many morphodynamic factors that are not accounted in that parameter and that may be also relevant when introducing the morphodynamic information to the infragravity swash parameterizations. In a recent work, Baldock et al. (2017) showed that the current morphodynamic conditions highly depends on the order of the previous morphodynamic beach states and that more than one equilibrium shape may exist for the same constant wave

conditions. Atkinson et al. (2017), in turn, tested the influence of the tidal stage (high tide, mid tide or low tide) on the capability of runup models to predict the oscillations in the swash zone. The performance of the runup models was different in each tidal moment. The current water level determines the part of the profile that is submerged, the breaking pattern and other process that may occur in the surf zone. During low tide, the breaking process becomes important and more dissipative conditions are expected. The opposite occurs during high tide. The result achieved by Atkinson et al. (2017) may be related to the capacity of each model to represent the different morphodynamic characteristics observed in each tidal moment. However, the parameterization of such complex process is not clear yet and further analyses are necessary regarding the best way to take them into account in the morphodynamic parameter. Furthermore, the tidal level determines the water saturation of the seabed in the swash zone (Raubenheimer et al., 1995), what can have a direct effect on swash values. Vousdoukas (2014) showed that, during mid and low tide, the mean uprush and backwash velocities were higher due to the saturation of the ground that takes to low capacity of filtering the water. Those factors are usually not accounted in swash parameterizations, which have the objective to be simple and pragmatic. With the aim of verifying the prediction capability of the formula proposed here in each tidal moment, the dataset used in this work was separated according to the tidal stage. The cutoff tidal elevations were arbitrarily taken as the level correspondent to $+\text{std}(\text{tide})$ and $-\text{std}(\text{tide})$ ($\text{std}=\text{standard deviation}$) to separate high-mid tide and mid-low tide, respectively. The regression fit between measured and calculated values for the three groups indicate that eq. 3.5 is capable of representing properly the S_{igH} in all tidal moments (Figure 3.10).

3.5. Summary and Conclusions

This chapter presented the analysis of parameters related to the infragravity swash on beaches. Taking the parameterizations presented by Stockdon et al. (2006) and Ruggiero et al. (2001) as a starting point, an empirical formulation was defined

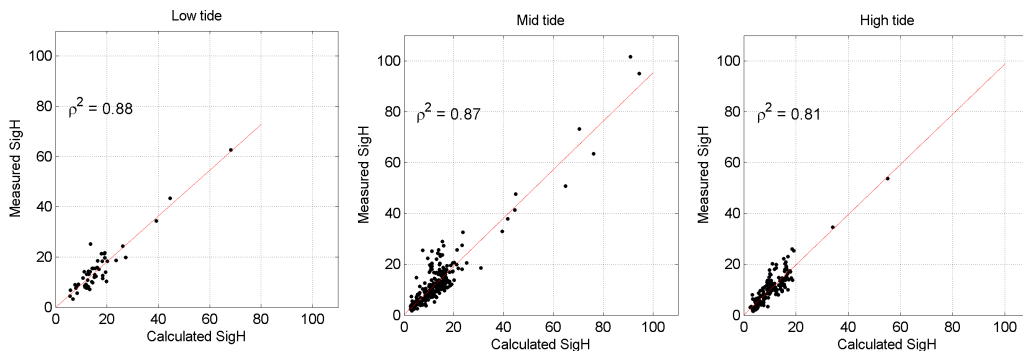


Figure 3.10: Linear regression fit between measured and calculated S_{igH} (using eq. 3.5) for data obtained during different tidal moments (high, mid and low tide).

based on field data from 10 experiments. The aim was to include the effect of the morphology and morphodynamic of the beach in a simple infragravity swash parameterization.

Performance analysis confirmed the S2006 model's ability to predict runup in beaches with different characteristics. However, high dispersion indicated the need to account for other parameters. The R2001 model also showed to be in agreement with measured data. The improvement in the correlation when adding the square roots of the foreshore slope, indicates that there is a link with slope of the profile. The dependence, however, is not linear and that may be the reason why the relation between S_{ig} and $\tan\beta$ could not be verified in earlier efforts.

A clear tendency was verified when relating the vertical excursion of the infragravity swash to the parameter $(H_0L_0/\tan\beta)^{0.5}$. Beaches with different morphological characteristics presented different swash behavior, highlighting the need for a parameterization that differentiated morphodynamic conditions. The representation of the infragravity swash by its horizontal component resulted in significant improvement in the estimations, and the slope of the regression between S_{igH} and the parameter $(H_0L_0/\tan\beta)^{0.5}$ showed to be related to the morphodynamic condition of the beach. These results highlight the effect of the morphodynamic beach state on the low frequency oscillations at the beach and, hence, on determining infragravity swash values. The use of Ω^* (eq. 2.2), however is a first proxy, and further analyzes regarding other factors that may be important are necessary.

Based on the results obtained, two empirical parameterizations were proposed for infragravity swash predictions (eqs. 3.4 and 3.5) and the choice to use one or the other will depend on the available data from the site of interest. Given the importance of the morphodynamic beach state, the use of eq. 3.5 is recommended. On the other hand, the first equation is suitable for those situations where sediment information (to calculate the beach state) is not available, or in any situation where ascertaining the morphodynamic condition through Ω^* (eq. 2.2) is not possible.

Chapter 4

Incident swash analysis and parameterization

4.1. Introduction

The preceding chapter dealt with the analysis and parameterization of the low frequency component of the swash, S_{ig} ($f < 0.05Hz$). In this chapter, the same process will be carried out concerning the high frequency component, S_{inc} ($f > 0.05Hz$).

As explained before (see State of the Art in Chapter 1), there is a connection between the amount of reflection of the wave energy and the amplitude of the swash at shoreline. The data measured in Somo beach also highlighted the importance of taking the reflection process into account when analyzing swash values (see Chapter 2). The higher the reflection is, the higher the relative swash (S/H) is expected to be. Part of the reflection process can be described by the Iribarren number (Raubenheimer and Guza, 1996; Seelig and Ahrens, 1981) used in many runup and swash parameterizations. However, a single formula comprising ξ_0 may not be enough to describe the incident swash in conditions of different amount of reflection at the shoreline (*i.e.* different beach morphodynamic state).

Muttray et al. (2006) proposed that the runup on a structure is related to the amplitude of the stationary wave at the shoreline and, so, it can be parameterized using the reflection coefficient. A similar relation applied to beaches was not tested yet, possibly due to the lack of knowledge about the wave reflection on beaches.

Guza et al. (1984) (hereinafter G1984), in turn, based on the hypothesis of reflection and saturation proposed by Miche, presented three different formulas to calculate the swash of monochromatic waves in conditions of different amount of reflection:

$$\frac{S}{H} = \begin{cases} 3\xi_0^2/\pi & \text{if } \xi_0 < \xi_c \text{ (saturated regime)} \\ (2\pi\beta)^{-1/4}\xi_0 & \text{if } \xi_c/3 < \xi_0 < \xi_c \text{ (transition regime)} \\ (\pi/2\tan\beta)^{1/2} & \text{if } \xi_c < \xi_0 \text{ (reflective regime)} \end{cases} \quad (4.1)$$

where ξ_0 is the Iribarren number and $\xi_c = \left| \frac{\pi^3}{2\tan\beta} \right|^{1/4}$ is the minimum value for complete reflection.

The relation presented by G1984 have been shown to be qualitatively consistent with field measurements and modeled data (Elgar et al., 1994; Raubenheimer and Guza, 1996). However, a quantitative analysis to allow the application of this monochromatic based model to real beaches (and irregular waves) have not been devised yet.

Hence, the analysis presented in this chapter was based on the two relations described above (Muttray et al., 2006 and G1984). Both approaches were tested to provide some insight into the environmental parameters to quantify the wave reflection and the incident swash. Finally, with the aim of improving the S_{inc} estimations on beaches, a new parameterization was developed.

4.2. Methods

The analysis regarding the high frequency swash on beaches was addressed in two different lines. First, we used the dataset from Somo beach to analyze the reflection coefficient and its effect on swash values. Afterwards, we directed our analysis to the monochromatic based model presented by G1984, and developed a new parameterization for describing the incident swash of irregular waves in different morphodynamic conditions.

4.2.1. Dataset

The dataset from the MUSCLE-Beach Experiment (2016 and 2017) and the dataset from previous works (the same used in Chapter 3) were used to accomplish the goals proposed in this chapter.

4.2.2. S_{inc} estimation using G1984 and S2006 formulas

To allow further comparison to the results presented in the following items of this chapter, the prediction capability of the formulas proposed by S2006 (based on the Hunt scaling $\tan\beta(H_0L_0)^{0.5}$), and the formulas proposed by G1984 was verified. The former for being the most extensive formula based on field measurements proposed until now and the later, because it is the one which the following analysis and parameterization will be based on.

The incident swash according to S2006 is calculated as:

$$S_{inc} = 0.75 \tan\beta(H_0L_0)^{0.5} \quad (4.2)$$

The swash based on G1984 is calculated according to the regime in which the dataset is included (eq. 4.1). G1984 model was based on monochromatic wave

data and some adaptations were necessary to apply it to calculate the incident swash of irregular waves:

- S_{inc} values obtained from spectral analysis were used instead of total S ;
- the parameters H , L and T , used in eq. 4.1 and also in ξ_0 and ξ_c formulas, were replaced by the spectral parameters H_0 , L_0 and T_p .

4.2.3. Wave reflection and the incident swash at Somo beach

Somo data was analysed to verify the applicability of the reflection coefficient to calculate the incident swash. The steps of the analysis are shown in Figure 4.1. The free-surface and cross-shore velocity series were used to calculate the reflection coefficient (K_r^2) of each sea state. The relation between K_r^2 and different parameters was assessed and the fit to between S_{inc}/H_0 and measured and theoretical K_r^2 was verified.

The squared reflection coefficient (K_r^2) was calculated from the sea surface elevations and cross-shore current fluctuations measured by collocated pressure sensors and velocimeter. The coefficient K_r^2 was obtained at the profiles where velocity and pressure were measured at the same position (P2-2016, P3-2016, P2/2017-1 and P2/2017-2 - Figure 4.2). For the second field experiment, the most seaward measurement point was used.

The estimation of K_r^2 from collocated sensors assumes dominant cross-shore wave propagation. This is particularly true for the measurements taken nearshore at Somo beach, where the cross-shore velocity U was always much higher than the longshore velocity V (Figure 4.3):

The process to calculate K_r^2 is described bellow.

- I. Measured η was separated into shoreward (incoming) and seaward (reflected) waves. Shoreward and seaward signals were crudely estimated using the

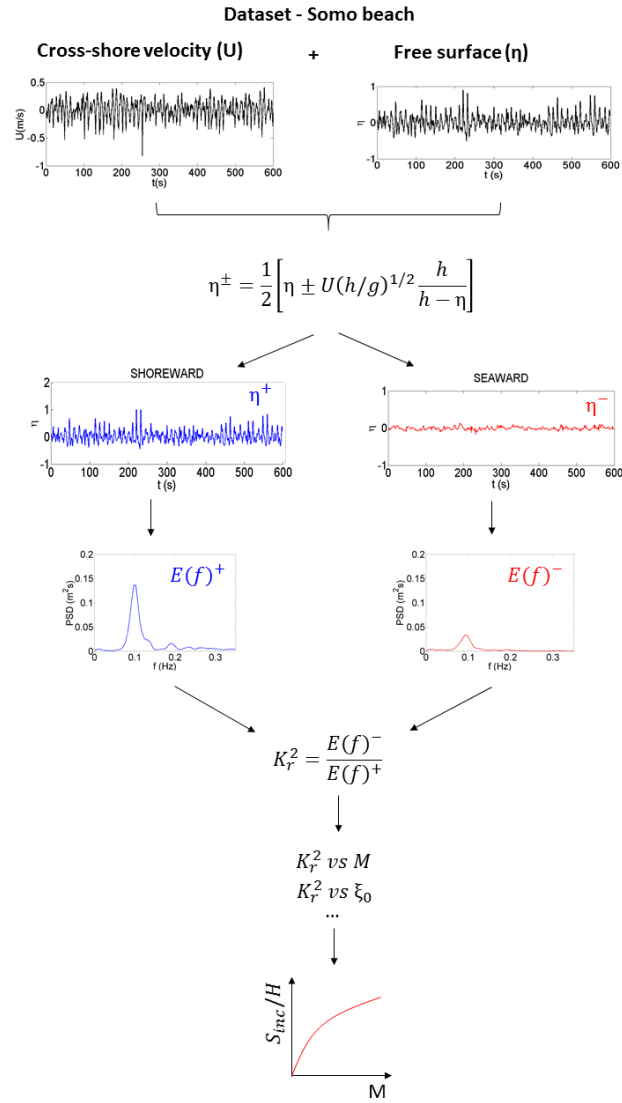


Figure 4.1: Methodology applied to verify the relation between S_{inc}/H_0 and K_r^2 .

method based on the quasi-nonlinear long wave theory proposed by Kubota et al. (1990) (eq. 4.3 and eq. 4.4):

$$\eta^+ = \frac{1}{2} \left[\eta + U \left(\frac{h}{g} \right)^{1/2} \frac{h}{h - \eta} \right] \quad (4.3)$$

$$\eta^- = \frac{1}{2} \left[\eta - U \left(\frac{h}{g} \right)^{1/2} \frac{h}{h - \eta} \right] \quad (4.4)$$

where η is the free surface elevation, U is the cross-shore velocity and h is the water depth at the measurement point. Superscripts $^+$ and $^-$ indicate

MUSCLE-Beach 2016 (P2 and P3)



MUSCLE-Beach 2017 (P2)

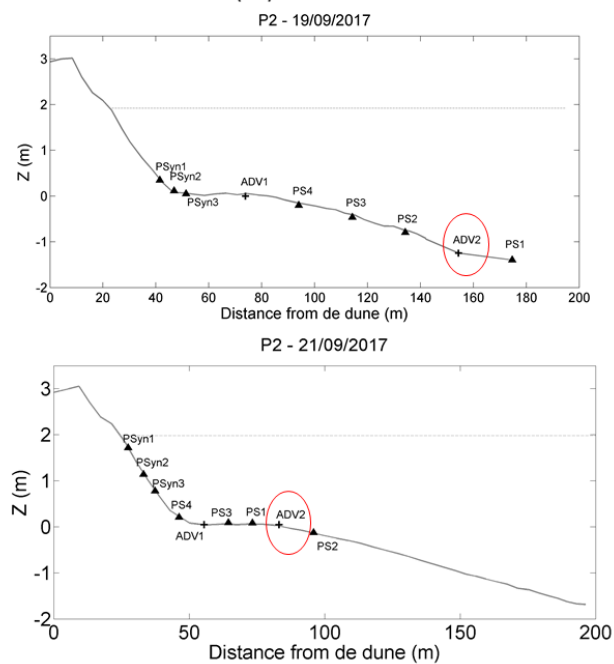


Figure 4.2: Location of the collocated pressure sensor and velocimeter used to calculate K_r^2 .

shoreward and seaward series. Similar method was applied in previous works (e.g. Raubenheimer et al., 1995) and this one, specifically, was chosen because it was validated for real beaches in sites with similar characteristics to those observed at Somo beach during the experiment (similar $\tan\beta$, wave height and period).

- II. The energy spectra $E(f)$ were calculated for both η^+ and η^- .
- III. Finally, the reflection coefficient was calculated as the ratio between the seaward and the shoreward energy integrated along the frequencies of interest

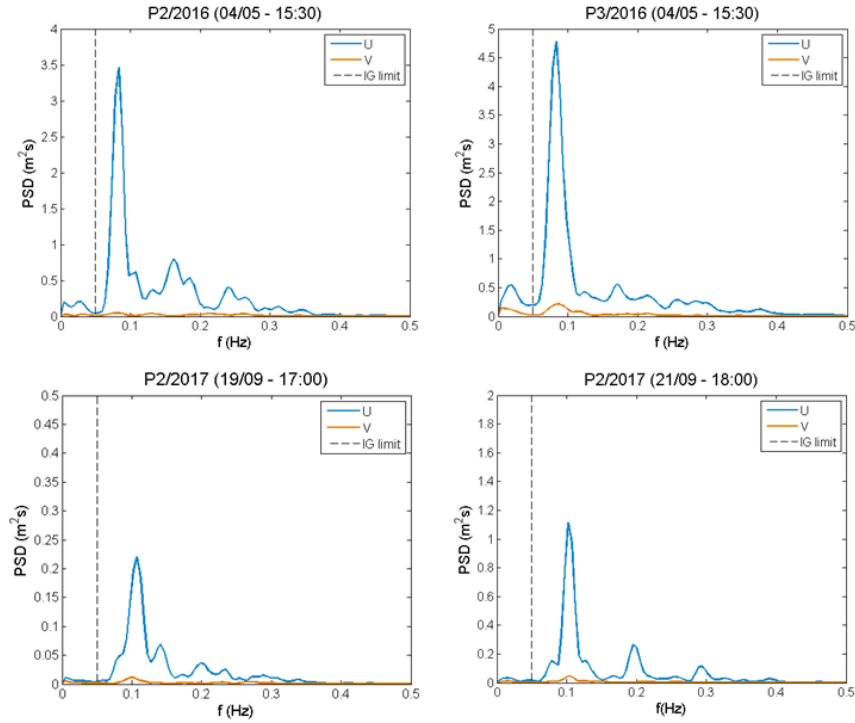


Figure 4.3: Energy spectra of cross-shore velocity U and longshore velocity V at the measurement points.

(eq. 4.5). Here, the final K_r^2 was obtained integrating the incoming and reflected energy along the incident band frequencies (from 0.05 Hz to 0.5 Hz).

$$K_r^2 = \frac{\int E^-(f)dx}{\int E^+(f)dx} \quad (4.5)$$

The analysis with theoretical K_r^2 was based mainly on Miche's number (eq. 4.6), although other parameters were also tested.

$$K_r^2 \approx M = \begin{cases} \frac{16g^2 \tan^5 \beta}{(2\pi)^5 H^2 f^4} & \text{if } M < 1 \\ 1 & \text{if } M \geq 1 \end{cases} \quad (4.6)$$

where M is the Miche's number used as reflection coefficient, g is the acceleration due to gravity and f , is the wave frequency. When applied to irregular waves, M is usually calculated using H_0 and the mean frequency f_m (Ardhuin and Roland, 2012).

4.2.4. S_{inc} parameterization for different morphodynamic conditions based on G1984 model

Looking to the formulas presented by G1984 (eq. 4.1), it was possible to identify one simple form that applies for the saturated, transition and reflective regimes:

$$\frac{S}{H} = a * \tan\beta^b \left(\frac{H}{L}\right)^c \quad (4.7)$$

where a , b and c are coefficients that change according to the regime, such that:

$$S/H = \begin{cases} (3/\pi)\tan\beta^2 \left(\frac{H}{L}\right)^{-1} & \text{(saturated)} \\ (2\pi)^{-0.25}\tan\beta^{0.75} \left(\frac{H}{L}\right)^{-0.5} & \text{(transition)} \\ (\pi/2)^{0.5}\tan\beta^{-0.5} \left(\frac{H}{L}\right)^0 & \text{(reflective)} \end{cases} \quad (4.8)$$

Hunt scaling $\tan\beta(H_0L_0)^{0.5}$ used by S2006 in their S_{inc} parameterization can also be described by the same relation (with $a = 1$, $b = 1$ and $c = -0.5$). The same is true for any relation with the Iribarren number. Thus, in the present work, the structure presented in eq. 4.7 was used to establish the new incident swash parameterization.

the relation between the relative swash (S/H), the foreshores slope ($\tan\beta$) and the wave steepness (H/L) was assessed first, using the whole dataset, and then using only data with similar morphodynamic characteristics. That means that, in this second approach, the coefficients a , b and c were obtained using the dataset from reflective ($\Omega^* \leq 1.5$), intermediate ($1.5 < \Omega^* \leq 5.5$) and dissipative ($\Omega^* > 5.5$) conditions, separately.

4.2.5. Evaluations of S_{inc} parameterization

The parameterization proposed here was evaluated in terms of the whole dataset and in terms of morphodynamic beach state. The results were compared to those obtained using previous parameterizations.

4.3. Results

4.3.1. S_{inc} estimation using G1984 and S2006 formulas

Before establishing the S_{inc} parameterization, the prediction capability of S2006 and G1984 models was tested. To calculate the swash using G1984, it was necessary to identify the regime in which the data was included (according to ξ_0 and ξ_c). The distribution of the dataset used in this work along the three regimes proposed by G1984 is presented in Figure 4.4. All data are distributed over saturated and transition zones and no fully reflective conditions were observed.

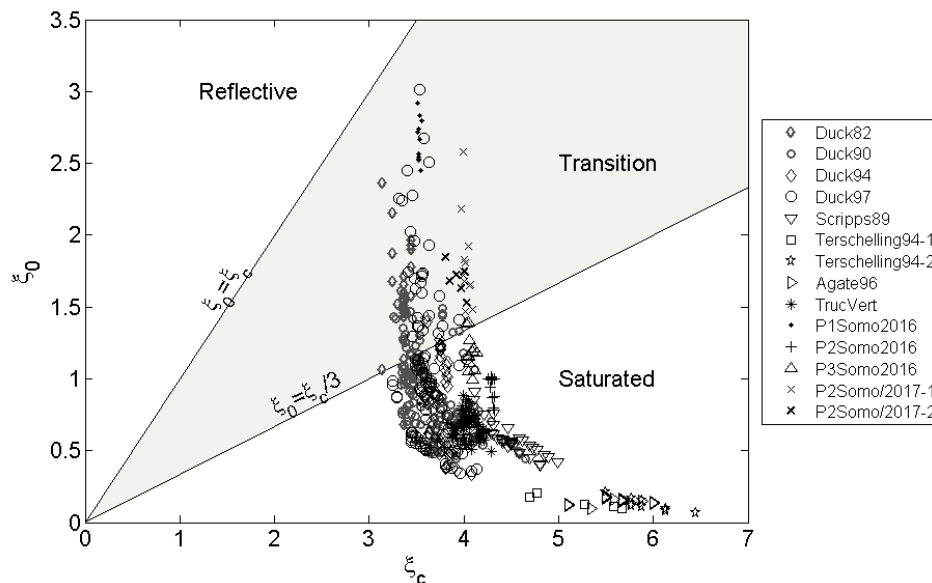


Figure 4.4: Distribution of the dataset used in this work according to the conditions proposed by Guza et al (1984). ξ_0 is the Iribarren number and ξ_c is the minimum value for complete reflection.

The correlation between measured and calculated S_{inc} using both models is presented in Figure 4.5. The tendency of the incident swash is well represented by S2006, although high scatter was observed. Correlation analysis resulted in $\rho^2 = 0.31$ when using that model. Incident swash values obtained from G1984 equations were poorly correlated to measurements, with $\rho^2 = 0.07$. The values obtained for the data that were positioned near to the reflective regime in Figure 4.4 (*i.e.* P1 Somo 2016), were particularly overpredicted. Apparently, the equation for the transitional regime does not apply for those data, a theme that will be further discussed in the next items. The dataset from the extreme dissipative beaches (Terschelling and Agate) are positioned over the line of ideal fit and seemed to be well represented by the saturated conditions.

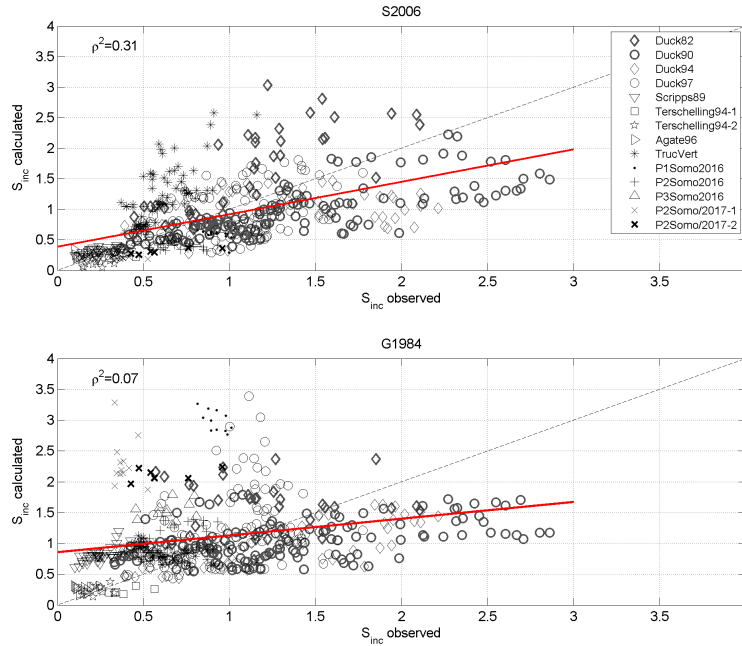


Figure 4.5: Linear regression between S_{inc} observed and calculated with S2006 (up) and G1984 (down) parameterizations. The dashed line represents the ideal fit over which the values would be perfect correlated. The red line is the fit between measured and calculated values.

To assess the validity of both parameterizations when calculating S_{inc} in conditions of different amount of reflection, the correlation was verified for each group of data considering the different morphodynamic beach state. Given the importance of the incident swash on reflective beaches, the dataset from profile P1, Somo beach

TABLE 4.1: Performance evaluation of G1984 and S2006 for all dataset and for different morphodynamic conditions

Condition	G1984		S2006	
	RMSE(m)	ρ^2	RMSE(m)	ρ^2
Dissipative Beaches	0.26	0.38	0.40	0.32
Intermediate beaches	0.60	0	0.46	0.47
Reflective beaches	0.56	0.24	0.08	0.32
All data	0.55	0.07	0.44	0.31

(only reflective condition with $\Omega^* < 1.5$), was assessed alone. However, conclusions obtained from here must be taken carefully given the low variability of that dataset.

Statistical results of the analysis between measured and calculated S_{inc} are presented in table 4.1. S2006 represented better the intermediate conditions ($\rho^2 = 0.47$) if compared to the results from the other beach states (reflective and dissipative beaches resulted in $\rho^2 = 0.32$).

When analysing the dataset calculated with G1984, the correlations show low prediction capability for the majority of the conditions analysed. This was expected due to the monochromatic approach in which the formulas were developed. Still, the analysis regarding dissipative beaches showed better fit than it was obtained with S2006. Lower RMSE (0.26 m) and higher ρ^2 (0.38) were obtained using G1984 model for this beach type. These results indicate some weakness on the representation of the incident swash of dissipative beaches by S2006 model.

Under dissipative conditions, the dissipation due to wave breaking is important and it makes sense that an approximation to the saturated regime results in better correlation with measured incident swash values. This fact becomes clear if we analyse the dataset from dissipative beaches separately. Figure 4.6a shows the plot of S_{inc}/H_0 as a function of the Iribarren number for the dataset classified as dissipative. The fit to ξ_0^2 , as proposed by Guza for saturated conditions, represents better the distribution of the dataset if compared to the function of ξ_0 used by S2006 for all beach types. The error between the measured data and the fitted curve using ξ_0 ($S_{inc}/H_0 = K\xi_0$) and using ξ_0^2 ($S_{inc}/H_0 = K\xi_0^2$) is presented in Figure 4.6b. Lower error was verified along the whole range of ξ_0 when applying

the function of ξ_0^2 . This confirms that G1984 parameters and coefficients result in better estimation of the incident swash on dissipative beaches.

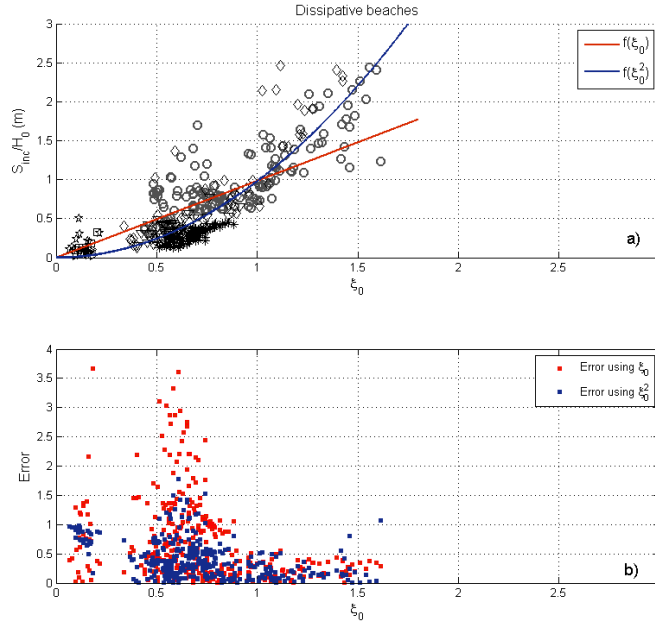


Figure 4.6: a) Relation between S_{inc}/H_0 and ξ_0 for dissipative beaches. Red and blue lines represent the linear and the quadratic relation between both variables respectively. Black Symbols represent the same beaches as presented in previous figures. b) Error associated with each fit ($Error = |(Predicted - Observed)/Observed|$). Note that the morphodynamic beach state was determined using Ω^* .

4.3.2. Wave reflection and the incident swash at Somo beach

The reflection coefficient obtained from the measurements undertaken at Somo beach and its relation to the incident swash were assessed and the results are presented below.

Examples of the shoreward and seaward (reflected) wave series (η), their energy spectra and the resultant $K_r^2(f)$ are presented in Figure 4.7 and Figure 4.8. The shoreward signal was always more significant than the seaward signal, typical behaviour observed on natural beaches. In general, $K_r^2(f)$ was high at infragravity

¹K = the slope of the linear regression.

frequencies ($0.003 < f < 0.05 \text{ Hz}$) (some values higher than 1) during both experiments. This is the result of the longwave resistance to dissipation. Infragravity waves (low f) usually results in low steepness, low wave dissipation due to breaking and, so, higher reflection.

Significant differences are evident in $K_r^2(f)$ values at incident frequencies ($0.05 < f < 0.5 \text{ Hz}$) from both experiments (Figure 4.7 and Figure 4.8).

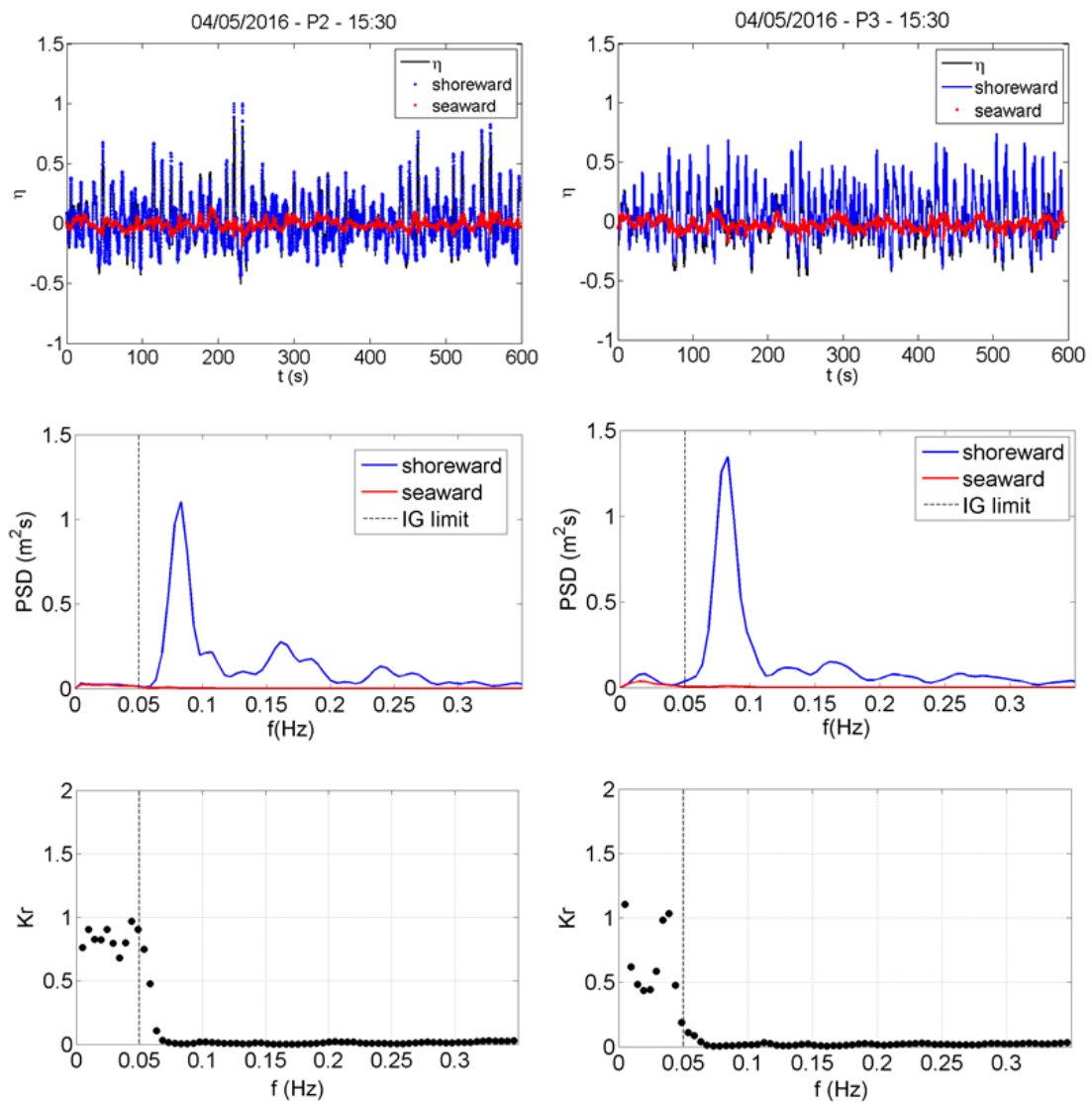


Figure 4.7: Example of the shoreward and seaward (reflected) wave series (upper panels), wave energy density (middle panels) and $K_r^2(f)$ (lower panels) at profiles P2 and P3, during the first experiment (05/2016).

During MUSCLE-Beach 2016 (Figure 4.7), K_r^2 values within the incident band were very small, less than 0.05, increasing to a maximum 0.8 in the vicinity of the

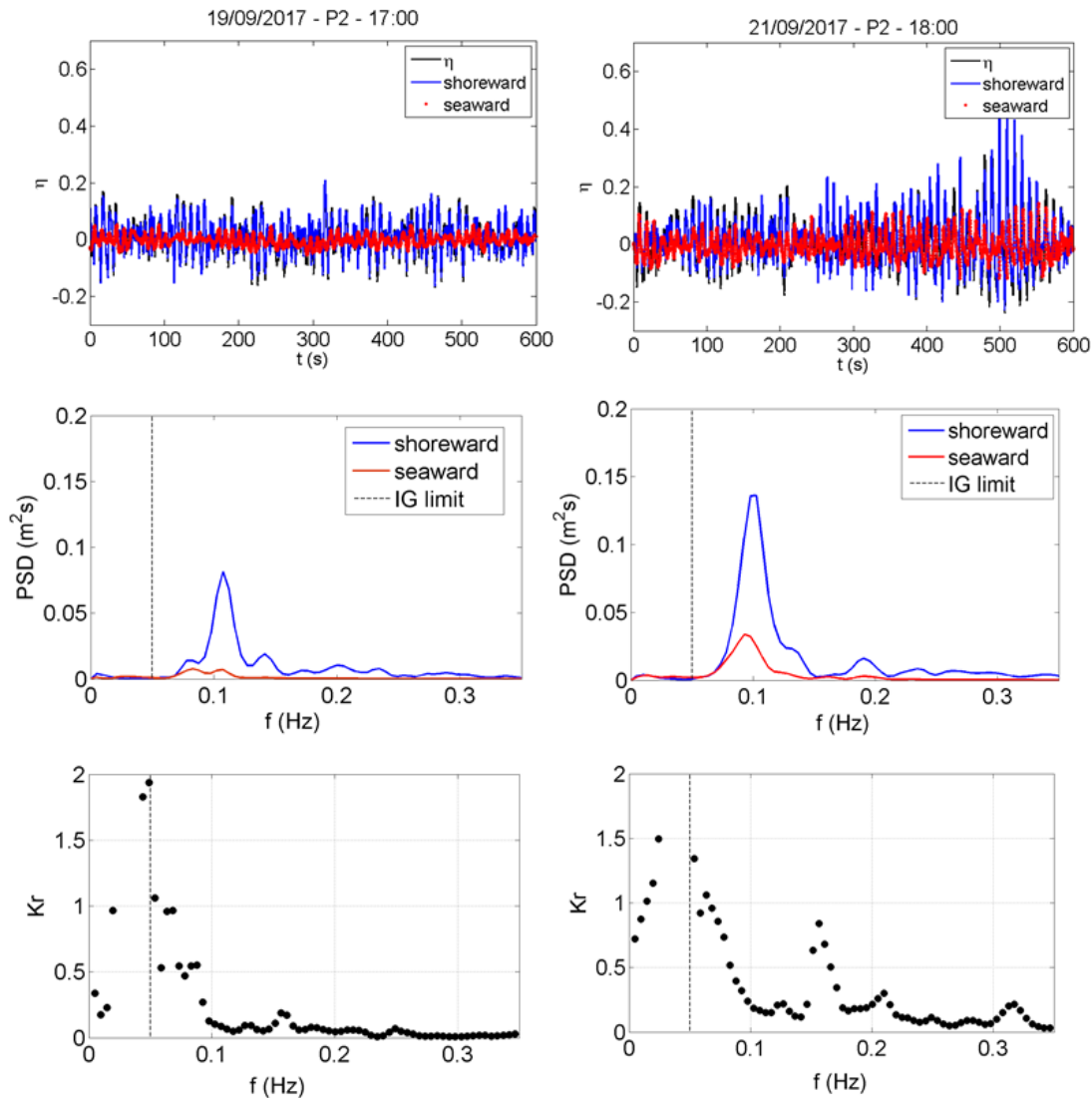


Figure 4.8: Example of the shoreward and seaward (reflected) wave series (upper panels), wave energy density (middle panels) and $K_r^2(f)$ (lower panels) at profiles P2, for the two days of the second experiment (09/2017).

infragravity band. During MUSCLE-Beach 2017 (Figure 4.8), values were higher (around 0.2) with a peak at 0.16 Hz and increasing from 0.2 to 1 in the zone between 0.1 Hz to 0.05 Hz. Particularly, the series measured on 21st September 2017, the day in which the nodal structure was observed, registered the highest amount of reflection. This is evident if we look to the η series and the energy spectra. The seaward signal was more representative in that day than it was observed in the other days. Total K_r^2 (integrated along incident frequencies) from the 21st September 2017 was around 0.25, while during the other days values were always less than 0.1.

TABLE 4.2: Correlation between the reflection coefficient and different wave and beach parameters ($y = Kx$).

Relation	Slope (K)	ρ^2
K_r^2 vs $\tan\beta$	1.46	0.16
K_r^2 vs H_0	0.10	-0.58
K_r^2 vs L_0	0.0003	0.29
K_r^2 vs $(H_0/L_0)^{-0.5}$	0.003	0.17
K_r^2 vs ξ_0	0.061	0.30
K_r^2 vs ξ_0^2	0.04	0.25
K_r^2 vs M	8.72	0.67

Previous works have shown that the reflection of the short waves (incident band) is highly affected by the wave frequency and the beach slope (Elgar et al., 1994). For the dataset measured in Somo beach, K_r^2 was proportional to $\tan\beta^{4.3}$ and f_m^4 (Figure 4.9a and Figure 4.9b). This result is consistent with eq. 4.6, which represents M as a function of $\tan\beta^5$ and f_m^4 .

The correlation between K_r^2 and different beach and wave parameters is presented in Table 4.2. The higher correlation was observed when relating K_r^2 and M (see also Figure 4.9c). M (a combination of frequency, energy and beach slope information) have already been related to the reflection coefficient in previous works (Ardhuin and Roland, 2012; Tatavarti et al., 1988). Although Miche's formula was developed based on monochromatic waves, it is consistent to measured data and can be used as a first approximation to parameterize the reflection on beaches.

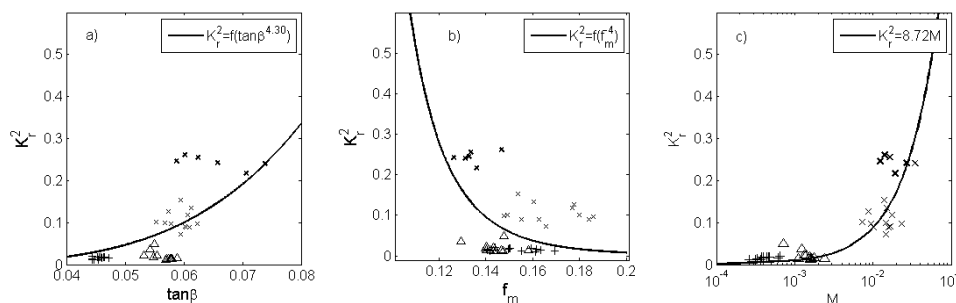


Figure 4.9: Relation between the reflection coefficient K_r^2 and the foreshore slope $\tan\beta$ (a), the mean frequency f_m (b) and the Miche's number M (c).

The relation between K_r^2 and the relative incident swash S_{inc}/H_0 is presented in Figure 4.10a. Higher S_{inc}/H_0 have been observed in conditions of higher K_r^2 . A parameterization using this kind of relation was already presented for estimating

the wave runup on structures (Muttray et al., 2006; Tautenhain et al., 1982), and can be a way to improve the S_{inc} predictions on beaches. The practical application to other beaches, however, demands the use of theoretical K_r^2 based on typical environmental parameters. Hence, once the relation between S_{inc}/H_0 and K_r^2 was verified, the following was to test the relation using M .

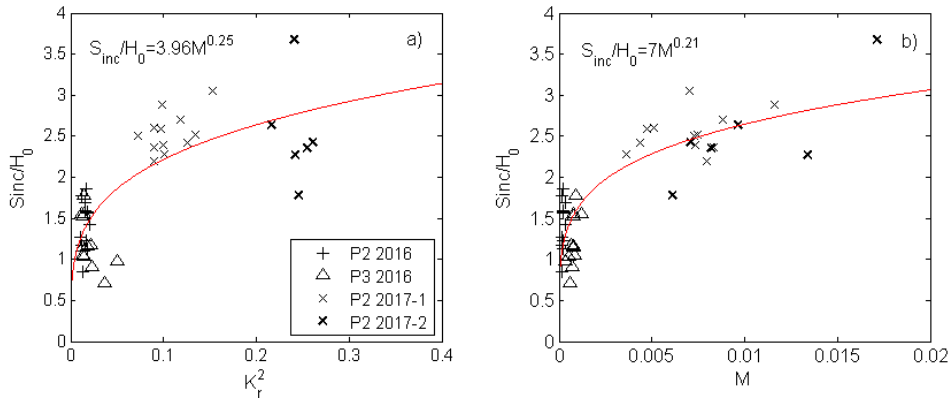


Figure 4.10: Relation between S_{inc}/H_0 and the measured reflection coefficient (a) and the Miche's number M (b).

The parameter M showed to characterize well the relative incident swash (Figure 4.10b) with high correlation being observed from that relation ($\rho^2 = 0.72$) spite of the scatter of the dataset. When comparing M to the S_{inc}/H_0 obtained from the other beaches (M calculated with f_p instead of f_m), the correlation is also high ($\rho^2 = 0.65$) (Figure 4.11a) with the exponent of the term M similar to the one verified using only the dataset from Somo beach. However, higher scatter was observed and, because of that, the distribution between measured and calculated S_{inc} did not show improvement from the results observed using previous parameterization (*i.e.* S2006) (Figure 4.11b).

These results indicate that although M is related to K_r^2 and some relation can also be observed with S_{inc}/H_0 , that parameter is not enough to correctly describe the swash on beaches. Larger database of measured K_r^2 in different morphodynamic conditions would be necessary to establish the correct parameterization of the reflection coefficient to be used in incident swash predictions.

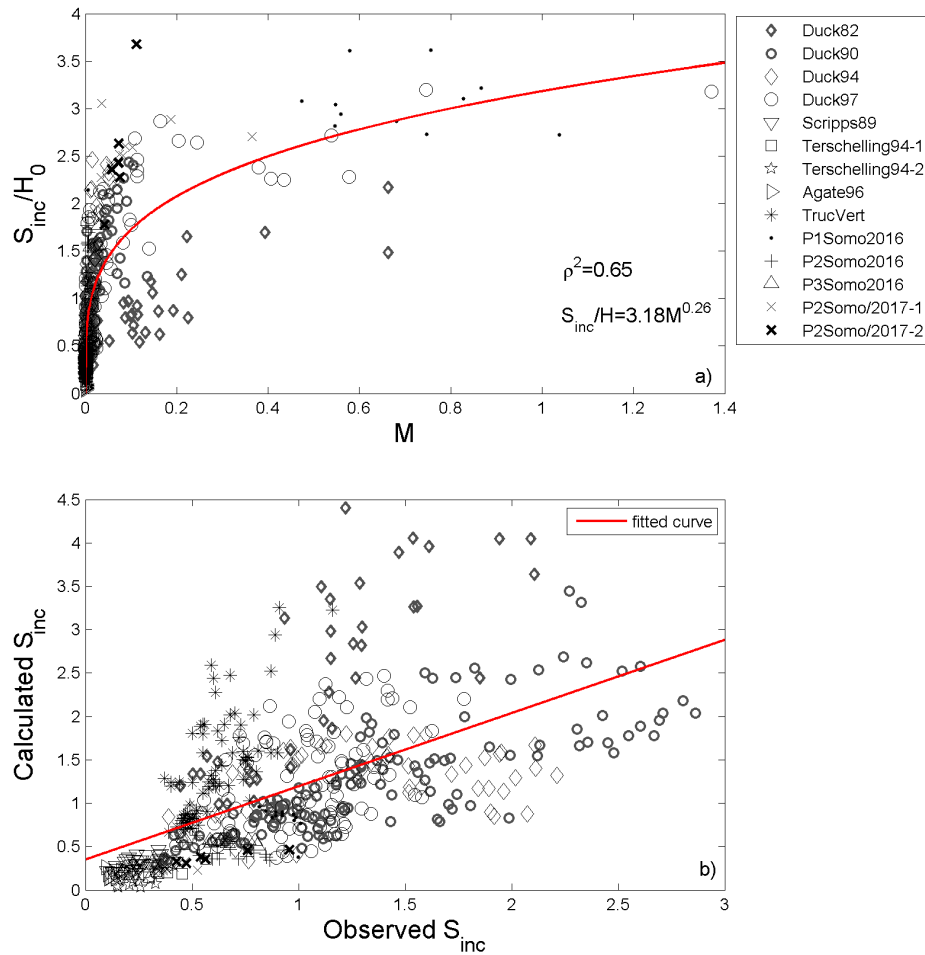


Figure 4.11: Relation between S_{inc}/H_0 and the parameter M using the whole database available in this work.

4.3.3. S_{inc} parameterization for different morphodynamic conditions based on G1984 model

The last step was to test the use of eq. 4.7 for predicting the incident swash. First, the whole dataset was used in the regression and the coefficients a , b and c were obtained ($a = 0.42$, $b = 0.99$ and $c = -0.65$). The S_{inc} values obtained from that relation resulted in low correlation ($\rho^2 = 0.32$) and high scatter (Figure 4.12). Besides, the coefficients were not so distant from those presented by S2006 ($a = 0.75$, $b = 1$ and $c = -0.5$) and the resultant distribution between measured and calculated data was quite similar (colored dots represents S2006 results in Figure 4.12). Once again, the problem of representing the incident swash under different morphodynamic conditions with one single formula is evidenced.

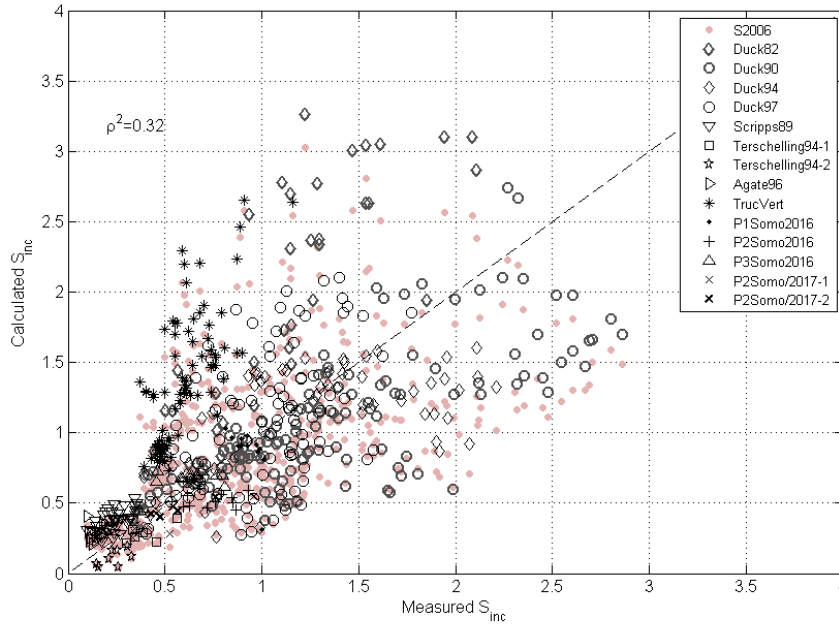


Figure 4.12: Scatterplot between measured S_{inc} and S_{inc} calculated using the coefficients obtained with the fit for the whole dataset ($a = 0.42$, $b = 0.99$ and $c = -0.65$) and resultant $\rho^2 = 0.32$. Light colored dots represent the distribution of S_{inc} calculated with S2006 model. The dashed line represents the ideal fit over which the values would be perfectly correlated.

The following was to analyse the use of eq. 4.7 when fitted according to each morphodynamic condition. The final formula and coefficients established for each beach type are presented in eq. 4.9.

$$\frac{S_{inc}}{H_0} = a \cdot \tan \beta^b \left(\frac{H_0}{L_0} \right)^c \begin{cases} a = 2.83; b = 2.12; c = -0.82 \text{ (dissipative: } \Omega^* > 5.5) \\ a = 0.15; b = 0.56; c = -0.64 \text{ (intermediate: } 1.5 < \Omega^* \leq 5.5) \\ a = 0.50; b = -0.37; c = -0.15 \text{ (reflective: } \Omega^* \leq 1.5) \end{cases} \quad (4.9)$$

Coefficients b and c showed to vary with the morphodynamic beach state. b values increased from reflective to dissipative states while c values were always negative, increasing from dissipative to reflective states. The coefficients b and c obtained from the fit to dissipative and reflective beaches (eq. 4.9) are similar to those proposed by Guza et al. (1984) to characterize the saturated ($b = 2$ and $c = -1$) and reflective ($b = -0.5$ and $c = 0$) regimes (eq. 4.8). The scatterplot between

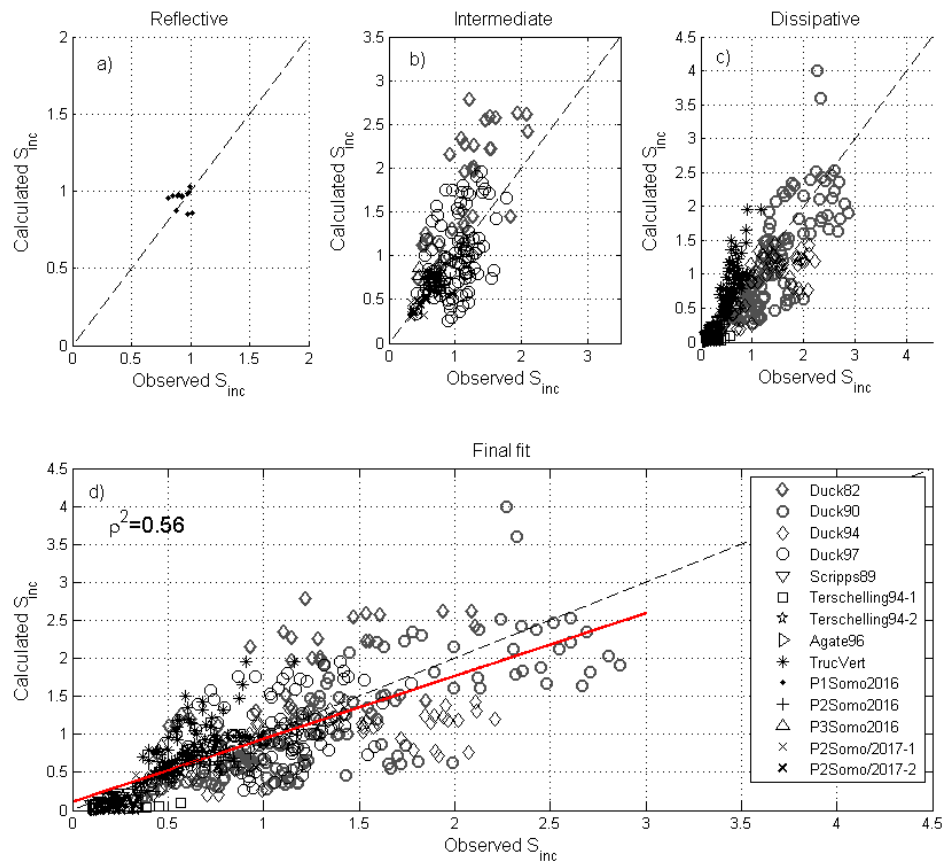


Figure 4.13: Scatterplot between measured and calculated S_{inc} for each beach type (up) and the final regression fit (down) using the three formulas. The dashed line represents the fit over which the values would be perfectly correlated.

measured and calculated data for each morphodynamic condition and also for the totality of the dataset (merging the results obtained from the three equations - *Final fit*) are presented in Figure 4.13. The results show high correlation when fitting the formula for each beach state separately. The tendency of S_{inc} was well represented by the formulas proposed here, and the dataset was distributed around the line of ideal fit (Figure 4.13a, 4.13b and 4.13c).

The statistics of the correlation using eq. 4.9 is presented in Table 4.3. The correlation between S_{inc} and the parameters proposed in that equation was high for all beach types ($\rho^2 > 0.42$) and specially for intermediate and dissipative beaches with $\rho^2 = 0.70$ and $\rho^2 = 0.71$ respectively (Table 4.3). The final fit between measured and calculated S_{inc} resulted in $\rho^2 = 0.56$ (Figure 4.13), an improvement of 0.25 if compared to the fit obtained using S2006 ($\rho^2 = 0.31$).

TABLE 4.3: Coefficients of the regression between S_{inc}/H_0 and the parameters proposed in eq. 4.7 ($S_{inc}/H_0 = a * \tan\beta^b (H_0/L_0)^c$) for different beach types

Condition	THIS WORK				
	Coefficients			Statistics	
	a	b	c	RMSE (m)	ρ^2
Dissipative beaches	2.83	2.12	-0.82	0.29	0.71
Intermediate beaches	0.15	0.56	-0.64	0.44	0.70
Reflective beaches	0.5	-0.37	-0.15	0.33	0.42

The comparison between the results obtained with i) eq. 4.9, ii) eq. 4.7 fitted to the whole dataset (Figure 4.13) iii) and S2006, indicate the need for distinguishing incident swash formulas according to the beach state.

4.4. Discussion

Reflection coefficients observed during the second experiment carried out in Somo beach showed high amount of reflection not only in the infragravity frequencies but also within the incident band, extending until a frequency of about 0.1 Hz. The same behavior was verified by Raubenheimer and Guza (1996) when analysing data from Scripps beach (California). According to those authors, in conditions of high ξ_0 the stationary wave energy can be significant in incident frequencies, until $f \approx 0.08$ Hz, and so the K_r^2 will be high. On the contrary, in situations of low ξ_0 the waves are progressives and the K_r^2 is expected to be lower. This is consistent to the data observed in Somo. During the experiment MUCLE-Beach 2017, ξ_0 was high (always higher than 1.5) and high $K_r^2(f)$ values extended until $f \approx 0.1$ Hz, what support the idea of a nodal structure within the high frequency suggested in the first analyses of the field measurements. Some studies have shown that under highly reflective conditions, standing waves within the incident band can result in edge waves that causes high longshore variations on runup values (Almar et al., 2018). The detection of edge waves was not the objective of MUSCLE-Beach experiments and the presence of trapped waves could not be verified. Even though, it was shown that cross-shore propagation was dominant nearshore in both

infragravity and incident frequencies (see U and V spectra in Figure 4.3), what dismiss the hypothesis of the occurrence of edge waves during the measurement period.

Following with the idea that the amount of reflection is directly relate to the incident swash values, the relation between the oscillations at the shoreline and the reflection coefficient was tested. This kind of relation have already been used to stablish runup parameterizations in previous works (Muttray et al., 2006; Tautenhain et al., 1982), although those studies were focused on predicting the runup on coastal structures. The application of similar relation to beaches seems obvious. However, obtaining K_r^2 at the coast is not an easy task. Measuring the K_r^2 in these environments includes the use of many equipment to measure wave and current in the surf zone, and such data are not always available. An apparent simple solution would be the use of parameterized K_r^2 , nevertheless, since only few studies were carried out with the aim of measuring the wave reflection on natural beaches, parameterizations to describe K_r^2 are very limited.

The reflection coefficient measured during MUSCLE-Beach experiments showed to be related to the parameter M . Elgar et al. (1994) and Ardhuin and Roland (2012) also showed that M can be used to describe the amount of reflection on natural coasts. The results obtained with the dataset from Somo beach are consistent to those works. The use of M to parameterize S_{inc} also seemed reasonable for Somo beach, however, the application to the whole dataset (Somo data and the dataset from previous works) did not presented a good relation. It seems that the parameter M , as calculated here, is still not the ideal to represent the swash on natural beaches.

On the other hand, the solution proposed in this work based on the formulas presented by Guza et al. (1984), showed to be a good way to represent the swash in conditions of different amount of reflection. The role of the foreshore slope and the wave steepness have shown to vary according to the morphodynamic conditions. One single formula comprising ξ_0 would not be capable of capturing the differences on the incident swash in distinct beach types.

The values of the coefficients b and c obtained in this work for reflective and dissipative beaches were similar to those presented in G1984 formulas for the reflective and saturated regimes, although the dataset used here did not extend until the reflective zone proposed by Guza. These results indicate that the formulas used to represent the reflective and saturated monochromatic regimes can be extended to explain the swash of reflective and dissipative conditions in real beaches. However, the limits between the three regimes are not the ideal to differentiate the three morphodynamic conditions analysed, which were mixed along the transitional and saturated regimes, as can be verified in Figure 4.14.

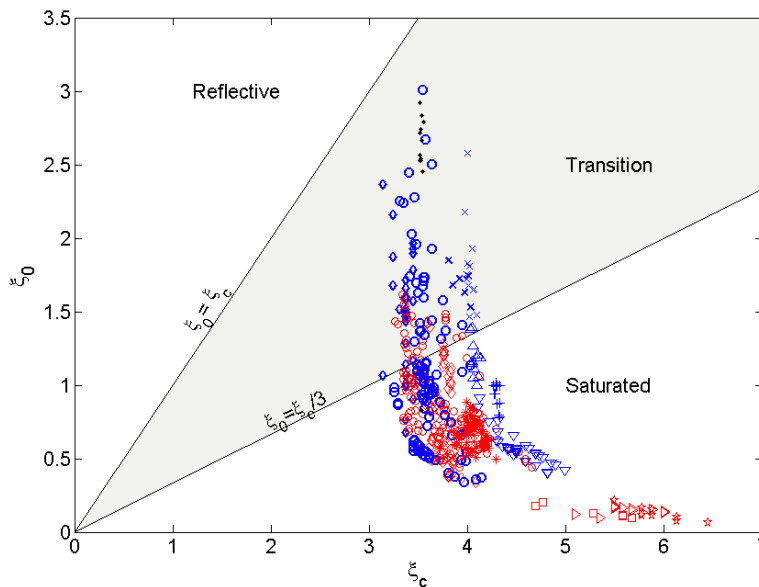


Figure 4.14: Distribution of the dataset used in this work according to the conditions proposed by Guza et al (1984). Symbols represent the same beaches as presented in previous figures. Black, blue and red symbols represents reflective, intermediate and dissipative conditions (according to Ω^*), respectively.

Previewing the different behaviour of the swash in beaches with dissipative characteristics, Stockdon et al. (2006) proposed an alternative formula for calculating the swash in those cases. They suggested that under dissipative conditions the swash component is dominated by the infragravity signal and, in this case, it does not depend on the foreshore slope (their infragravity swash was a function of H_0 and L_0 only). According to S2006, the total swash (including incident and infragravity frequencies) on dissipative beaches can be calculated simply as $S = 0.046(H_0L_0)^{0.5}$. Nevertheless, if we calculate the total swash for dissipative beaches using that

formula, the correlation with measured data is much lower ($\rho^2 = 0.18$) than the correlation obtained for the total swash calculated with S_{ig} and S_{inc} proposed in this work ($S = \sqrt{S_{ig}^2 + S_{inc}^2}$) ($\rho^2 = 0.64$). It is clear, then, that S2006 represents well the S_{inc} under intermediate conditions, but improvements can still be achieved regarding dissipative and reflective beaches.

As stated in Chapter 3 when assessing infragravity swash predictions, some works have shown that the tidal stage can have some effect on runup estimations (Atkinson et al., 2017). So far we have seen that the tidal stage does not represent great differences on the S_{ig} estimations when using the formulas proposed in Chapter 3 (differences in ρ^2 values were lower than 0.1 between tidal stages). The same analysis was carried out to verify the performance of the S_{inc} formula during different tidal moments. The relation between measured and calculated S_{inc}/H_0 in low, mid and high tide is presented in Figure 4.15. Calculated values showed good correlation to measured ones in all tidal moments (ρ^2 always higher than 0.52). However, in contrast to the results obtained for the low frequency swash, the differences were a little bit greater in the correlations of the three tidal stages. Better predictions were obtained during high tide ($\rho^2 = 0.73$), followed by mid ($\rho^2 = 0.64$) and low tide ($\rho^2 = 0.52$). The tidal level seems to affect more the incident swash predictions than it does to the infragravity swash. Atkinson et al. (2017) showed that most empirical runup models (they tested 11 R_2 models and 3 R_{max} models) tend to present lower correlation during low tide. Holman and Sallenger (1985) showed that the tidal level may affect the setup predictions (lower correlation was obtained during low tide), but it did not affect the swash estimations in their dataset. Based on that, they suggested that spilling breaker occurring during low tide affects the setup, but not the swash estimations. Their analysis, however, was limited to the total swash (including low and high frequencies) and the effect of the tide on the incident and infragravity swash was not assessed separately. Further analyses are necessary to elucidate the processes that may have influence on incident and infragravity swash predictions in the different tidal stages.

The improvement on incident swash predictions was only possible when discretizing the dataset according to the beach morphodynamic state and establishing the

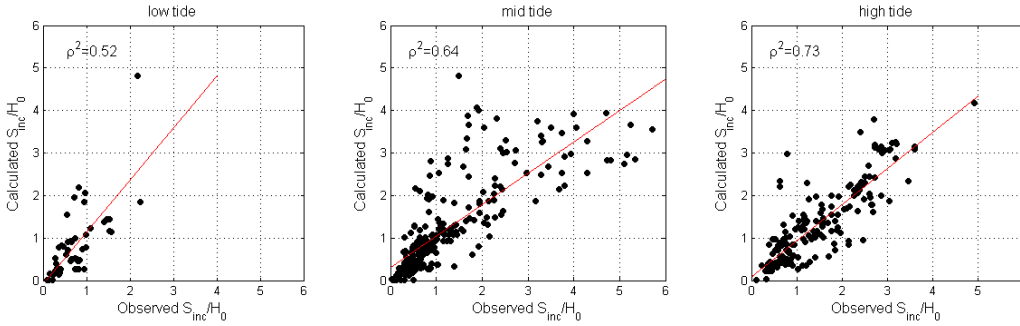


Figure 4.15: Linear regression fit between measured and calculated S_{inc}/H_0 (using eq. 4.9) for the data obtained during different tidal moments (high, mid and low tide).

S_{inc} parameterization for each group of data. The use of more than one formula to calculate the incident swash (and the runup) under different morphodynamic conditions is not a new idea and, besides G1984 model, something similar was proposed by Nielsen and Hanslow (1991) and even by S2006, as mentioned above. Holman and Sallenger (1985) also showed that, within the incident band, different dependencies can be observed in conditions of different ξ_0 . Although the unification in one single parameterization may be easier to understand and to apply, the distinction is necessary to reduce the errors in S_{inc} predictions.

Finally, it is important to state that high scatter will still be present in swash estimations. Many factors can contribute to the remaining errors. The first factor is the omission of parameters that may be important but we still do not take into account, searching for pragmatism when applying the empirical model or because an empirical relation with other parameters was not established yet. Other factor is the 2D approximation assumed by empirical swash formulas. The 2D proxy not always represents the real state at the beach. Intermediate beaches, for example, can present complex features like rips, longshore bar-through system and edge waves, that causes longshore variability of swash values, and are not accounted in empirical estimations.

4.5. Summary and Conclusions

This Chapter presented the analysis and parameterization of the incident swash on beaches. Specifically, the role of the amount of wave reflection under different morphodynamic conditions was analysed. The estimation of the incident swash was assessed under two different approaches. First, a direct relation between S_{inc}/H_0 and the reflection coefficient (K_r^2) was tested. The second approach was based on the formulas proposed by G1984 to calculate the swash in conditions of different amount of reflection.

Initial analysis using the dataset measured in Somo beach indicated a clear relation between high frequency swash and the reflection coefficient, confirming the main hypothesis of this chapter. However, establishing a parameterization with the reflection coefficient demands the use of theoretical K_r^2 , a subject very limited in the existent literature.

Based on the work presented by Guza et al. (1984) a general formula was proposed to describe the incident swash in different morphodynamic conditions. The coefficients of that basic formula were fitted to measured data and three equations, for reflective, intermediate and dissipative beaches, were devised. The analysis of the values predicted with those formulas indicated good correlation for all beach types. These results show that the basic structure observed in G1984 formulas, can be applied to swash parameterizations in different beach states. The use of more than one formula to characterize the swash under different morphodynamic conditions is necessary if we want to represent the swash oscillations accurately in all beach types.

Chapter 5

Application of the swash formulas to wave runup estimation

5.1. Introduction

Once the incident and the infragravity swash parameterization were defined, the next step was to verify the impact of the new formulas on the wave runup values. This chapter is dedicated to i) demonstrate the improvement on runup predictions when applying the S_{ig} and S_{inc} parameterizations to runup estimation and ii) verify the validity of the formulas for predicting the wave runup when applied to other beaches. For this second topic, the dataset measured at the beaches that compose the Itapocorói Bay, in the South of Brazil, was used.

5.2. Methods

5.2.1. Evaluations of wave runup estimation (R_2)

To assess the effect of applying S_{ig} and S_{inc} parameterizations on runup predictions, the structure of the wave runup formula presented by S2006 was used (eq. 5.1).

TABLE 5.1: Values attributed to coefficients a , b and c for dissipative, intermediate and reflective conditions.

Ω^*	a	b	c
Dissipative Beaches ($\Omega^* > 5.5$)	2.83	2.12	-0.82
Intermediate beaches ($1.5 \leq \Omega^* \leq 5.5$)	0.15	0.56	-0.64
Reflective beaches ($\Omega^* < 1.5$)	0.50	-0.37	-0.15

$$R_2 = 1.1 \left(\langle \eta \rangle + \frac{\sqrt{S_{inc}^2 + S_{ig}^2}}{2} \right) \quad (5.1)$$

Based on that structure, the formula to calculate the R_2 using the equations proposed here becomes:

$$R_2 = 1.1 \left(0.35 \tan \beta (H_0 L_0)^{0.5} + \frac{\sqrt{\left[(0.19 + 0.008 \Omega^*) \left(\frac{H_0 L_0}{\tan \beta} \right)^{0.5} \tan \beta \right]^2 + [a * \tan \beta^b H_0 \left(\frac{H_0}{L_0} \right)^c]^2}}{2} \right) \quad (5.2)$$

where a , b and c are the coefficients that vary according to the morphodynamic beach state, as presented in Table 5.1.

The R_2 was calculated using the S_{ig} and S_{inc} as proposed in previous chapters for the same dataset (MUSCLE-beach experiments and recompiled data). The results were compared to those obtained with the parameterizations proposed in previous works.

5.2.2. Application to Itapocorói Bay

The dataset from the experiment carried out on Itajuba, Piçarras and Alegre Beaches (Vieira da Silva et al., 2017) (Figure 5.1), was used to verify the R_2 predictions when using the S_{ig} and S_{inc} formulas on reflective and intermediate beaches.

Itajuba, Piçarras and Alegre are microtidal beaches that are located at Itapocorói Bay, in the Southern coast of Brazil. These three sectors of the bay are typically

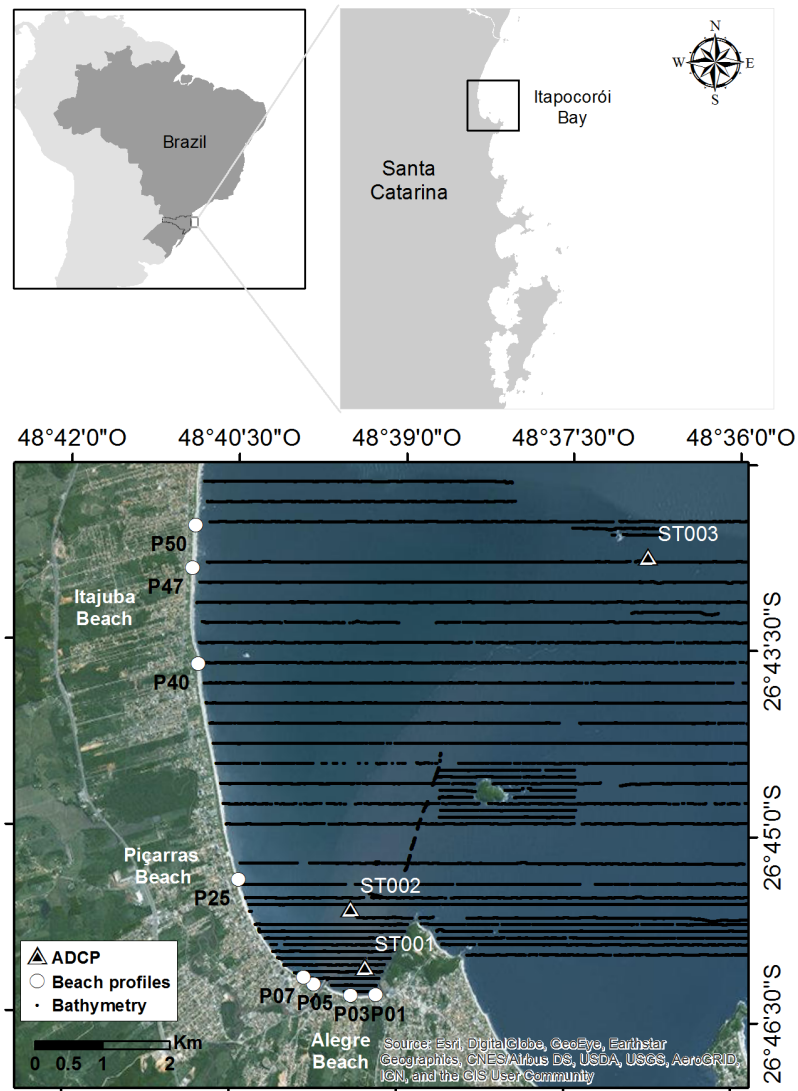


Figure 5.1: Location and measurement distribution along Itajuba, Piçarras and Alegre beaches.

characterized as intermediate beaches (Klein and Menezes, 2001), but may present reflective conditions according to the incident wave energy. The dataset measured in those beaches was obtained in a 34 days experiment, from 19th August to 22nd September 2011. Wave data were obtained by ADCP measurements in three points nearshore (ST001, ST002 and ST003). Beach profile topography was measured every two days, from 22/Aug to 21/Sep on profiles P01, P03, P05; P07 and P47; from 12/Sep to 21/Sep on profile P25; and from 24/Aug to 21/Sep on profile P40. The maximum uprush of the waves at the beach was measured with a GPS equipment (same procedure explained in Chapter 2 of this thesis) during 30 min

every measurement day. Detailed bathymetry was measured with echo sounder between 2nd and 6th November. Details about the experiment can be found in Vieira da Silva et al. (2017).

The procedure to obtain the environmental data to be used in the parameterizations is described below:

- RUNUP 2% (R_2): R_{max} values were fitted to a Gaussian curve and the runup exceeded by 2% of the waves were obtained from the Cumulative Distribution Function (CDF).
- WAVE PARAMETERS: Wave data from the ADCPs ST001 and ST002 were deshoaled to 80 m depth, same procedure carried out with the rest of the data used in this thesis. Wave parameters deshoaled from ST001 were used in runup estimation of profiles P01 and P03, while ST002 data was used to calculate the runup on P05, P07 and P25. To obtain wave parameters for the profiles P40 to P50, the wave series measured at ST003 was propagated until a point in front of each of those profiles using the OLUCA-SP model. The wave parameters were then deshoaled assuming linear theory and shore-normal approach.
- FORESHORE SLOPE: The foreshore slope was obtained from the topography of each beach profile. Since runup measurements were not continuous, it was not possible to obtain the $\tan\beta$ by the same procedure as carried out with Somo dataset. The foreshore slope was then obtained as the slope between the Z values of maximum and minimum R_{max} (Figure 5.2 and Figure 5.3).
- D50 AND BEACH MORPHODYNAMIC STATE: $D50$ values varied from 0.20 mm to 0.65 mm in the profiles along the beach (Figure 5.3). Based on the $D50$ and on the wave parameters, the morphodynamic beach state was calculated. To take into account the previous sea state, wave series obtained from the database GOW in a point selected in front of the beach (Figure 5.4) was used. The embayed form of the beach leads to transformation of the

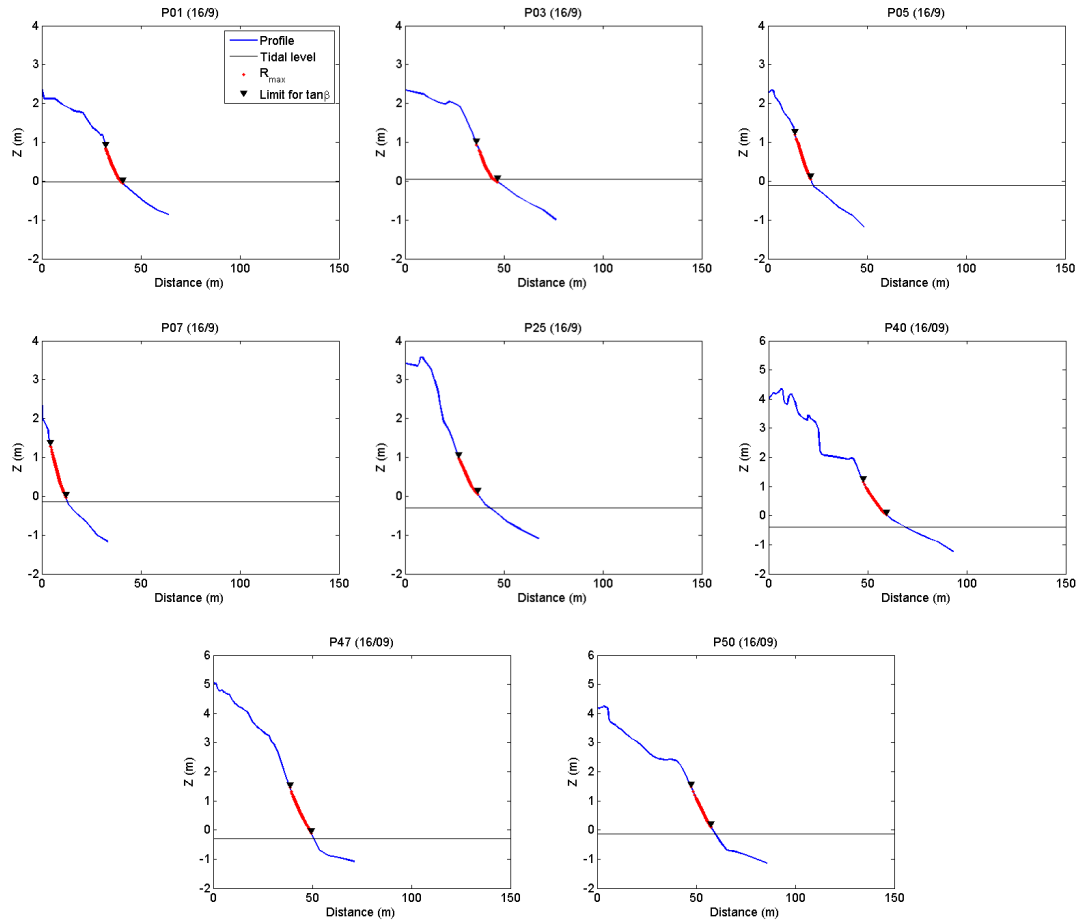


Figure 5.2: Example of the topography (blue line) and runup (red dots) measured in each beach profile. Black triangles indicate the limits between which the foreshore slope was calculated.

waves and a wave gradient may be observed along the shoreline. Because of that, the dataset from the GOW point could not be used to directly estimate Ω^* , since the variations on the wave runup due to the wave gradient would not be considered. The solution was to propagate the waves using the OLUCA-SP model until a point in front of the profiles and, then, deshoal the wave series to a depth equals to 80 m. The procedure is the same applied to calculate Ω^* in Somo beach. The series for the 30 days previous to the measurements at the beach were used then, to calculate the Ω^* as proposed in eq. 2.2.

A resume of the parameters obtained from the process explained above can be found in Table A1, Appendix 1. Based on those data, the wave runup calculated

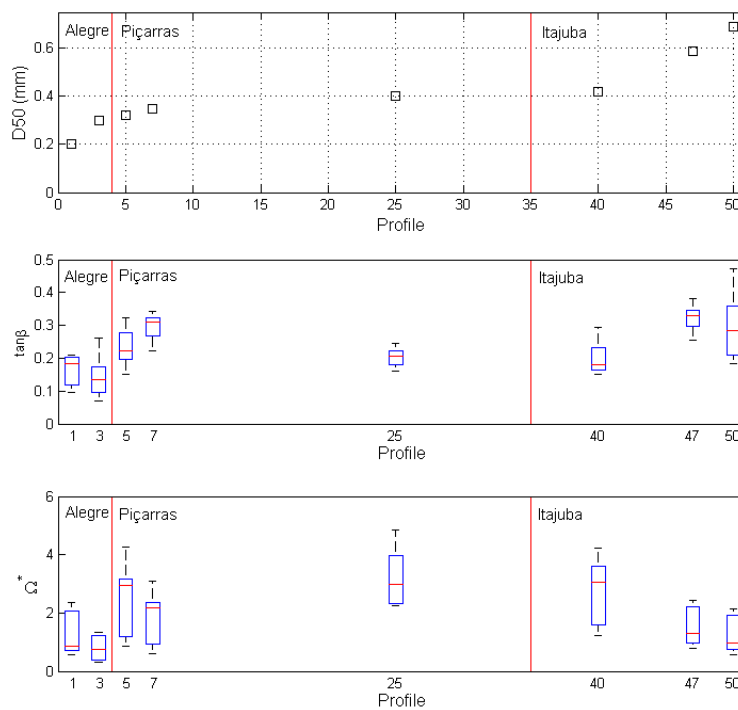


Figure 5.3: D_{50} , mean $\tan\beta$ and Ω^* distribution along the beach. On the boxplot, the central mark is the median, the edges of the box are the 25th and 75th percentiles, the whiskers extend to the most extreme datapoints.

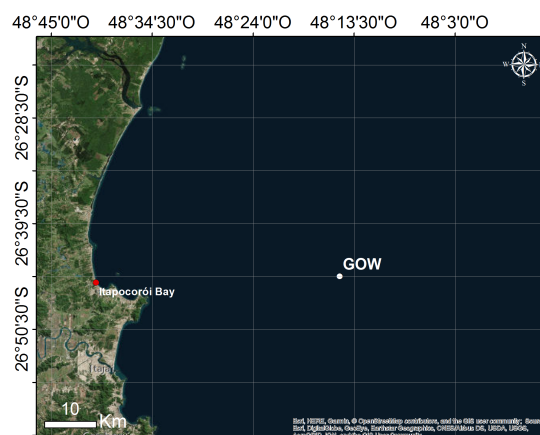


Figure 5.4: GOW point used to calculate the beach state according to the beach memory (Ω^*).

with the formulas proposed here was assessed.

5.3. Results

5.3.1. Evaluation of wave runup estimation (R_2)

The estimation of wave runup values (R_2) was evaluated. Figure 5.5 shows the distribution of measured data and the values calculated using the formulas proposed here (as expressed in eq. 5.2). The tendency of the dataset is well represented and the fitted curve (black thick line) lies very near to the ideal fit (black thin line). High correlation between measured and calculated R_2 values were observed ($\rho^2 = 0.76$) and the fit for each beach type indicates good prediction under all morphodynamic conditions (ρ^2 always higher than 0.70) (Table 5.2). For comparison and verification of the improvement on runup estimations, the S2006 fit, obtained from the linear regression between measured values and the R_2 calculated with S2006 formulas, is also presented in Figure 5.5 (gray dashed line). By comparing both curves, it is possible to verify improvement in the predictions of high values that were underestimated by S2006 model.

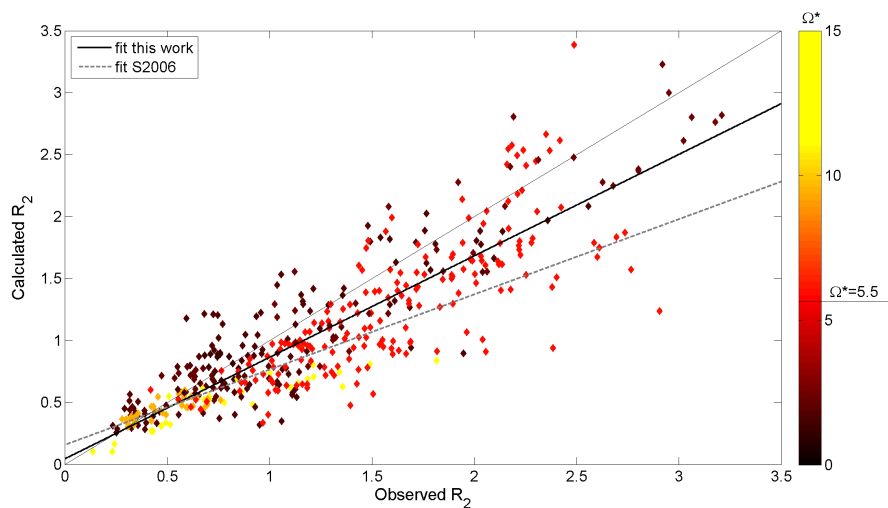


Figure 5.5: Scatterplot between measured and calculated R_2 . Coloured symbols indicate the beach morphodynamic state according to Ω^* . Black thin line represents the ideal fit, black thick line represents the fit obtained when using the formulas proposed here (eq. 5.2) and gray dashed line is the fit obtained using the formulas proposed by Stockdon et al. (2006) (eq. 1.11).

There is, however, a significant scatter in the R_2 results showed in Figure 5.5 and the distribution seems to broader in the upper part of the curve. The dataset from dissipative beaches was particularly underpredicted, what is surprising since improvements in both S_{ig} and S_{inc} estimations were obtained with the new parameterizations for that beach type. The distribution between measured and calculated values of the swash amplitude (calculated using the formulas proposed in this work) and the setup (using S2006 formula) is presented in Figure 5.6. Although some scatter is observed in swash amplitude distribution (Figure 5.6a), the underestimation of the dataset from dissipative beaches was not verified in calculated swash values. On the other hand, the setup values from dissipative beaches are scattered and mostly distributed under the ideal fit. That means that an important part of the error in runup predictions comes from the estimations of the setup component, not assessed in this work.

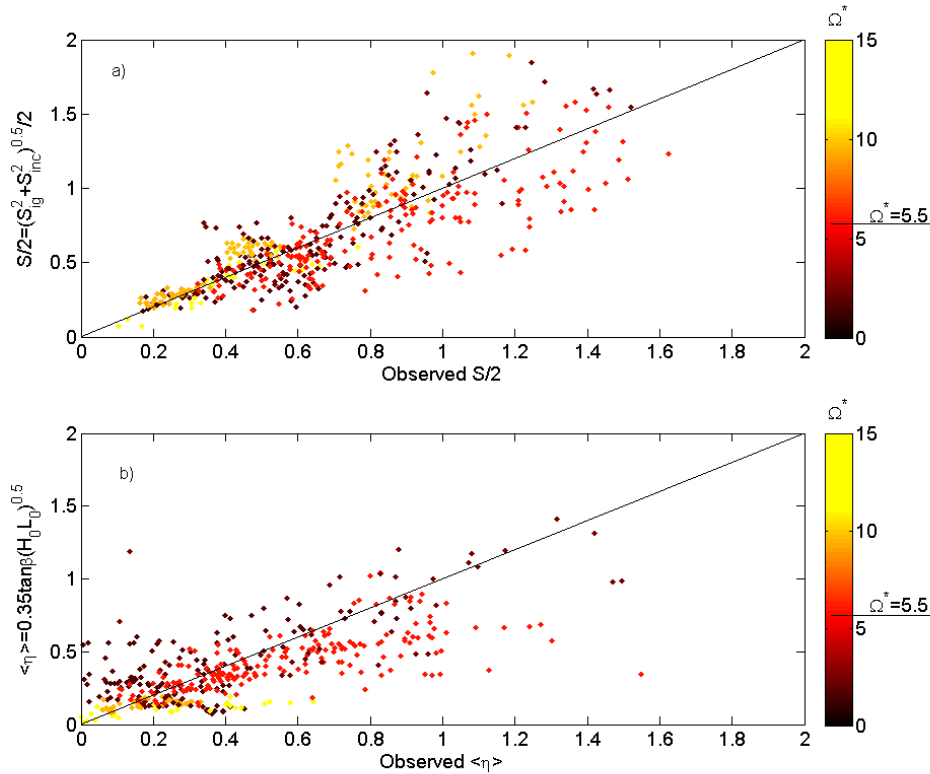


Figure 5.6: Scatterplot between measured and calculated values of the wave runup components: a) swash amplitude ($S/2$) calculated using both infragravity and incident swash formulas proposed in this work and b) setup level ($\langle \eta \rangle$) calculated according to S2006. Coloured symbols indicate the beach morphodynamic state according to Ω^* .

TABLE 5.2: Performance assessment of the R_2 calculated with the S_{inc} and S_{ig} parameterization from S2006 and from those proposed in this work, using the dataset from Somo beach and those recompiled from previous works.

Condition	S2006		This work	
	RMSE(m)	ρ^2	RMSE(m)	ρ^2
Dissipative Beaches	0.19	0.74	0.21	0.87
Intermediate beaches	0.24	0.84	0.22	0.86
Reflective beaches	0.09	0.12	0.02	0.70
All data	0.24	0.73	0.31	0.76

5.3.2. Application to Itapocorói Bay

The data measured along the Itapocorói Bay indicated both reflective and intermediate conditions. This dataset was assessed to verify the effect of using the parameterization proposed in this work on the wave runup estimations in those beach types. Setup, incident swash, infragravity swash and runup values calculated for each profile along the experiments are presented in Figure 5.7. The scatterplot between measured and calculated R_2 are presented in Figure 5.8. The wave runup calculated with the formulas proposed in this work showed to reduce the scatter around the ideal fit and correct overestimation of higher values (blue circles in the figure) if compared to S2006. The RMSE calculated with the whole dataset from the Itapocorói Bay was reduced from 0.96 m using S2006 to 0.71 m using the formulas presented in this work.

The difference between both predictions is even more clear if we compare the errors for each measurement day. The difference between the error resultant from the R_2 calculated using the formulas proposed here and the errors from the estimations using S2006 were calculated as presented in eq. 5.3.

$$\Delta err = \left| \frac{R_{2m} - R_{2c}}{R_{2m}} \right|_{thiswork} - \left| \frac{R_{2m} - R_{2c}}{R_{2m}} \right|_{S2006} \quad (5.3)$$

where Δerr is the difference between the errors obtained with the parameterization proposed in this work and the errors obtained using S2006; R_{2m} is the measured runup and R_{2c} is the calculated runup.

The results obtained in each profile are presented in Figure 5.9. Negative values (red triangles) indicate those cases in which there was a reduction in the error if compared to S2006, and positive values (black triangles) indicate those cases in which the error was higher. The distance from the line zero, indicate how large was the improvement or worsen in the predictions. As it can be seen, most of the cases showed reduction on the errors. Negative values were predominant in all profiles, with exception of profile P01, in which the differences were smaller (always lower than 0.2 for positive values). The biggest difference was observed in northern profiles, where the improvement reached values higher than a meter. It is worth noting that errors due to setup estimations were present in both results.

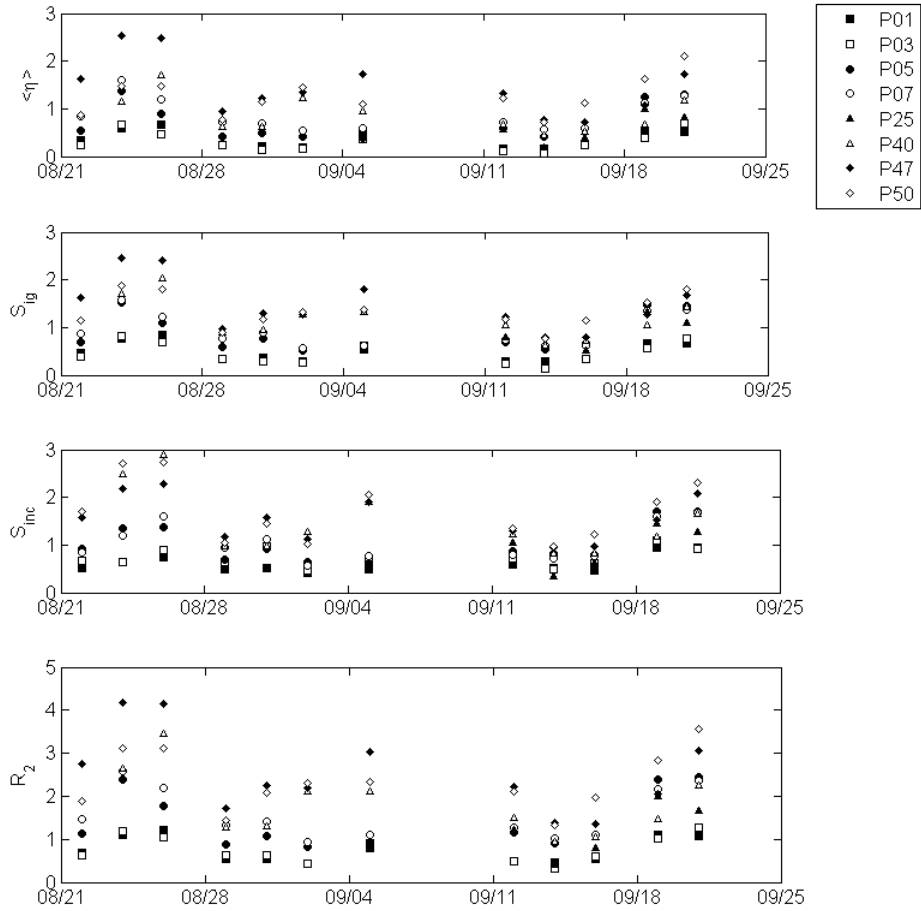


Figure 5.7: Setup $\langle \eta \rangle$, infragravity swash S_{ig} , incident swash S_{inc} and wave runup R_2 calculated with the formulas proposed in this work for Itapocorói bay.

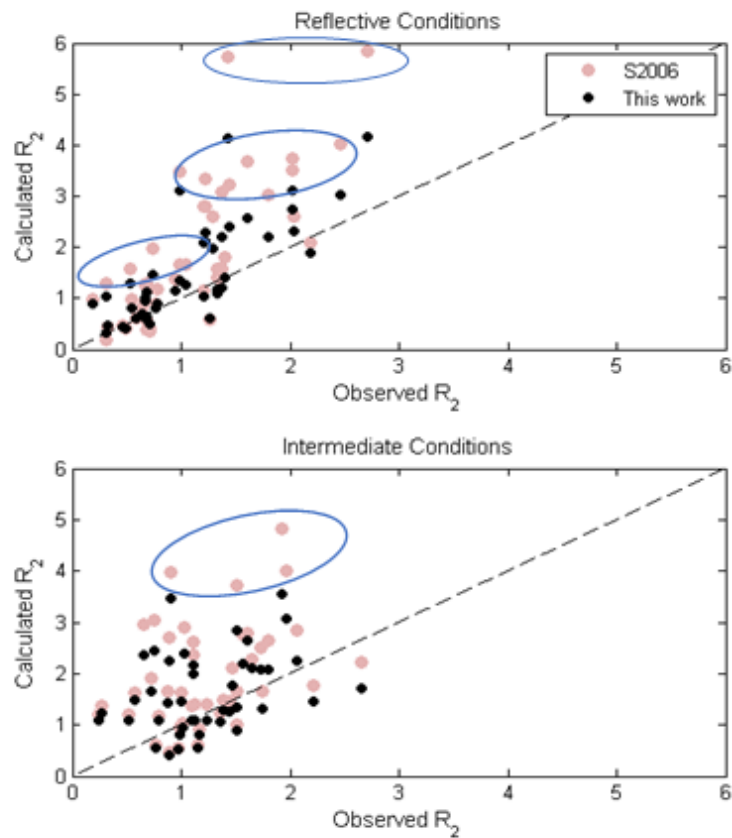


Figure 5.8: Estimated vs observed R_2 from reflective conditions on Itapocorói bay. Blue circles indicate the main overestimation resultant from S2006 model and reduced with the formula proposed here.

5.4. Discussion

The analysis concerning the wave runup estimation using the formulas proposed in this work, demonstrated the effect of the improvements obtained in S_{ig} and S_{inc} estimations on R_2 values. Some scatter can still be verified when analyzing the relation between measured and calculated runup values, partially due to the remaining scatter on swash predictions, but an important part of the errors seems to come from setup estimations. The dataset from dissipative beaches was particularly underpredicted by the setup formula proposed by S2006, based on Hunt scaling ($\langle \eta \rangle = \tan\beta(H_0L_0)^{0.5} = H_s\xi_0$); and that underprediction had some effect of runup estimations. Holman and Sallenger (1985) demonstrated that the wave setup shows good agreement to the Hunt's formula during mid and high tide, but no correlation was observed during low tide. They attributed the lower correlation

to the influence of the offshore bar, and suggested that the relation does not apply for low tidal levels, since the foreshore slope does not reflect the total profile shape. This could be the reason why S2006 formula for predicting the wave setup did not show good results for dissipative beaches, although specific analysis of the setup process and parameterization are necessary to confirm that hypothesis.

5.5. Summary and Conclusions

This chapter presented the analysis of the effect of using the incident and infragravity swash formulas proposed in his work to wave runup predictions. The analysis showed good agreement between measured and calculated runup in all beach types. As observed for S_{ig} and S_{inc} predictions, there was a great contribution for dissipative beaches. Even though, the values for that beach state were mostly displayed under the ideal fit. Part of the errors arises from the setup estimation that results in underpredicted values on dissipative conditions. Improvements on the prediction of the wave runup on dissipative beaches are especially important, since most of high energy storms are characterized by dissipative conditions.

After observing satisfactory results for intermediate and dissipative beaches when assessing the S_{inc} and S_{ig} parameterization in the previous chapters, only few conclusions could be made concerning the prediction capability of the formulations on reflective beaches. Although the parameterization for reflective beaches was established based only on the dataset from profile P1 at Somo beach, the results of the runup estimation on the reflective and intermediate Brazilian beaches, attested the validity of the parameterizations achieved in this work for all morphodynamic beach states.

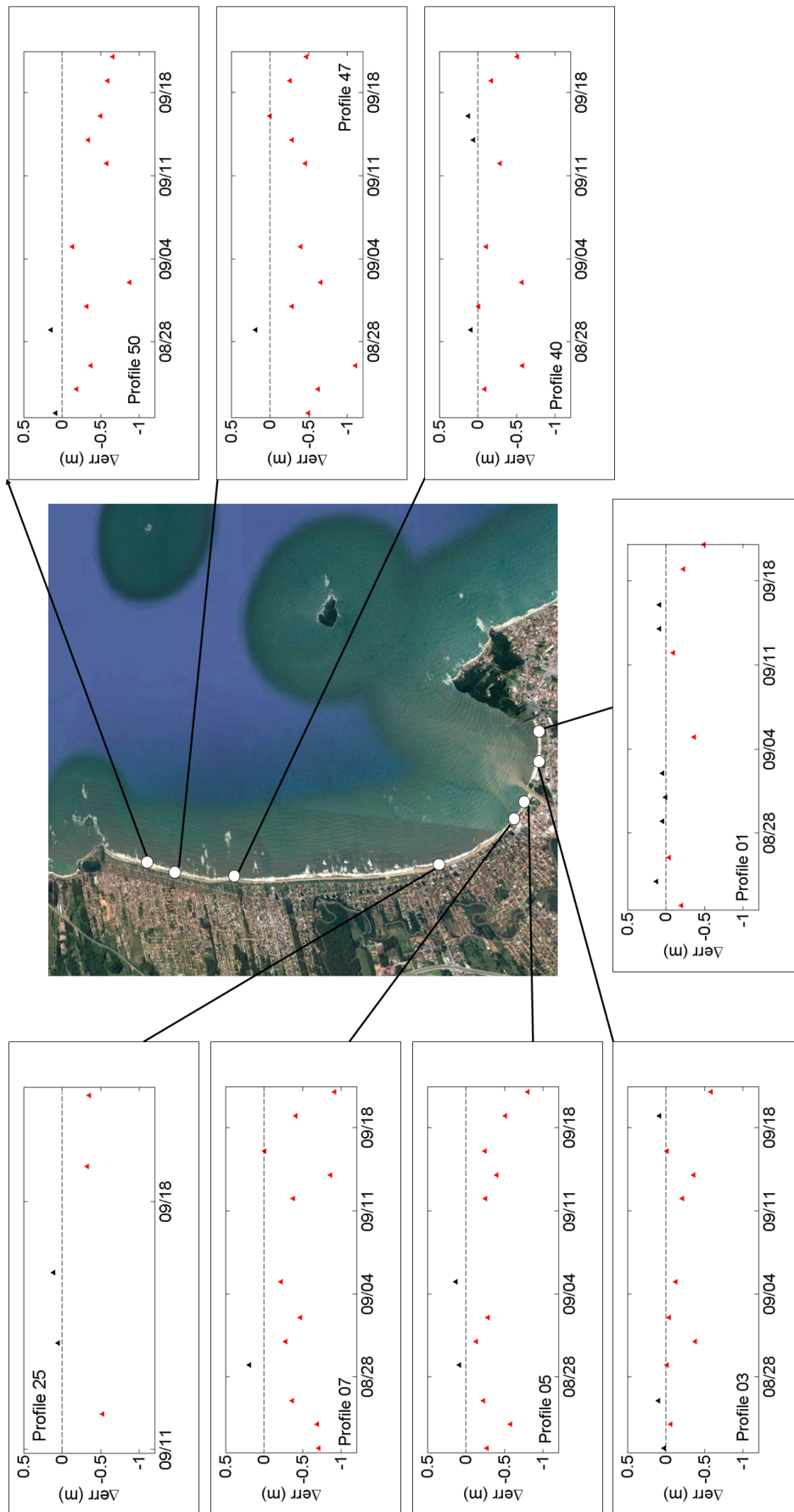


Figure 5.9: Difference between the errors from S2006 and from the model proposed here as stated in eq. 5.3.

Chapter 6

Conclusions and future research

The main goal of this thesis was to broaden the knowledge on swash zone processes and to improve empirical parameterizations by considering the beach morphodynamic conditions. This chapter presents the conclusions, main contributions of the work and some suggestions for future research.

6.1. Conclusions

6.1.1. Main conclusions on the analysis of measured wave, morphology and runup

Two field experiments were undertaken at Somo beach (North Spain) to elucidate the processes occurring in the surf and swash zone that lead to oscillations at the shoreline. The dataset was then used in the development of the new swash parameterizations.

The first experiment (MUSCLE-Beach 2016) was designed to observe the morphology, wave, current and runup behavior on profiles under different morphodynamic conditions. The aim of that experiment was to distinguish wave processes and beach characteristics that may be critical to the swash oscillations in each beach

type. The results from this experiment indicated clear differences on the swash from profiles with different morphodynamic characteristics. The distribution of the swash energy along the frequency bands and the shape of the swash spectra were distinct. An important point was highlighted regarding the determination of the beach state. To take into account the previous wave conditions was crucial to properly defining the morphodynamic of the profiles at Somo beach.

The second experiment (MUSCLE-Beach 2017) was planned to answer additional questions regarding the evolution of the waves along the beach profile. This experiment was carried out in more reflective conditions and measured data evidenced the presence of a standing wave along the profile. These results drew the attention to the importance of the reflection process on swash values.

An additional contribution of MUSCLE-Beach experiments, was that it was possible to enlarge the database of wave, runup and topography used in this work. Besides, all dataset was made available on internet, so it can be used by other researchers that may have interest on studying the wave runup and other processes on beaches. The dataset from Somo can be found in Mendeley platform (<http://dx.doi.org/10.17632/6yh2b327gd.2>) and comprises the following information:

- Wave spectra and parameters
- Reflection coefficients
- Beach profiles topography
- Timestacks

6.1.2. Main conclusions on the analysis and parameterization of the infragravity swash

The role of the morphodynamic beach state on low frequency swash values was assessed in the third chapter of this thesis. The lack of parameters related to the

beach morphology was identified as a limitation in previous infragravity swash parameterizations. Therefore, the analyses were carried out with the aim of including the effect of the morphodynamic of the beach state in a simple parameterization.

A new parameter $\left[(H_0 L_0 / \tan \beta)^{0.5} \right]$ was proposed which included the square root of the foreshore slope. The improvement in the correlations when adding that parameter indicates that there is a link with the slope of the profile. The dependence, however, is not linear and that is the reason why earlier efforts could not find a relation to the profile shape. The correlation to $\tan \beta^{-0.5}$ suggest a relation with the behaviour of long waves reflected in the coast. In conditions of low wave steepness, the waves reflect on the coast forming a standing wave structure. That being the case, the swash can be represented by the standing wave solution near the shoreline, which is describe by $\tan \beta^{-0.5}$.

The representation of the infragravity swash by its horizontal component improved the estimations and the slope of the regression between S_{igH} and the parameter $(H_0 L_0 / \tan \beta)^{0.5}$ showed to be related to the beach morphodynamic state through Ω^* . These results highlight the effect of the beach morphodynamic state on the low frequency oscillations at the beach.

Based on the results obtained, two empirical parameterizations were proposed for infragravity swash predictions and the choice to use one or the other depends on the available data from the site of interest.

6.1.3. Main conclusions on the analysis and parameterization of the incident swash

The amount of wave energy reflection at the beach was analyzed and its role on the high frequency swash was assessed. The analyses of the incident swash were based in two different approaches. First, the effect of the reflection coefficient over the relative incident swash was assessed. Then, basing the analysis on the model

proposed by Guza et al. (1984) for monochromatic waves, a new parameterization to calculate the incident swash on natural beaches was proposed.

Initial analysis using the dataset measured in Somo beach indicated a clear relation between high frequency swash and the reflection coefficient, confirming the role of the wave reflection on the incident swash. However, establishing a parameterization with the reflection coefficient demands the use of theoretical K_r^2 , a subject very limited in the existent literature.

Based on the work presented by Guza et al. (1984) a general formula was proposed to describe the incident swash in conditions of different amount of reflection. The main difference from this formula to the formulas proposed in previous works is the role of the fore shore slope and the role of the wave steepness. We started from the hypothesis that the exponents of those parameters change according to the beach state. Three equations for reflective, intermediate and dissipative beaches were devised. The analysis of the values predicted with those formulas indicated good correlation for all beach types.

6.1.4. Main conclusion on the application of the swash formulas to runup estimation

The analysis of the effect of using the proposed incident and swash formulas on wave runup predictions showed good agreement between measured and calculated runup in all morphodynamic conditions. As observed in S_{ig} and S_{inc} estimations, significant contribution was observed for intermediate and dissipative beaches. Improvements on the prediction of the wave runup on dissipative state are especially important, since most of high energy storm conditions are characterized by dissipative conditions.

The results of the runup estimation on the Brazilian beaches, attested the validity of the parameterizations achieved in this work for intermediate and reflective conditions.

6.2. Scientific contributions

Dataset

- Gomes da Silva, P.; Medina, R.; González, M.; Garnier, R. (2017), “Observations of wave, runup and beach characteristics during the MUSCLE-Beach Experiment”, Mendeley Data, v2. doi: 10.17632/6yh2b327gd.2

Publications

- Gomes da Silva, P., Dalinghaus, C., González, M., Gutiérrez, O., Espejo, A., Abascal, A.J. and Klein, A.F.K. (2016) Estimating flooding level through the Brazilian coast using reanalysis data. *Journal of Coastal Research*. Vol. SI, pp. 1092-1096. doi: 10.2112/SI75-219.1
- Gomes da Silva, P., Medina, R., González, M. and Garnier, R. (2018) Infragravity swash parameterization on beaches: The role of the profile shape and the morphodynamic beach state. *Coastal Engineering*. Vol. 136, pp. 41-55. doi: 10.1016/j.coastaleng.2018.02.002
- Gomes da Silva, P., Medina, R. and González, M. (2018) On the role of the reflection on incident swash parameterization. (submitted to *Coastal Engineering*).

Conferences

- Gomes da Silva, P., Medina, R., González, M. and Garnier, R. (2017) The role of the beach morphodynamic state on infragravity swash on beaches: field observations. *Proceedings of the 19th EGU General Assembly, EGU2017*, Vienna, Austria.
- Gomes da Silva, P., Medina, R., González, M. and Garnier, R. (2017). Influencia de las bajas frecuencias en el runup en playas: mediciones en la

playas de Somo, Santander. Proceedings of the 14th Jornadas Españolas de Ingeniería de Costas y Puertos, Alicante, Spain

- Gomes da Silva, P., Medina, R., González, M. and Garnier, R. (2017) Field measurement and parameterization of the infragravity swash excursion on beaches. Proceedings of the International Short Course and Conference on Applied Coastal Research, Santander, Spain.
- Gomes da Silva, P., Medina, R., González, M. and Garnier, R. (2018) Field measurement and swash parameterization on beaches. Proceedings of the 36th International Conference on Coastal Engineering (ICCE), Baltimore, USA.

6.3. Future research

During the development of this thesis new research questions have arised. We can then, based in those questions, suggest some topics to be explored in future research that could take to further development regarding the swash analysis and parameterization.

- The first point concerns the performance of the swash formulas in different tidal moments. Atkinson et al. (2017) have shown that the prediction capability of runup models depends on the tidal stage. The analysis carried out in this thesis was based mainly on dataset from meso and microtidal beaches. Although Somo beach is included in a zone with large tidal variations (tidal range ≈ 5 m), it was only possible to analyse the high tide period from MUSCLE-Beach experiment. It would be interesting to assess the applicability of the formulas proposed here to the different tidal moments in sites with high tidal ranges and verify how the changes along the tidal cycle may affect infragravity and incident swash predictions, and what processes are responsible for the differences on the performance of swash models.

- It has been shown that the infragravity swash is related to the foreshore slope through the parameter $\tan\beta^{-0.5}$. Such relation suggested that the dependence on that parameter is related to the standing wave solution at the vicinity of the shoreline, as presented by Guza and Thornton (1982). Further analysis, however, are necessary to prove that the inverse dependence on the square root of the fore shore slope is, in fact, due to the standing wave behaviour of the infragravity waves.
- The analysis of the effect of using the S_{ig} and S_{inc} formulas on the wave runup showed good agreement to measured data. However, the wave runup comprises a quasi-steady component, the wave setup, that was not approached in this research. The estimation of that component is responsible for an important part of the errors observed on runup estimations. Although assessment and improvement on wave setup parameterization was not the objective of this work, this analysis could take to better runup predictions and to reduction on the scatter between measured and calculated values.
- The choice of the parameters to be used in swash parameterizations are usually based on variables that partially explain the processes occurring in the surfzone. However, many of those variables can be redundant, like D_{50} and $\tan\beta$, or L_0 and H_0 , that are directly related. Besides, sometimes the use of combined parameters can result in synergy improving the predictions when used together, like it was seen for the Iribarren number during decades of studies. Statistical methods like the Bayesian Networks or those used in the field of Information Theory are efficient on quantifying the information in one variable that can be explained by the others, coupled or not. Bayesian Networks, for example, have already been applied in recent studies to explain coastal processes like erosion on coastlines (Beuzen et al., 2017) and vulnerability to the sea level rise (Gutierrez et al., 2011). Information theory, in turn, have been used to assess complex and non-linear dependencies between driving forces and response in natural systems (e.g. ecohydrological systems in Goodwell and Kumar, 2017). However, none of those metrics have been applied in the study of surf and swash zone processes yet. The use of this

kind of methodology could imply a breakthrough in swash predictions in times that large databases becomes available.

- Very few works were undertaken with the aim of registering the wave reflection on beaches. A gap in the literature was verified with respect to the parameterization of the reflection coefficient on those environments. Given the importance of that parameter, and given the clear link between the reflection coefficient and the swash observed in Somo beach, a simple formulation to quantify the wave reflection through typical environmental parameters could represent large advance in swash analysis and parameterizations. The establishment of such formula would demand, however, high efforts on measuring wave and currents along many beach profiles and under different morphodynamic conditions. A short way to get to the same result could be the use of numerical models validated with measured data.
- Some works have highlighted the importance of the shape of the wave spectra on runup values (Guza and Feddersen, 2012; van Oorschot and d'Angremond, 1968). The directional and frequency spreading are connected to the occurrence of wave groups in the surf zone and to the amount of reflection on the beach. Although the use of those parameters on swash and runup predictions have shown to improve runup estimations, very few studies were carried out in that line.
- Previous studies (Mansard and Funke, 1949; Ruju et al., 2014; van Dongeren et al., 2007) have shown that long and short waves interaction within the surfzone can affect the swash values. Specifically, the presence of wave groups can generate swash modulation in the coastline, a process that have effect on low and high frequency swash. Additional studies are necessary to comprehend and parameterize the effect of wave groupness on swash values.

Appendix A

Appendix 1 - Tables

A resume of the environmental parameters used in this research is presented here.

Figure A.1 shows the location of each field experiment site.

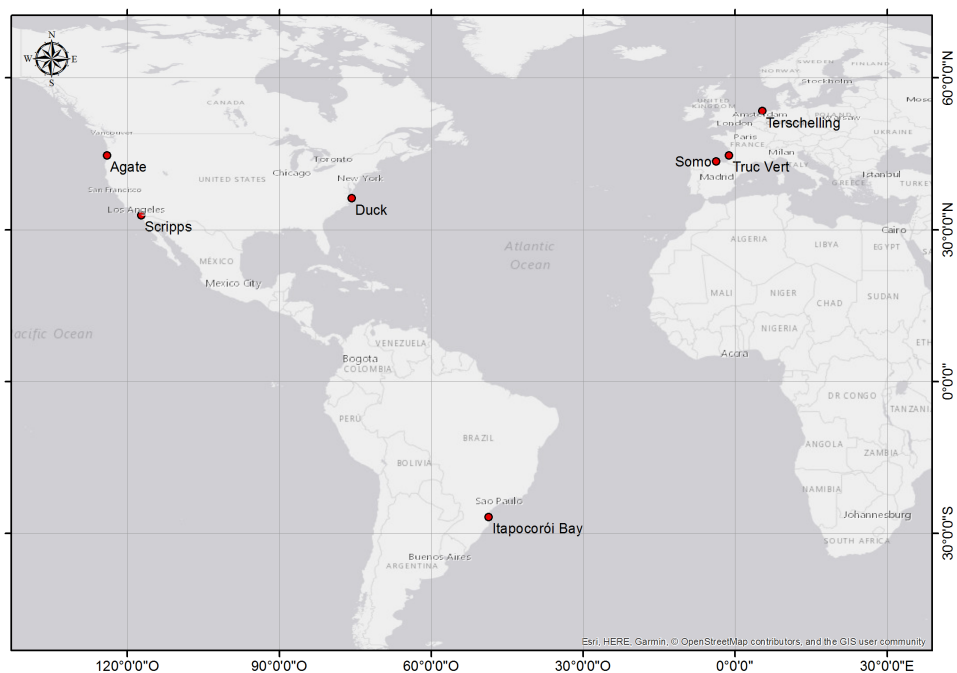


Figure A.1: Field experiment sites.

TABLE A.1: Summary of the environmental parameter from Somo (Gomes da Silva et al, 2017); Truc Vert (Senechal et al, 2011), Itapocoroi (Vieira da Silva et al, 2017) beaches. Sub-index 0 indicates parameters obtained from measurement points and deshooled to a depth of 80 m. N is the number of data in each dataset.

Site/Experiment	Date	Available Data	$\bar{H}_0 \pm \sigma$ (m)	$\bar{T}_p \pm \sigma$ (s)	$\overline{\tan\beta} \pm \sigma$	D50 (mm)	$\bar{\Omega} \pm \sigma$	Ω^*	$\overline{\xi_{0^r}} \pm \sigma$	N
Somo - P1 (Spain) MUSCLE-2016	04/May/2016	$H_0, T_p, R_2, \eta,$	0.31 ± 0.05	11.16 ± 2.17	0.10 ± 0.0001	0.28	0.95 ± 0.66	1.41	2.51 ± 0.56	12
		$S_{tt}, S_{inc}, Sig,$ $\tan\beta, D50$					$(0.67 \text{ to } 0.84)$			
Somo - P2 (Spain) MUSCLE-2016	04/May/2016	$H_0, T_p, R_2, \eta,$	0.52 ± 0.06	11.97 ± 0.76	0.04 ± 0.0001	0.34	1.05 ± 0.14	2.39	0.93 ± 0.08	12
		$S_{tt}, S_{inc}, Sig,$ $\tan\beta, D50$					$(0.87 \text{ to } 1.34)$			
Somo - P3 (Spain) MUSCLE-2016	04/May/2016	$H_0, T_p, R_2, \eta,$	0.55 ± 0.08	12.40 ± 0.48	0.06 ± 0.00	0.35	1.02 ± 0.16	2.32	0.68 ± 0.10	12
		$S_{tt}, S_{inc}, Sig,$ $\tan\beta, D50$					$(0.78 \text{ to } 1.31)$			
Somo - P2 (Spain) MUSCLE-2017	19/Sep/2017	$H_0, T_p, R_2, \eta,$	0.15 ± 0.01	9.78 ± 1.13	0.06 ± 0.003	0.29	0.45 ± 0.07	1.85	1.87 ± 0.33	13
		$S_{tt}, S_{inc}, Sig,$ $\tan\beta, D50$					$(0.31 \text{ to } 0.52)$			
Somo - P2 (Spain) MUSCLE-2017	21/Sep/2017	$H_0, T_p, R_2, \eta,$	0.22 ± 0.02	10.13 ± 0.21	0.06 ± 0.004	0.29	0.63 ± 0.05	1.90	1.71 ± 0.12	13
		$S_{tt}, S_{inc}, Sig,$ $\tan\beta, D50$					$(0.58 \text{ to } 0.78)$			
Truc Vert (France) ECORS - TrucVert'08	Mar/2008	$H_0, T_p, R_2, \eta,$	2.37 ± 1.18	13.64 ± 1.59	0.06 ± 0.1	0.35	3.92 ± 1.70	9.81	0.68 ± 0.12	88
		$S_{tt}, S_{inc}, Sig,$ $\tan\beta, D50$					$(2.08 \text{ to } 9.80)$			
Itapocoroi Bay (Brazil)	Aug and Sep 2011	H_0, T_p, R_2	0.58 ± 0.35	8.87 ± 3.30	0.21 ± 0.07	0.20 to 0.42	1.73 ± 1.13	0.32 to 4.84	3.41 ± 1.71	53
		$\tan\beta, D50$					$(0.32 \text{ to } 4.84)$			

TABLE A.2: Summary of the environmental parameters from Stockdon et al (2006) used in this work. Sub-index 0 indicates parameters obtained from measurements points deshoaled to a depth of 80 m. N is the number of data in each dataset.

Site/Experiment	Date	Available Data	$\overline{H_0} \pm \sigma$ (m)	$\overline{T_p} \pm \sigma$ (s)	$\overline{\tan\beta} \pm \sigma$	D50 (mm)	$\overline{\Omega} \pm \sigma$	Ω^*	$\overline{\xi_0} \pm \sigma$	N
Duck (USA) <i>Duck82</i>	Oct/1982	$H_0, T_p, R_2, \eta,$ $S_{tt}, S_{inc}, Sig,$ $\tan\beta, D50$	1.71 ± 0.87	11.86 ± 3.08	0.12 ± 0.2	0.75	1.48 ± 0.77 (0.59 to 3.99)	2.39	1.44 ± 0.45	36
Scripps (USA)	Jun/1989	$H_0, T_p, R_2, \eta,$ $S_{tt}, S_{inc}, Sig,$ $\tan\beta, D50$	0.69 ± 0.11	10	0.04 ± 0.01	0.2	2.95 ± 0.49 (2.33 to 3.61)	9.58	0.57 ± 0.11	41
Duck (USA) <i>Duck90 - Delilah</i>	Oct/1990	$H_0, T_p, R_2, \eta,$ $S_{tt}, S_{inc}, Sig,$ $\tan\beta, D50$	1.40 ± 0.45	9.25 ± 1.99	0.09 ± 0.02	0.36	3.6 ± 1.38 (0.96 to 6.38)	5.91	0.90 ± 0.31	138
Tescheling (Netherlands)	Apr/1994	$H_0, T_p, R_2, \eta,$ $S_{tt}, S_{inc}, Sig,$ $\tan\beta, D50$	2.83 ± 0.91	8.73 ± 1.56	0.02 ± 0.01	0.22	12.34 ± 2.66 (8.35 to 15.4)	15.85	0.14 ± 0.04	6
Tescheling (Netherlands)	Oct/1994	$H_{s0}, T_p, R_2, \eta,$ $S_{tt}, S_{inc}, Sig,$ $\tan\beta, D50$	1.08 ± 0.47	7.89 ± 2.29	0.01	0.22	5.33 ± 1.96 (3.71 to 9.28)	12.49	0.13 ± 0.05	8
Duck (USA) <i>Duck94</i>	Oct/1994	$H_0, T_p, R_2, \eta,$ $S_{tt}, S_{inc}, Sig,$ $\tan\beta, D50$	1.89 ± 0.83	10.51 ± 2.61	0.08 ± 0.01	0.25 to 2	6.06 ± 4.08 (0.37 to 13.37)	6.0	0.81 ± 0.32	52
Agate (USA)	Feb/1996	$H_0, T_p, R_2, \eta,$ $S_{tt}, S_{inc}, Sig,$ $\tan\beta, D50$	2.48 ± 0.51	11.85 ± 2.54	0.02	0.2	9.82 ± 4.65 (6.15 to 18.71)	17.42	0.15 ± 0.02	52
Duck (USA) <i>Duck97 - SanddyDuck</i>	Oct/1997	$H_0, T_p, R_2, \eta,$ $S_{tt}, S_{inc}, Sig,$ $\tan\beta, D50$	1.37 ± 0.79	9.48 ± 2.71	0.09 ± 0.02	0.90 to 1.66	1.21 ± 0.83 (0.19 to 3.01)	1.78	1.1 ± 0.57	95

TABLE A.3: Summary of the runup, setup and swash statistics for all field experiments analysed in this thesis.

Site/Experiment	$\overline{R_2} \pm \sigma$ (m)	$\overline{\langle \eta \rangle} \pm \sigma$ (m)	$\overline{S_{ig}} \pm \sigma$ (m)	$\overline{S_{inc}} \pm \sigma$ (m)
Somo - P1 (Spain) <i>MUSCLE-2016</i>	0.77 ± 0.06	0.15 ± 0.05	0.34 ± 0.04	0.93 ± 0.06
Somo - P2 (Spain) <i>MUSCLE-2016</i>	0.69 ± 0.06	0.22 ± 0.04	0.62 ± 0.15	0.73 ± 0.13
Somo - P3 (Spain) <i>MUSCLE-2016</i>	0.61 ± 0.07	0.13 ± 0.05	0.68 ± 0.10	0.65 ± 0.11
Somo - P2 (Spain) <i>MUSCLE-2017</i>	0.35 ± 0.07	0.37 ± 0.03	0.16 ± 0.05	0.43 ± 0.12
Somo - P2 (Spain) <i>MUSCLE-2017</i>	0.36 ± 0.06	0.18 ± 0.05	0.32 ± 0.11	0.64 ± 0.22
Truc Vert (France) <i>ECORS - TrucVert'08</i>	-	-	1.33 ± 0.46	0.59 ± 0.14
Itapocoroi Bay (Brazil - 2011)	0.88 ± 0.38	-	-	-
Duck (USA) <i>Duck82</i>	1.95 ± 0.73	0.78 ± 0.36	1.18 ± 0.62	1.15 ± 0.44
Scripps <i>UCA 1994</i>	0.51 ± 0.14	0.18 ± 0.09	0.44 ± 0.09	0.24 ± 0.07
Duck (USA) <i>Duck90</i>	1.48 ± 0.48	0.49 ± 0.22	0.91 ± 0.28	1.33 ± 0.62
Tescheling <i>Netherlands/1994-1</i>	0.83 ± 0.28	0.27 ± 0.19	0.68 ± 0.17	0.40 ± 0.10
Tescheling <i>Netherlands/1994-2</i>	0.37 ± 0.14	0.05 ± 0.04	0.40 ± 0.18	0.24 ± 0.07
Duck (USA) <i>Duck94</i>	1.95 ± 0.45	0.80 ± 0.28	1.35 ± 0.41	1.30 ± 0.53
Agate <i>USA 1996</i>	1.08 ± 0.35	0.38 ± 0.14	1.06 ± 0.27	0.16 ± 0.05
Duck (USA) <i>Duck97</i>	1.17 ± 0.45	0.32 ± 0.21	0.88 ± 0.39	1.02 ± 0.29

Bibliography

- Almar, R., Lerma, A. N., Castelle, B., and Scott, T. On the influence of reflection over a rhythmic swash zone on surf zone dynamics. *Ocean Dynamics*, pages 1–11, 2018.
- Andriolo, U. and Sánchez-García, H. Measuring wave runup and intertidal beach topography from online-streaming surfcam. In *XI Jornadas do Mar 2016*. Portuguese Marine Naval School, 12 2016.
- Ardhuin, F. and Roland, A. Coastal wave reflection, directional spread, and seismoacoustic noise sources. *Journal of Geophysical Research: Oceans*, 117(C11), 2012.
- Atkinson, A. L., Power, H. E., Moura, T., Hammond, T., Callaghan, D. P., and Baldock, T. E. Assessment of runup predictions by empirical models on non-truncated beaches on the south-east australian coast. *Coastal Engineering*, 119: 15 – 31, 2017. ISSN 0378-3839. doi: 10.1016/j.coastaleng.2016.10.001.
- Baldock, T. E., Birrien, F., Atkinson, A., Shimamoto, T., Wu, S., Callaghan, D. P., and Nielsen, P. Morphological hysteresis in the evolution of beach profiles under sequences of wave climates - part 1; observations. *Coastal Engineering*, 128:92 – 105, 2017. ISSN 0378-3839. doi: <https://doi.org/10.1016/j.coastaleng.2017.08.005>.
- Battjes, J. Surf similarity. In *Coastal Engineering 1974*, pages 466–480. Elsevier, 1975.

- Beuzen, T., Splinter, K. D., Turner, I. L., Harley, M. D., and Marshall, L. Predicting storm erosion on sandy coastlines using a bayesian network. *Australasian Coasts & Ports 2017: Working with Nature*, page 102, 2017.
- Carrier, G. F. and Greenspan, H. P. Water waves of finite amplitude on a sloping beach. *Journal of Fluid Mechanics*, 4(1):97–109, 1958. doi: 10.1017/S0022112058000331.
- Dean, R. G. Heuristic models of sand transport in the surf zone. In *First Australian Conference on Coastal Engineering, 1973: Engineering Dynamics of the Coastal Zone*, page 215. Institution of Engineers, Australia, 1973.
- Elgar, S., Herbers, T. H. C., and Guza, R. T. Reflection of ocean surface gravity waves from a natural beach. *Journal of Physical Oceanography*, 24(7):1503–1511, 1994.
- Gomes da Silva, P., Dalinghaus, C., González, O., M. and Gutiérrez, Espejo, A., Abascal, A. J., and Klein, A. H. F. Estimating flooding level through the brazilian coast using reanalysis data. *Journal of Coastal Research*, 75(sp1): 1092–1096, 2016.
- Gomes da Silva, P., Medina, R., González, M., and Garnier, R. Observations of wave, runup and beach characteristics during the muscle-beach experiment. <http://dx.doi.org/10.17632/6yh2b327gd.2>, 2017.
- González, M., Medina, R., Gonzalez-Ondina, J., Osorio, A., Méndez, F. J., and García, E. An integrated coastal modeling system for analyzing beach processes and beach restoration projects, smc. *Computers and Geosciences*, 33(7):916 – 931, 2007. ISSN 0098-3004. doi: <https://doi.org/10.1016/j.cageo.2006.12.005>.
- Goodwell, A. E. and Kumar, P. Temporal information partitioning: Characterizing synergy, uniqueness, and redundancy in interacting environmental variables. *Water Resources Research*, 53(7):5920–5942, 2017. doi: 10.1002/2016WR020216.
- Gourlay, M. R. and Meulen, T. Beach and dune erosion tests (i). *M0935*, 1968.

- Gutierrez, B. T., Plant, N. G., and Thieler, E. R. A bayesian network to predict coastal vulnerability to sea level rise. *Journal of Geophysical Research: Earth Surface*, 116(F2), 2011.
- Guza, R. T. and Bowen, A. J. Resonant interactions for waves breaking on a beach. In *Coastal Engineering 1976*, volume 15. Elsevier, 1976.
- Guza, R. T. and Feddersen, F. Effect of wave frequency and directional spread on shoreline runup. *Geophysical Research Letters*, 39(11), 2012.
- Guza, R. T. and Thornton, E. B. Swash oscillations on a natural beach. *Journal of Geophysical Research: Oceans*, 87(C1):483–491, 1982.
- Guza, R., Thornton, E., and Holman, R. Swash on steep and shallow beaches. *Coastal Engineering Proceedings*, 1(19), 1984.
- Holland, K. T. and Holman, R. A. Field observations of beach cusps and swash motions. *Marine Geology*, 134(1):77–93, 1996. ISSN 0025-3227. doi: 10.1016/0025-3227(96)00025-4.
- Holland, K., Raubenheimer, R., Guza, R., and Holman, R. Runup kinematics on a natural beach. *Journal of Geophysical Research: Oceans*, 100(C3):4985–4993, 1995. doi: 10.1029/94JC02664.
- Holman, R. A. Extreme value statistics for wave run-up on a natural beach. *Coastal Engineering*, 9(6):527–544, 1986.
- Holman, R. A. and Sallenger, A. H. Setup and swash on a natural beach. *Journal of Geophysical Research: Oceans*, 90(C1):945–953, 1985.
- Hughes, M., Moseley, A. S., and Baldock, T. Probability distributions for wave runup on beaches. *Coastal Engineering*, 57:575–584, 06 2010.
- Hughes, M. G., Aagaard, T., Baldock, T. E., and Power, H. E. Spectral signatures for swash on reflective, intermediate and dissipative beaches. *Marine Geology*, 355:88–97, 2014.

- Hunt, I. A. Design of sea-walls and breakwaters. *Transactions of the American Society of Civil Engineers*, 126(4):542–570, 1959.
- Iribarren, C. R. Protection des ports. In *XVIIth International Naval Congress (Lisbon, Portugal), 1949*, pages 31–80, 1949.
- Klein, A. H. F. and Menezes, J. T. Beach morphodynamics and profile sequence for a headland bay coast. *Journal of Coastal Research*, 17(4):812–835, 2001.
- Kubota, S., Mizuguchi, M., and Takezawa, M. Reflection from swash zone on natural beaches. In *Coastal Engineering 1988*, pages 570–583, 1990.
- Losada, M. A., Medina, R., Vidal, C., and Roldán, A. Historical evolution and morphological analysis of "el puntal" spit, santander (spain). *Journal of Coastal Research*, 7(3):711–722, 1991.
- Mansard, E. P. D. and Funke, E. R. The measurements of incident and reflected spectra using a least squares method. In *XVIIth International Naval Congress (Lisbon, Portugal), 1949*, pages 31–80, 1949.
- Masselink, G. and Puleo, J. A. Swash-zone morphodynamics. *Continental Shelf Research*, 26(5):661–680, 2006.
- Medina, R. and Méndez, F. J. Inundación costera originada por la dinámica marina. *Ingeniería y Territorio*, 74:68–75, 2006.
- Méhauté, L., Koh, R. C. Y., and Hwang, L. A synthesis on wave run-up. *Journal of the Waterways and Harbors Division*, pages 77–92, 1968.
- Meyer, R. E. and Taylor, A. D. *Runup on beaches*. Academic, SanDiego, California, 1972.
- Miche, M. Le pouvoir réfléchissant des ouvrages maritimes exposés à l'action de la houle. *Annales de Ponts et Chaussées*, 121 (285-319), 1951.
- Muttray, M., Oumeraci, H., and ten Oever, E. Wave reflection and wave run-up at rubble mound breakwaters. In *Coastal Engineering 2006*, 2006.

- Nielsen, P. Wave setup: A field study. *Journal of Geophysical Research: Oceans*, 93(C12):15643–15652, 1988.
- Nielsen, P. and Hanslow, D. J. Wave runup distributions on natural beaches. *Journal of Coastal Research*, pages 1139–1152, 1991.
- Park, H. and Cox, D. T. Empirical wave run-up formula for wave, storm surge and berm width. *Coastal Engineering*, 115:67–78, 2016.
- Poate, T. G., McCall, R. T., and Masselink, G. A new parameterisation for runup on gravel beaches. *Coastal Engineering*, 117:176–190, 2016.
- Power, H. E., Atkinson, A. L., Hammond, T., and Baldock, T. E. Accuracy of wave runup formula on contrasting southeast australian beaches. In *Proceedings of the 21st Australian Coastal and Ocean Engineering Conference, (Sydney, Australia)*, pages 618–623, 2013.
- Raubenheimer, B. and Guza, R. Observations and predictions of run-up. *Journal of Geophysical Research: Oceans*, 101(C11):25575–25587, 1996. doi: 10.1029/96JC02432.
- Raubenheimer, B., Guza, R. T., Elgar, S., and Kobayashi, N. Swash on a gently sloping beach. *Journal of Geophysical Research: Oceans*, 100(C5):8751–8760, 1995.
- Reguero, B. G., Menéndez, M., Méndez, F. J., Mínguez, R., and Losada, I. J. A global ocean wave (gow) calibrated reanalysis from 1948 onwards. *Coastal Engineering*, 65:38–55, 2012. ISSN 0378-3839. doi: 10.1016/j.coastaleng.2012.03.003.
- Ruessink, B. G., Kleinhan, M. G., and den Beukel, P. G. L. Observations of swash under highly dissipative conditions. *Journal of Geophysical Research: Oceans*, 103(C2):3111–3118, 1998.
- Ruggiero, P., Komar, P. D., McDougal, W. G., Marra, J. J., and Beach, R. A. Wave runup, extreme water levels and the erosion of properties backing beaches. *Journal of Coastal Research*, pages 407–419, 2001.

- Ruggiero, P., Holman, R. A., and Beach, R. A. Wave run-up on a high-energy dissipative beach. *Journal of Geophysical Research: Oceans*, 109(C6), 2004. doi: 10.1029/2003JC002160.
- Ruju, A., Lara, J. L., and Losada, I. J. Numerical analysis of run-up oscillations under dissipative conditions. *Coastal Engineering*, 86:45–56, 2014.
- Sallenger, A. H. Storm impact scale for barrier islands. *Journal of Coastal Research*, pages 890–895, 2000.
- Seelig, W. N. and Ahrens, J. P. *Estimation of wave reflection and energy dissipation coefficients for beaches, revetments, and breakwaters*. U.S. Army, Corps of Engineers, 1981.
- Senechal, N., Coco, G., Bryan, K. R., and Holman, R. A. Wave runup during extreme storm conditions. *Journal of Geophysical Research: Oceans*, 116(C7), 2011.
- Staubke, D. and Cialone, M. Sediment dynamics and profile interactions: Duck94. *Coastal Engineering*, 100:4985–4993, 1996.
- Stockdon, H. F. and Holman, R. A. Observations of wave runup, setup, and swash on natural beaches. <https://pubs.usgs.gov/ds/602/>, 2011.
- Stockdon, H. F., Holman, R. A., Howd, P. A., and Sallenger, A. H. Empirical parameterization of setup, swash, and runup. *Coastal engineering*, 53(7):573–588, 2006.
- Stockdon, H. F., Thompson, D. M., Plant, N. G., and Long, J. W. Evaluation of wave runup predictions from numerical and parametric models. *Coastal Engineering*, 92:1–11, 2014.
- Tatavarti, R., Huntley, D., and Bowen, A. J. Incoming and outgoing wave interactions on beaches. In *Coastal Engineering 1988*, pages 136–150, 1988.
- Tautenhain, E., Kohlhase, S., and Partenscky, H. W. Wave run-up at sea dikes under oblique wave approach. In *Coastal Engineering 1982*, pages 804–810, 1982. doi: 10.1061/9780872623736.050.

- van Dongeren, A., Battjes, J., Janssen, T., van Noorloos, J., Steenhauer, K., Steenbergen, G., and Reniers, A. Shoaling and shoreline dissipation of low-frequency waves. *Journal of Geophysical Research: Oceans*, 112(C2), 2007. doi: 10.1029/2006JC003701.
- van Oorschot, J. H. and d'Angremond, K. The effect of wave energy spectra on wave run-up. In *Coastal Engineering 1968*, 1968. doi: 10.1061/9780872620131.057.
- Vieira da Silva, G., Gomes da Silva, P., Araujo, R., Klein, A., and Toldo Jr, E. Swah on steep and shallow beaches. *Wave run-up on embayed beaches. Study case: Itapocoroí bay Southern Brazil*, 65, 2017.
- Vousdoukas, M. I. Observations of wave runup and groundwater seepage line motions on a reflective-to-intermediate, meso-tidal beach. *Marine Geology*, 350: 52–70, 2014.
- Vousdoukas, M. I., Velegarakis, A. F., Dimou, K., Zervakis, V., and Conley, D. C. Wave run-up observations in microtidal, sediment-starved pocket beaches of the eastern mediterranean. *Journal of Marine Systems*, 78:S37–S47, 2009.
- Vousdoukas, M. I., Wziatek, D., and Almeida, L. P. Coastal vulnerability assessment based on video wave run-up observations at a mesotidal, steep-sloped beach. *Ocean Dynamics*, 62(1):123–137, 2012.
- Wright, L. D. and Short, A. D. Morphodynamic variability of surf zones and beaches: a synthesis. *Marine geology*, 56(1-4):93–118, 1984.
- Wright, L., Short, A., and Green, M. Short-term changes in the morphodynamic states of beaches and surf zones: An empirical predictive model. *Marine Geology*, 62(3):339–364, 1985.